REPORT DOCUMENTATION PAGE

AD-A253 667

1. AGENCY USE ONLY (Leave blank)	2. REPORT DATE	3. REPORT TYPE AND DATES COVERED
	6/30/92	Final Technical Report 11/1/88-4/30/92

4. TITLE AND SUBTITLE
Epitaxial Magnetic Oxides

5. FUNDING NUMBERS
AFOSR-89-0097

6. AUTHOR(S) M.H. Kryder, D.D. Stancil, D.E. Laughlin, W. Wang, M. Ramesh, J. Peruyero, P.H.L. Rasky, S. Silliman, A. Zeltser, W. Eppler, X. Sui, D.J. Rogers

7. PERFORMING ORGANIZATION NAME(S) AND ADDRESS(ES)
Carnegie Mellon Univesity
Pittsburgh, PA 15213-3890

AFOSR-

8. PERFORMING ORGANIZATION REPORT NUMBER
3
21

9. SPONSORING/MONITORING AGENCY NAME(S) AND ADDRESS(ES)
Air Force Office of Scientific Research
Bolling Air Force Base
Washington, DC 20332-6448

10. SPONSORING/MONITORING AGENCY REPORT NUMBER
2305/C1

11. SUPPLEMENTARY NOTES

12a. DISTRIBUTION/AVAILABILITY STATEMENT
Approved for Public Release
Distribution Unlimited

12b. DISTRIBUTION CODE

13. ABSTRACT *(Maximum 200 words)*

Research was carried out on the heteroepitaxial growth of magnetic oxides (garnets and hexaferrites) on a variety of substrates. These new materials technologies are being used for the development of novel microwave, millimeter wave and optical signal processing devices. Liquid phase epitaxy (LPE) sputtering and pyrolysis (thermal decomposition of spin coated material) have been used to grow these materials. For integrated microwave and optical signal processing devices, two-layer LPE grown garnets with one layer having a narrow resonance linewidth (<1 Oe) and the other a high Faraday rotation (>0.1°/μm) have been developed. Silicon-on-garnet technology was developed and demonstrated capable of producing high quality integrated semiconductor and magnetic devices on a common substrate.

Sputter deposition and pyrolysis were developed as alternative lower temperature processes capable of depositing garnets onto nongarnet substrates, and thin film hexaferrites with near-bulk values of magnetization and uniaxial anisotropy were grown by sputter deposition.

14. SUBJECT TERMS	15. NUMBER OF PAGES
garnets, hexaferrites, microwave materials, millimeter wave materials, magneto-optical materials, sputtering, liquid phase epitaxy	148
	16. PRICE CODE

17. SECURITY CLASSIFICATION OF REPORT	18. SECURITY CLASSIFICATION OF THIS PAGE	19. SECURITY CLASSIFICATION OF ABSTRACT	20. LIMITATION OF ABSTRACT
Unclassified	Unclassified	Unclassified	

EPITAXIAL MAGNETIC OXIDES
FINAL TECHNICAL REPORT
June, 1992

1. Introduction

The objectives of this research program have been to develop new magnetic-oxide heteroepitaxial materials for new integrated microwave, millimeter wave and optical signal processing devices. There have been four thrusts to the work carried out in this program. One thrust was to develop new garnet heterostructures which would make possible a new class of integrated microwave and optical signal processing devices. Another was to develop silicon-on-garnet technology so that silicon and magnetic garnet devices could be integrated onto a single substrate. A third was to develop alternative lower temperature processes than liquid phase epitaxy which could be used to grow garnets on nongarnet substrates. A fourth was to develop techniques which would make possible the growth of thin film hexaferrites for new microwave and millimeter wave devices.

The research carried out in each of these areas is briefly summarized below. Detailed reports on each thrust are contained in accompanying reports.

2. Garnet Heterostructures for Microwave and Optical Signal Processing

All of the experimental and theoretical investigations of optical-MSW interactions to date have involved a single film of garnet which served simultaneously as a guide for the optical and magnetostatic modes. This places rather stringent material requirements upon the film since it must simultaneously exhibit low optical absorption, low ferromagnetic resonance linewidth, and high Faraday rotation. We have recently proposed that the desired properties can be more easily realized in a structure consisting of two or more layers. In such a case, alternating layers could be optimized for magnetic and optical properties.

The first layer in the proposed garnet heterostructure is a thin film of yttrium iron garnet (YIG) grown on a gadolinium gallium garnet (GGG) substrate. This is followed by an epitaxial layer of GGG and then an overlayer of bismuth-lutetium iron garnet. In this structure, the YIG layer is optimized for MSW propagation, while the (Bi,Lu)IG overlayer is optimized for optical mode propagation.

Under this program, we concentrated our efforts on growth techniques for the (Bi,Lu)IG layer, since this material is the most difficult to grow with the required properties. We studied films grown with liquid phase epitaxy from two different melts: one based on bismuth oxide and the other based on lead oxide. Significant results were obtained using both melts, although further improvements are needed.

At the low growth temperature required for the incorporation of necessary amounts of bismuth for a significant Faraday rotation value, the standard LPE melt is highly viscous and flux adhesion impairs the surface morphology of the films. Na_2O is known to be effective in decreasing this viscosity and therefore promoting flux removal in the LPE crystal growth of rare-earth garnet films. However, prior to our work, no controlled study of the effect on magnetic and magneto-optic properties of the inclusion of Na^{1+} had been made.

Significantly, we found that while the incorporation of Na_2O in the melt improved surface morphology, the Faraday rotation was unchanged, and the only microwave effect was the introduction of 100-200 Oe of growth-induced anisotropy. This anisotropy could be removed by annealing, but may also be used to fine tune the frequency of the MSW passband. Since the MSW passband frequency is a critical parameter in the proper operation of the heterostructure, this may prove to be an important new capability.

A significant difficulty with the bismuth oxide melt, however, is that the films always have significant absorption lines in the MSW passband from higher-order degenerate exchange modes. Because of this, we also explored films grown from a lead-oxide melt.

(Bi,Lu)IG films grown with a lead oxide melt showed smooth MSW passbands, but the insertion loss was high and the FMR linewidth was typically 2-3 Oe. Since the addition of MgO is known to improve both microwave and optical losses when added to the bismuth oxide melt, we studied its effect when added to a lead-oxide melt. We found that although the optical loss was unchanged, the FMR linewidth was reduced to 1 Oe or below.

A disadvantage of the use of a lead oxide melt is that the incorporation of lead contributes to optical absorption. The relatively high optical loss at 1.3 μm of 10-20 dB/cm could perhaps be reduced with the use of a high temperature anneal in forming gas. Consequently, we believe this new melt may show the most promise yet of achieving (Bi,Lu)IG films with the required optical and microwave properties.

3. Silicon-on-Garnet Technology

The feasibility of combining silicon and magnetic garnet technologies on a single substrate was demonstrated. Functional MOSFETs and silicon magnetodiodes were fabricated in both laser-annealed and 600°C vacuum-annealed polysilicon deposited onto magnetic garnets coated with SiO_2 and Si_3N_4.

Fabrication of silicon-on-garnet magnetodiodes is straightforward from a structural point of view; the substrates used in this work were (111) GGG, and each substrate had a single bubble film on it. A double-layer spacer, consisting of SiO_2 and Si_3N_4, was used to isolate the silicon device layer from the bubble film. Low pressure chemical vapor deposition was used to deposit these materials with laser recrystallization being employed to increase the grain size of the silicon device layer. The oxide and nitride layers can also be deposited by sputtering and plasma enhanced CVD -- the advantage with these processes is that process induced decomposition (which is observed to some degree or another during the oxide, nitride, and polysilicon depositions) is not a major issue. It is further noted that sputtering appears to be the better of the two processes since results with SiO_2 films show that oxide layers deposited by plasma enhanced CVD require high temperature densification while sputter deposited ones do not. Use of undensified plasma Si_3N_4 spacers caused major adhesion problems in silicon-on-garnet structures: the nitride and silicon layers flaked and peeled off in the processing that followed the laser recrystallization. Use of undensified plasma SiO_2 layers is not possible since post-recrystallized silicon films contain an unacceptably high density of holes. Process induced cracking of the oxide, nitride, and silicon layers has also been seen after laser recrystallization, and it appears that the magnitude of this problem can be minimized in a well controlled process.

Cross sectional TEM work revealed that the laser recrystallization of the silicon device layer damaged the topmost 0.09 to 0.16 μm of the magnetic bubble film. This layer was found to be polycrystalline and is believed to be nonmagnetic in its macroscopic properties. The thickness of the damaged bubble layer should be reduced by increasing the spacer layer thicknesses.

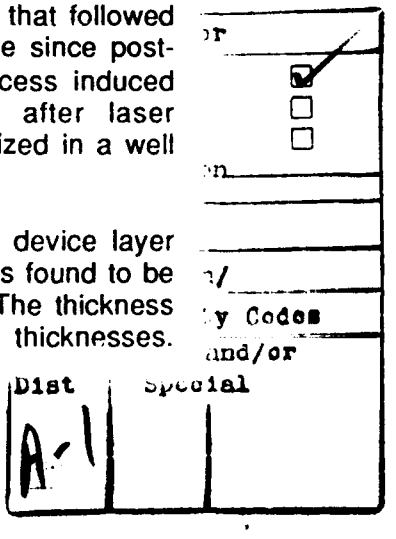

Decreased sensor performance (due to increased sensor/domain separation) could then be offset by using silicon-on-garnet MOSFETs to amplify the reduced magnetodiode output signals.

Silicon-on-garnet fabrication processes with high temperature process steps have been found to alter the room temperature magnetic properties of bubble films. Films containing the Al diluent are much more sensitive to process induced changes in magnetization than are films containing only the Ga diluent, presumably because less energy is required to transfer the smaller Al ion between sublattice sites. The process steps which most strongly affected film properties were the LPCVD depositions, the laser recrystallization, and the 850°C gate oxidation. In fact, it was shown that loss of oxygen from the bubble film during the LPCVD SiO_2 spacer deposition caused major bubble film coercivity increases along with decreased domain wall mobilities. Our work with ion-implanted contiguous-disk propagation patterns has shown that domain propagation in material with such properties is highly unlikely.

Low temperature fabrication processes were found to be considerably less harsh on magnetic bubble films, and it appears that loss of oxygen from the bubble film is not a major problem in the process we developed. Coercivity increases for this process are small. Moreover, it is found that changes to perpendicular anisotropy are not significant; changes to magnetization and the characteristic length are, however, but it is important to note that these changes can be mitigated by selecting the appropriate starting material.

Working magnetodiodes have been fabricated on silicon and magnetic bubble substrates coated with SiO_2 and Si_3N_4. These devices are important because the current and/or voltage of this type of device can be modulated by an in-plane magnetic field. The magnetic field sensitivity is greatest when the device is biased in the low-current positive resistance region; at larger currents, the sensitivity is found to fall off due to charge trapping effects that are associated with the nitride and/or gate oxide layers. Charge trapping effects are more pronounced for magnetodiodes fabricated on bubble substrates, and the difference can be explained by a variation in the degree to which the oxide and nitride layers are contaminated with bubble film ions.

Differential-magnetodiode bubble domain sensors have been shown to have outputs in the 2.2 to 9.1 mV range with two micrometer bubbles. Addition of on-chip silicon-on-garnet MOSFET based amplifiers is expected to lead to improved sensitivities and highly versatile computing structures.

MOSFETs have been fabricated on silicon and magnetic bubble substrates with three different processes. The first used a sputtered SiO_2 layer to isolate the silicon device layer from the substrate, and it was found that this isolation was very poor for the bubble substrate. Improved isolation was achieved in the second process which used a $SiO_2 + Si_3N_4$ spacer system -- gate oxide breakdown did not occur until oxide fields exceeded 3.8×10^7 V/m. Electron mobilities for devices fabricated on this double layer spacer were typically in the 100 to 200 cm^2/V-sec range. The best isolation, however, was achieved with a low temperature silicon-on-garnet fabrication process: process temperatures for this third technology did not exceed 600°C, and we note that gate oxide breakdown fields exceeded 2×10^8 V/cm.

4. Growth of Garnets by Sputtering and Pyrolysis

Although liquid phase epitaxy produces high quality garnet thin films, it would be desirable to have alternative growth techniques which are less costly, require lower temperatures and can be used with substrates other than single crystal garnets. Accordingly, a study has been carried out to evaluate the feasibility of depositing garnets by rf magnetron sputtering and by pyrolysis (thermal decomposition of spin coated oxides). It was shown possible to produce garnet thin

films using these techniques on a variety of substrates. On amorphous substrates, the films are polycrystalline, but nevertheless have desirable properties. These films require lower processing temperatures (670°C versus ~900°C for liquid phase epitaxy) and allow easy ionic substitution. The chemical composition has a large influence on magnetic properties such as compensation temperature and Curie temperature, and, through these, controls other material parameters such as coercivity. For sputter deposited films, it was shown that the composition can be finely adjusted by the sputtering parameters. It was also shown to be important to keep resputtering from the growing film to a minimum to achieve a high bismuth content, which is desirable in magneto-optic devices.

The properties of polycrystalline films grown by sputtering or thermal decomposition of spin coated oxides were found to be strongly influenced by the microstructure of the films. To achieve uniform properties, it was found to be desirable to have an extremely fine grain size. Accordingly, extensive studies were done of the crystallization processes in these materials. A simple and rapid technique for characterizing the grain size and distribution in these films was developed. In-situ annealing studies in a transmission electron microscope showed that the grain size is determined by the initial nucleation density of the garnet phases and, therefore, to decrease the grain size, it is necessary to increase the nucleation density. It was also found that the large bismuth ion readily segregates to spherical regions distributed throughout the film in the as-deposited state, and that, as the film is heated, the bismuth transforms into β-Bi_2O_3.

5. Growth of Hexaferrite Thin Films

A study of the feasibility of growing high quality thin films of hexaferrites was also carried out. Hexaferrite materials are used extensively in microwave and millimeter-wave devices today, and are also of potential interest for magnetic and magneto-optical recording technology. All devices made today utilize bulk hexaferrite materials; however, thin film hexaferrites, if available, would substantially reduce cost, enhance performance and make possible new applications.

The methods of deposition studied here included magnetron sputtering and liquid phase epitaxy. The sputter deposited films exhibited good c-axis texture, magnetization within 10% of bulk single crystal hexaferrite and uniaxial perpendicular anisotropy within about 50% of bulk value. To achieve these properties it was found to be extremely important to control the sputtering parameters during deposition of the films. Generally, it was found that low sputtering power and low argon pressure resulted in better c-axis orientation, higher magnetization and larger perpendicular anisotropy. In addition, target composition is critical. It was found necessary to have a slight excess of barium in the target to achieve near-stoichiometry in the film. Additional refinements in target composition and in-situ annealing of the films during deposition are expected to yield films with magnetic properties even closer to those of bulk hexaferrites.

Attempts to grow high quality hexaferrite films by liquid phase epitaxy onto sputter-deposited hexaferrite films on sapphire were much less successful. Typically, other phases were present in the LPE films; high, uncontrolled growth rates resulted; and films were very nonuniform due to problems with flux adhesion. R.F. magnetron sputter deposition appears to be much more promising as a growth technique for thin hexaferrite films.

6. Detailed Reports by Thrust

Attached to this summary are four detailed reports entitled:

(1) YIG-(BiLu)IG Heterostructures for Microwave and Optical Signal Processing

Devices

(2) Bismuth-Doped Lutetium Iron Garnet Thin Films for the MSW-Optical Mode Interaction

(3) Polycrystalline Iron Garnet Thin Films

(4) Magnetic Hexaferrite Films

The first two describe work related to the liquid phase epitaxial growth of garnet heterostructures. The third describes the work on fabricating high quality garnet thin films by sputtering and pyrolysis. The fourth describes the work on deposition of hexaferrite thin films. A detailed report on the silicon-on-garnet technology was previously published as the Ph.D. dissertation of P. H. L. Rasky and submitted as part of the second Annual Technical Report of Grant AFOSR-89-0097 for the time period Nov. 1, 1989-Oct. 31, 1990. Accordingly, it is not repeated here.

7. Publications

W. Eppler and M.H. Kryder, "The Effects of the Sputtering Conditions on Bismuth Doped Gadolinium Iron Garnet Films," *IEEE Trans. Magnet.*, MAG-25, 3743 (1989).

M. Ramesh, D.M. Gaultieri, S.D. Silliman, J. Peruyero and D.D. Stancil, "Effect of Sodium Doping of Rare-Earth Iron Garnet Films on Magnetic and Magneto-Optic Properties," *J. Appl. Phys.*, 70, 6289-6291 (1991).

William Wang and Mark H. Kryder, "Sputter Deposition of Hexaferrite Thin Films," submitted to *J. Appl. Phys.*

S.D. Silliman, D.M. Gaultieri and D.D. Stancil, "Improvement of FMR Linewidth in Bi-substituted Lutetium Iron Garnet Thin Films for the MSW-Optical Mode Interaction," to be submitted to *J. Appl. Phys.*

W. Eppler, D.J. Rogers, D.E. Laughlin and M.H. Kryder, "Microstructural Investigations of Bi Doped Fe Garnet Thin Films for Magneto-Optical Recording," submitted to Magnetism and Magnetic Materials Conf., Houston, TX, Dec. 1992, to be published in *J. Appl. Phys.*

8. Professional Personnel Associated with the Research Effort

M.H. Kryder, Professor of Electrical and Computer Engineering

D.D. Stancil, Professor of Electrical and Computer Engineering

D.E. Laughlin, Professor of Materials Science and Engineering

M. Ramesh, Research Engineer

D.J. Rogers, Postdoctoral Research Associate

A. Zeltser, Postdoctoral Research Associate

W. Eppler, Ph.D. Candidate

J.M. Peruyero, Graduate Student, M.S. completed (Course Option) August 1990

P.H.L. Rasky, Graduate Student, Ph.D. completed May 1990
Thesis Title: "Characterization of Silicon and Silicon-on-Garnet Devices with Applications to the Detection of Magnetic Bubble Domains in an Ion-Implanted Contiguous Disk Memory"

S.D. Silliman, Graduate Student, M.S. completed May 1992
M.S. Project Title: "Bismuth-Doped Lutetium Iron Garnet Thin Films for the MSW-Optical Mode Interaction"

X. Sui, Ph.D. Candidate

W. Wang, Graduate Student, M.S. completed May 1990
M.S. Project Title: "Sputter Deposition of Hexaferrite Thin Films for Magnetic and Microwave Applications"

9. Presentations

D.D. Stancil, "Optical Interactions with Magnetostatic Waves and Applications," Invited paper presented at the IEEE 1990 Ultrasonics Symp., Dec. 4-7, 1990.

M. Ramesh, J. Peruyero, D. Gualtieri, D. Stancil and S. Silliman, "Effect of Na on the Microwave and Optical Properties of (Bi-Lu)IG and YIG," presented at the 5th Joint MMM-Intermag Conf., Pittsburgh, PA, June 18-21, 1991.

S.D. Silliman, D.M. Gualtieri and D.D. Stancil, "Improvement of FMR Linewidth in Bi-Substituted Lutetium Iron Garnet Thin Films for the MSW-Optical Mode Interaction," submitted to 37th Annual MMM Conf. to be held in Houston, TX, Dec. 104, 1992.

D.D. Stancil, "Integrated Magneto-Optical Devices," Fall 1990 Colloquium Series, Electrical Engineering and Computer Science Department, George Washington University, Nov. 28, 1990.

W.E. Eppler, D.J. Rogers, D.E. Laughlin and M.H. Kryder, "Microstructural Investigations of Bi Doped Fe Garnet Thin Films for Magneto-Optical Recording," submitted to Magnetism and Magnetic Materials Conf., Houston, TX, Dec. 1992.

10. Consultations

Dr. Salvador Talisa, Dr. Kee-Chang Yu and Dr. Mike Daniel, Westinghouse Science and Technology Center. We met several times during the program to discuss research on MSW-optical materials and devices and have exchanged samples. They have also allowed us to make measurements in their laboratory and have lent equipment to us. Their work is supported in part by the Naval Research Laboratory.

Prof. John Kramer from the University of Delaware visited our laboratory on November 8, 1990 to discuss MSW-optical materials and devices. He is also supported by the Naval Research Laboratory.

Dr. Arthur Fisher, Dr. John Lee and Mr. John Butler, Naval Research Laboratory. Dr. Fisher and Mr. Butler visited CMU in Oct. 1989, and there have been numerous telephone and electronic mail communications with this group since that time. They are active in MSW-optical device research and have supported the above two groups.

Prof. Y. Ikamura, Osaka University, visited CMU on Nov. 7, 1990 and presented a seminar on integrated optics research at Osaka University. They are active in developing integrated optical devices using garnet thin films.

Dr. Devlin Gualtieri, Allied-Signal. We have worked closely with Dr. Gualtieri on the growth of Bi-YIG films. Dr. Gualtieri was instrumental in getting Allied-Signal to donate a Varian EPR Spectrometer to us which we used extensively to evaluate films grown under this program. He also grew a number of experimental films for us and was a significant contributor to two of our publications.

Dr. William Ross, Litton Data Systems, and Dr. Roger Belt, Airtron. D. Lambeth and D. Stancil are presently being supported by Litton Data Systems to do research on a new magneto-optical spatial light modulator for optical signal processing. This work involves processing of Bi-substituted garnets that have much in common with the MSW-optical work. Dr. Belt is also interested in materials for MSW-optical interactions. Both Dr. Ross and Dr. Belt have visited CMU several times during the program.

Dr. Hitoshi Tamada, Sony Corporation Corporate Research Labs. Dr. Tamada visited CMU briefly on Nov. 7, 1990 to discuss MSW-optical device interactions. Dr. Tamada has done some of the leading work on developing (Bi,Lu)IG films.

Prof. Chen Tsai, University of California-Irvine. Prof. Stancil visited Prof. Tsai on Nov. 2, 1990 to discuss MSW-optical devices. Prof. Tsai has done considerable work on the transverse interaction for spectrum analysis and beam deflection.

Dr. Philip Gerard of the Division d'Electronique de Technologie et d'Instramentation (LETI) in France on Nov. 8, 1990 to discuss hexaferrite thin film growth. Dr. Gerard has been involved in the epitaxial growth of thin film hexaferrites of LETI.

Dr. D.E. Grey, Dr. I.S. Jacobs and Dr. F.E. Luborsky of General Electric Corporate Research and Development have worked with us extensively on the growth of garnets and hexaferrites.

YIG-(Bi,Lu)IG Heterostructures for Microwave and Optical Signal Processing Devices

J.M. Peruyero
S.D. Silliman
D.D. Stancil

August 1990

YIG-(Bi,Lu)IG Heterostructures for Microwave and Optical Signal Processing Devices

1. Background

Heterostructures involving magnetic garnet films have a promising future for use in a new class of microwave and optical signal processing devices. [1] In particular, microwave magnetostatic waves interacting with optical guided modes can be used to realize device functions such as microwave and/or optical spectrum analysis, optical frequency shifting, and optical beam deflection.

To enhance the efficiency of the interaction while maintaining desirable microwave and optical properties, we are attempting to grow a multiple layer heterostructure. The first layer is a thin film of yttrium iron garnet (YIG) grown on a gadolinium gallium garnet (GGG) substrate. This is followed by an epitaxial layer of GGG and then an overlayer of bismuth-lutetium iron garnet. In this structure, the YIG layer is optimized for MSW propagation, while the (Bi,Lu)IG overlayer is optimized for optical mode propagation.

In this report, we discuss the growth and characterization of YIG films grown from a lead oxide melt, and (Bi,Lu)IG films grown from a bismuth oxide melt. We also provide a preliminary report of our success in growing a multilayer film.

2. Device Structure

The proposed multilayer device is shown in Figure 1. Layer 4 is the substrate layer which is composed of Gadolinium Gallium Garnet (GGG). The purpose of this layer is to provide a surface to use as a substrate for the epitaxial growth of a garnet layer. Layer 3 is a layer of YIG. This layer acts as the medium to support the propagation of magnetostatic forward volume waves (MSFVW). Layer 2 is a spacer layer whose purpose is to optically isolate layers 3 and 1. This layer will be composed of GGG. Finally, layer 1 will be a layer of $(BiLu)_3Fe_5O_{12}$. This layer will act as an optical waveguide. This device structure will be grown by liquid phase epitaxy (LPE).

There are several advantages of the multilayer structure over the single layer device structure. Most importantly, the use of only a single layered device places many material constraints on the layer. For instance, low FMR linewidth, high Faraday rotation, and low optical absorption are desirable properties in order for MSW-optical interactions to occur. Bi substituted YIG has been considered for this application since its Faraday rotation is approximately ten times that of pure YIG.[2] Since the layer must act simultaneously as a single mode optical waveguide and a MSW guide this places contradicting requirements on the single layer. In order to optimize it as a single mode optical waveguide the layer needs to be thin, whereas for a MSW guide thicker layers would be preferable. The multilayer device structure overcomes this problem by separately optimizing the desirable MSW properties in layer 3 and the optical properties in layer 1. Layer 3 will be composed of low FMR linewidth YIG which will allow for the propagation of MSFVW along the length of the device. Layer 1 will be the optical waveguide and will be composed of $(BiLu)_3Fe_5O_{12}$. The multilayer device structure eliminates the necessity of constructing a single layer that is optimized to simultaneously propagate MSW's and optical modes.

3. YIG Films

We have developed the capability to grow low FMR linewidth thin films of YIG whose thicknesses ranged anywhere from 6 μm to ~30 μm. Some of the films grown were able to propagate MSFVW. An example of a typical passband for a film is shown in Figure 2. This passband was taken on a film which was approximately 30 mm thick. The performance is satisfactory for layer 3 of the multilayer device.

4. $(BiLu)_3Fe_5O_{12}$ Films

4.1 Film Growth

We have also developed the capability to grow $(BiLu)_3Fe_5O_{12}$. We have been using the following melt composition:[3]

$$R_1=Fe_2O_3/Lu_2O_3=7.53$$

$$R_4=(Lu_2O_3+Fe_2O_3)/(Lu_2O_3+Fe_2O_3)3+Bi_2O_3)=17\% \text{ or } 18\%$$

$$R_6=MgO/(2Fe_2O_3+MgO)+0\%-3\%$$

This flux is employed because it doesn't contain PbO which can cause the incorporation of Pb in the film. This is undesirable because it increases both the FMR linewidth and the optical absorption.[3] As discussed in sections 4.2 and 4.3, we have had much success in growing $(BiLu)_3Fe_5O_{12}$ with low FMR linewidths and high Bi substitution.

However, we had problems with melt viscosity with these films. After the film growth, when the substrate is withdrawn from the melt, excess flux droplets tend to adhere to the surface (causing continued film growth under the droplets) instead of running off the film. This resulted in films with poor surface morphology.

This problem is usually corrected by adding appropriate amounts of additives to the melt to reduce the melt viscosity.[4,5] In our case, the additive we chose was sodium carbonate ($NaCO_3$). A series of films was grown after the melt was thus modified. The films were found to be cleaner, with smaller amounts of flux adhering to the film after growth. Additionally, it was found that the addition of $NaCO_3$ lowered the melt liquidus temperature significantly. After the addition of about 29 gms of $NaCO_3$ to the melt, films were grown typically at about 760 degrees C instead of the earlier growth temperatures of about 840 degrees C to achieve similar film composition. While characterizing these latter Bi-Lu films, it was observed that the addition of $NaCO_3$ also affected some magnetic properties of the film. This can be attributed to trace amounts of sodium ions being incorporated into the film. This is discussed further in a later section. Thus it is necessary to determine the appropriate amount of additives like $NaCO_3$ that would enhance the quality of the films, without adversely affecting their magnetic properties.

A melt is being developed to determine the appropriate amount of $NaCO_3$. Several films have been grown using this melt and are being studied as a function of the amount of additives present in the melt.

We have also successfully grown a two-layered film. A previously grown YIG film on a GGG substrate was used as a seed crystal for the growth of a Bi-Lu layer. The

characteristics of this multilayered film clearly indicated an excellent hetero-epitaxy between the layers.

4.2 Compositional and Structural Characterization

The garnet films were characterized by various standard (typically non-destructive) techniques such as the x-ray fluorescence spectrometer to analyze the chemical composition. The amount of bismuth in the film is a crucial parameter and could be accurately measured by this technique. It was found that the films had a nominal composition of $Bi_xLu_{3-x}Fe_5O_{12}$ where x, the amount of bismuth, ranged from about 0.4 to about 1.1 for our films. The value of x depends almost linearly on the amount of supercooling. To achieve larger values of x, the melt had to be cooled significantly below the liquidus temperature and this sometimes resulted in melt nucleation, a condition undesirable to produce good quality films. Thus there is a practical upper limit on the value of x for our films at around 1.1. Sodium ions, being too small in size, were not detected by this x-ray technique and thus their incorporation into the film could not be quantified directly. Indirect methods do exist to determine the presence of sodium ions and will be discussed later.

The lattice constants of the films were determined by x-ray diffraction. A plot of the experimentally measured lattice constants vs. the bismuth content is shown in Figure 3. The almost linear dependence is to be expected from the simple weighted average law. The theoretically predicted values are shown as a solid line and agree well with the experimental values. It is seen that the perfect lattice match between the film and GGG occurs for values of x around 0.9 and any excursion from this composition would result in stresses in the film. In fact, some lutetium rich films (x around 0.4) were under tremendous compressive stress and developed cracks and even broke. a good lattice match is also necessary to grow thicker films without cracking. Also, the lattice mismatch data is useful in evaluating the stress in the film and thus the stress-induced anisotropy.

The thickness of these films was measured by several techniques such as interferometry, x-ray fluorescence (x-ray attenuation) and by direct observation of the film cross section under an optical or electron microscope. All these measurements provided self-consistent values within the experimental errors. The thickness of the film is directly related to the amount of supercooling and the rotation rate of the substrate while in the melt.

4.3 Ferromagnetic Resonance

Figure 4 shows the FMR linewidth vs. growth temperature for the $(BiLu)_3Fe_5O_{12}$ films we grew prior to adding $NaCO_3$. It is evident that we have been able to grow films with linewidths which are significantly less than 1 Oe. In fact, the lowest linewidths we have attained are approximately 0.6 Oe. In addition, we have also been able to substitute significant amounts of Bi into the dodecahedral site of the garnet. Figure 5 shows Bi substitution vs. growth temperature for the same set of films. We have been able to grow films with x=0.9 that also have linewidths that are less than 1 Oe.

In addition to the cavity system used to make linewidth measurements, we have a specially designed micro-strip line, variable frequency, ferromagnetic resonance (FMR) spectrometer in our facility. The entire wafer can be placed in the micro-strip sample holder and studied extensively at various frequency-field configurations. Most of the films grown yielded clean FMR signals without much associated fine structure or

auxiliary signals due to inhomogeneities, indicating that the films are of very good quality. The FMR spectra from this system are used to determine the anisotropy fields of the films only. The experimental values of H_K are plotted in Figure 6 as a function of the bismuth content. The data points are split into two groups, one before the addition of $NaCO_3$ and the other after. It is clearly seen that the addition of $NaCO_3$ lowers the anisotropy fields substantially. The anisotropy energy in garnet films in general has two sources - the stress-induced anisotropy due to lattice mismatch and growth-induced anisotropy due to the non-random distribution of ions at various crystal sites. While stress-induced anisotropy can be calculated from lattice mismatch and magnetostriction values, a concise theory of growth-induced anisotropy does not exist at present, especially for bismuth based films. However, earlier work on magnetic bubbles has indicated that for (Bi,Lu)IG, growth-induced anisotropy is small compared to that typically induced by stress. This is also seen in Figure 6. In this figure, the theoretical stress-induced anisotropy is plotted (as a solid line) against the measured total anisotropy field. There is a substantial overlap between the theory and the experiment in films grown before $NaCO_3$ addition, indicating that the anisotropy is almost entirely due to stress. for films grown after the addition of $NaCO_3$, there is a substantial difference between the theoretical stress-induced anisotropy values and the experimental total anisotropy values, indicating the presence of a large growth-induced component, due to the incorporation of sodium ions in the film. The nonlinear behavior of the theoretical curve results from the fact that the magnetostriction coefficients for Bi-IG and Lu-IG have opposite signs. The linear behavior of the data at small x values is not in agreement with the calculation. This discrepancy is not yet understood.

Further evidence of this substantial, negative, growth-induced anisotropy in sodium-substituted films can be obtained by doing careful post-growth annealing. Two films from each group (sodium-substituted and sodium-free) were annealed at 1040 degrees C for 90 minutes and their FMR spectra were taken again. Annealing at such high temperatures should in principle randomize the ion distribution in the film lattice and thus effectively destroy any growth-induced anisotropy component. The anisotropy values before and after are plotted in Figure 7 for these four samples and it can be seen that there is very little change due to annealing in sodium-free films (thus pointing to negligible growth-induced anisotropy) whereas there is a substantial change in the films with sodium, indicating the presence of a large growth-induced anisotropy in these as-grown films. This also suggests that the effects of adding $NaCO_3$, such as lowering the anisotropy fields, can be annealed out in a controlled post-growth annealing cycle. Further studies are necessary to determine the optimum annealing schedule.

The presence of Na may also affect the microwave and optical attenuation. Future measurements are planned to examine this possibility.

The FMR spectrum of a two-layered film is shown in Figure 8. The two strong signals correspond to the two layers (YIG and (Bi,Lu)IG). The two weaker signals following the main signals correspond to the unwanted second harmonic frequency generated by the frequency source. This spectrum is reasonably clean, indicating the absence of any inhomogeneous intermediate layers and thus good heteroepitaxy between layers.

4.4 Magnetostatic Wave Excitation

In Section 4.3, we described FMR measurements showing line widths ΔH of significantly less than 1 Oe at 9 GHz in (Bi,Lu)IG films grown without sodium. Although such a low value of ΔH is necessary for good MSW propagation, this single parameter is not adequate to evaluate the films for MSW devices. For this reason, the transmission passbands

obtained from using the films in simple MSW delay lines were measured. Figure 9 shows the best passband obtained, and was measured by Dr. S. H. Talisa at Westinghouse Science and Technology Center in Pittsburgh. The strong absorption lines are caused by interactions between degenerate eigenmodes in the film. These undesirable features usually appear in films thinner than 10 mm, and become more pronounced as the growth rate is increased.[6] Reducing both the Na and Lu in the melt should permit slower growth rates and may minimize these notches.

4.5 Faraday Rotation

The strength of the MSW-optical interaction is determined primarily by the Faraday rotation effect. The Faraday rotation was measured using a magneto-optic loop tracer technique. This technique involves an incident wavelength in the infrared region of 1320 nm using a diode-pumped Nd:YAG laser, the desirable wavelength for magneto-optic devices. Referring to Figure 10, the laser light passes through a polarizer to achieve a single known polarization, then perpendicularly through the sample, where it undergoes the small rotation of polarization due to the Faraday effect. This light then passes through a Wollaston prism, which separates it into two perpendicular polarizations. Each polarization component is detected by a germanium photodetector. These two signals are input to a difference amplifier, the output of which is connected to an X-Y chart recorder with applied magnetic field on the abscissa. When the Faraday rotation angle ϕ_f is zero, the polarizations are aligned such that the intensities on both detectors are equal and the difference is zero. When the Faraday effect causes the polarization to change, the two components will differ, and the difference from the amplifier will be directly related to ϕ_f. The field is swept from negative saturation to positive saturation, and the output is read from the recorder.

The expected linear relationship between Bi content and Faraday effect is observed in Figure 11. At x=0.9, corresponding to the best lattice match, the Faraday rotation is about 0.12°/μm. This represents almost an order-of-magnitude improvement over pure YIG. These data have not been corrected for interference effects among the film layers.

5. Summary

We have demonstrated the ability to grow YIG, (Bi,Lu)IG, and a three-layer heterostructure consisting of GGG-YIG-(Bi,Lu)IG. The (Bi,Lu)IG films were grown with a bismuth oxide flux to prevent the increased optical and microwave losses associated with lead incorporation in conventional melts.

We have improved the surface morphology of the (Bi,Lu)IG films by the addition of $NaCO_3$ to reduce the viscosity of the melt. The presence of the sodium also caused a modest growth-induced anisotropy that can be removed by high-temperature annealing. The ability to control the anisotropy is desirable since the optical layer and the microwave layer of the heterostructure should have anisotropy fields differing by about 200 Oe. The presence of sodium may also affect the microwave and optical losses, however. For this reason, studies of the dependence of optical and microwave losses on Na content are planned.

6. References

1. Daniel D. Stancil, "Theoretical investigations for MSW optical interactions," Final Rep. on Contract N00173-88-M-X012, sponsored by the U.S. Naval Research Lab., Sept. 12, 1988, revised July, 1989.

2. P. Hansen, K. Witter, and W. Tolksdorf, "Magnetic and Magneto-Optic Properties of Lead- and Bismuth-Substituted Yttrium Iron Garnet Films," Phys. Rev., Vol. 27, June 1983.

3. H. Tamada, M. Kaneko, and T. Okamoto, "TM-TE Optical Mode Conversion Induced by a Transversely Propagating Magnetostatic Wave in a $(BiLu)_3Fe_5O_{12}$ Film," J. Appl. Phys., Vol. 64, Jan. 1988.

4. J.M. Robertson, "Improvement of Lead-Free Flux Systems for the Growth of Bismuth-Substituted Iron Garnet Films by Liquid Phase Epitaxy," J. Electrochem. Soc. **123** 1248 (1976).

5. J.E. Davies, "The surface tension of Bi_2O_3-based fluxes used for the growth of magnetic garnet films," J. Mat. Science Lett., **11** 976 (1976).

6. S.H. Talisa and J.D. Adam, "Bi:YIG Film Testing for MSW-Light Interaction Devices," Westinghouse Science and Technology Center Report.

7. Hitoshi Tamada, Masaki Saitoh, and Masahido Kaneko, "Improvements of optical and microwave properties of Bi-substituted magnetic garnets by O_3 annealing," J. Appl. Phys. **67** 949 (1990).

Figures

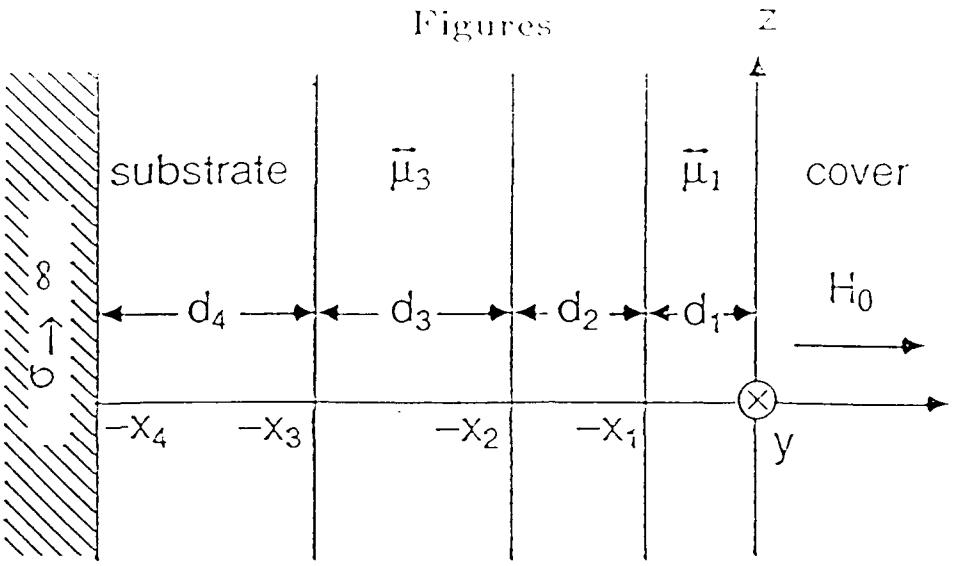

Multi-layer Structure

Figure 1

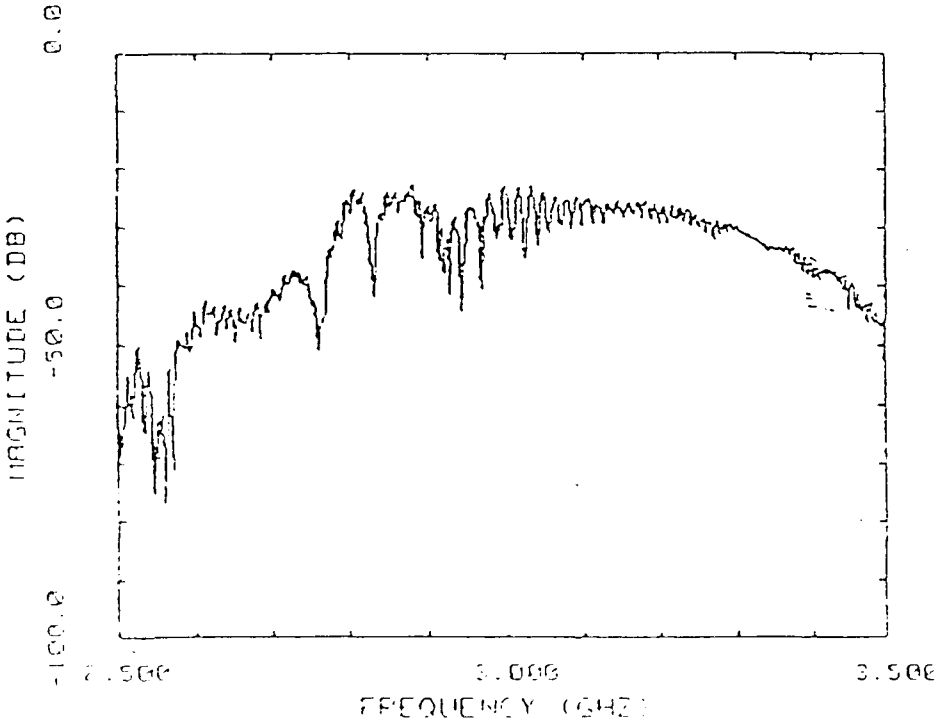

MSFVW Passband

Figure 2

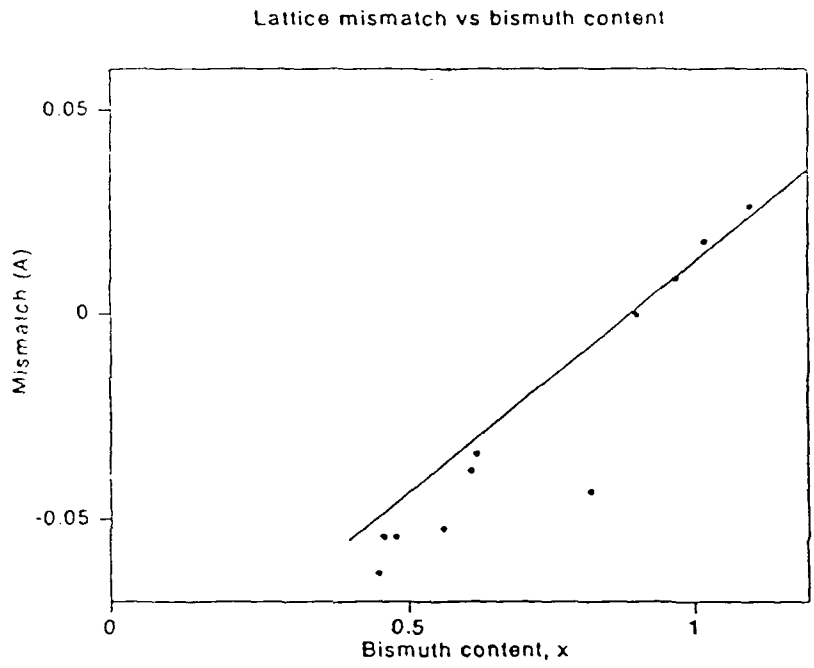

Figure 3. Lattice mismatch vs bismuth content. *Solid line is the theory.*

FMR linewidth vs. Temperature
$Bi_xLu_{3-x}Fe_5O_{12}$

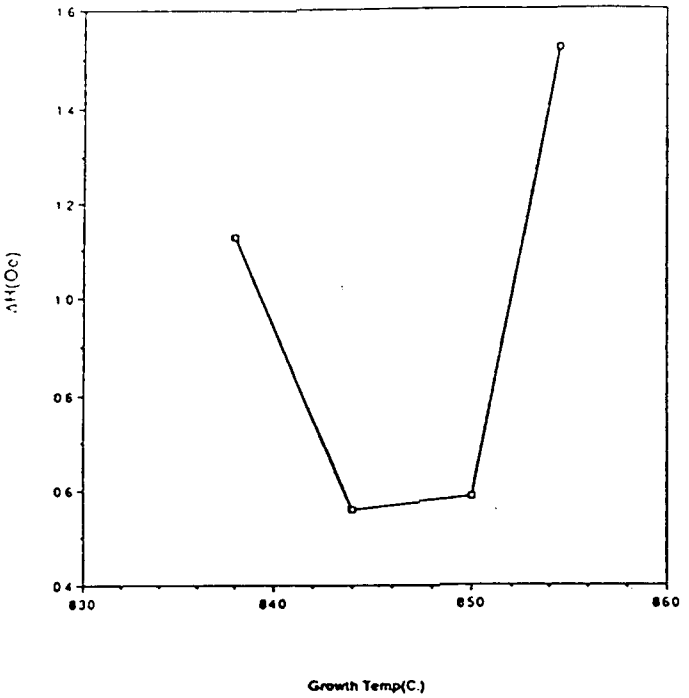

Figure 4

x vs. Temperature
$Bi_xLu_{3-x}Fe_5O_{12}$

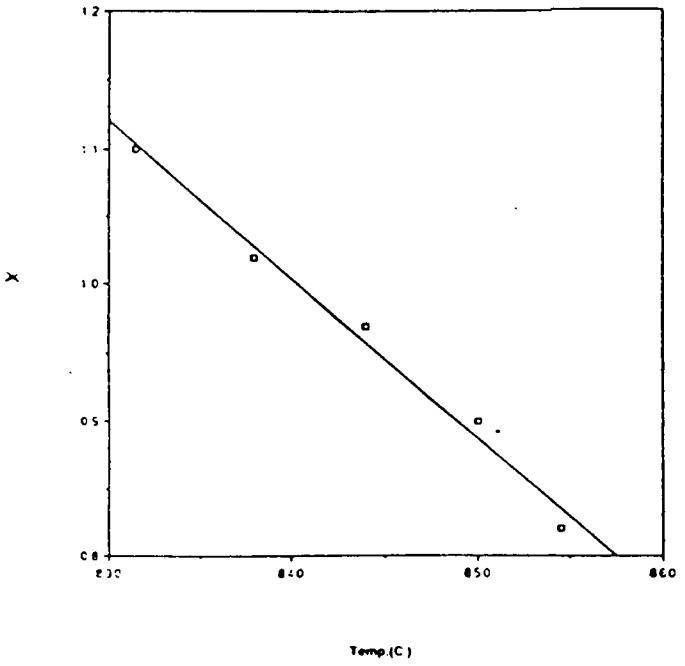

Figure 5

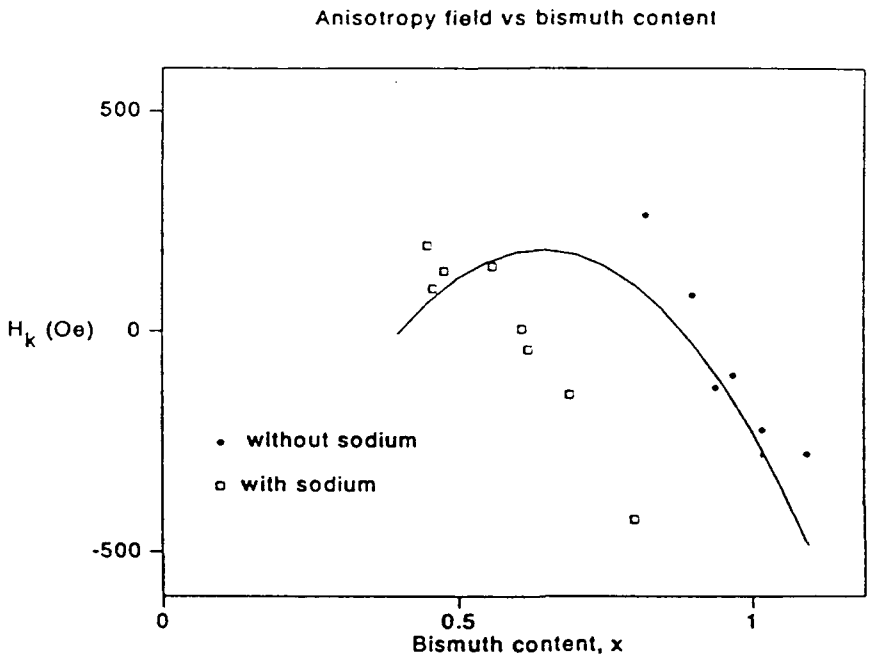

Figure 6. Anisotropy field vs bismuth content. Solid line is the theoretically calculated stress-induced anisotropy field values.

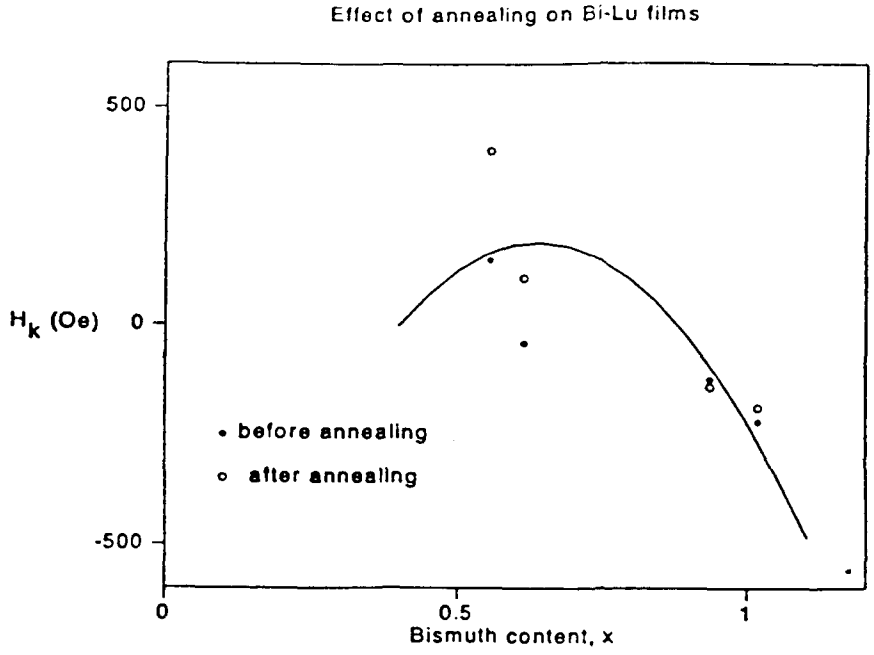

Figure 7. Effect of annealing on anisotropy. Solid line is the theoretically calculated stress-induced anisotropy field values. The four data points on the left correspond to films with sodium and the four data points on the right correspond to films without sodium.

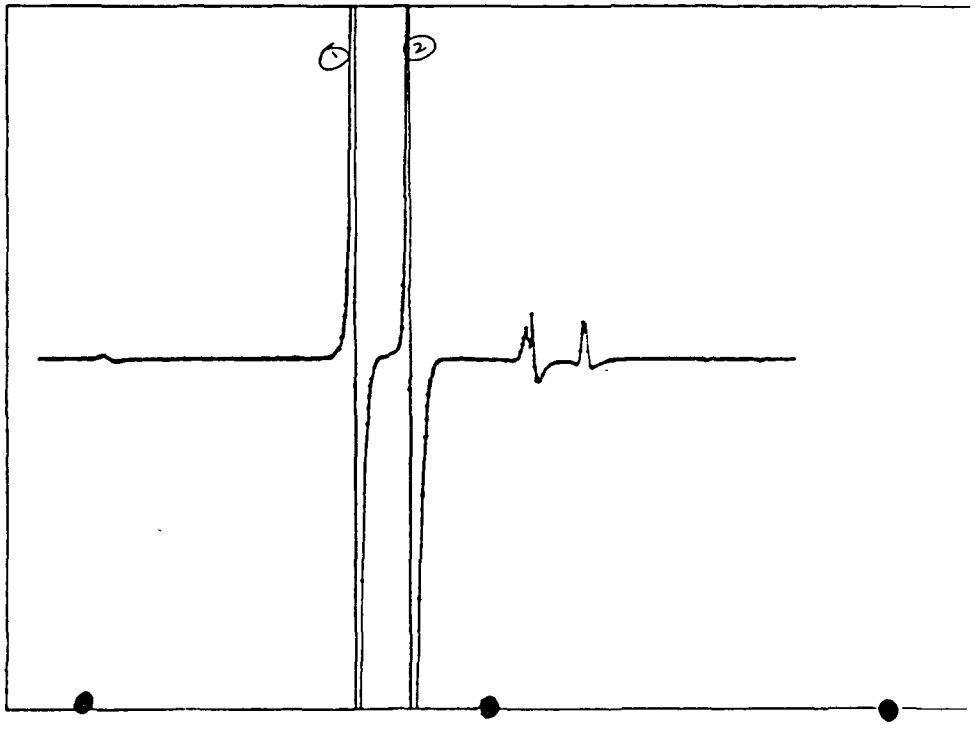

Figure 8. FMR signals from a double-layered film.

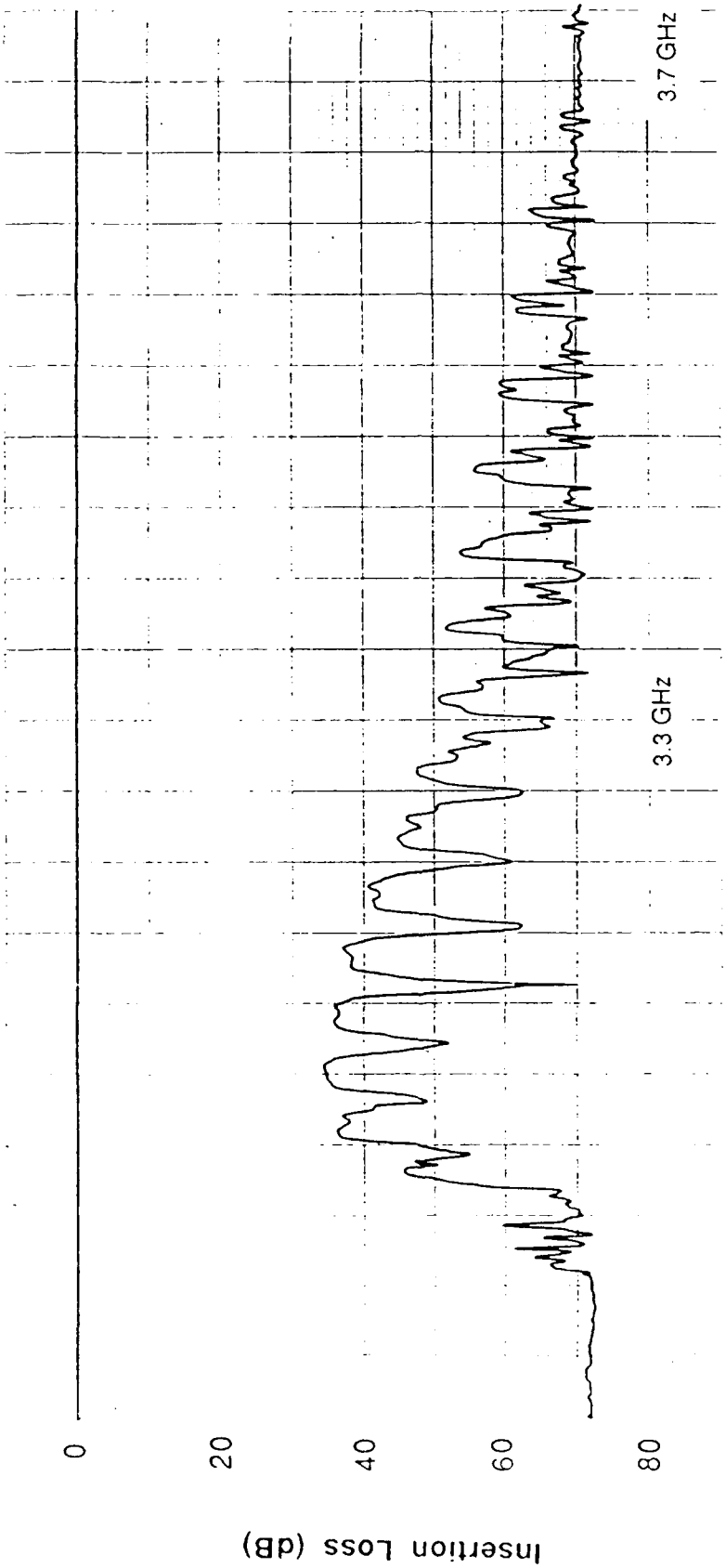

Figure 9. Magnetostatic forward volume wave transmission passband in (Bi,Lu)IG with x = 0.8 (measured by Dr. S. H. Talisa, Westinghouse Science and Technology Center).

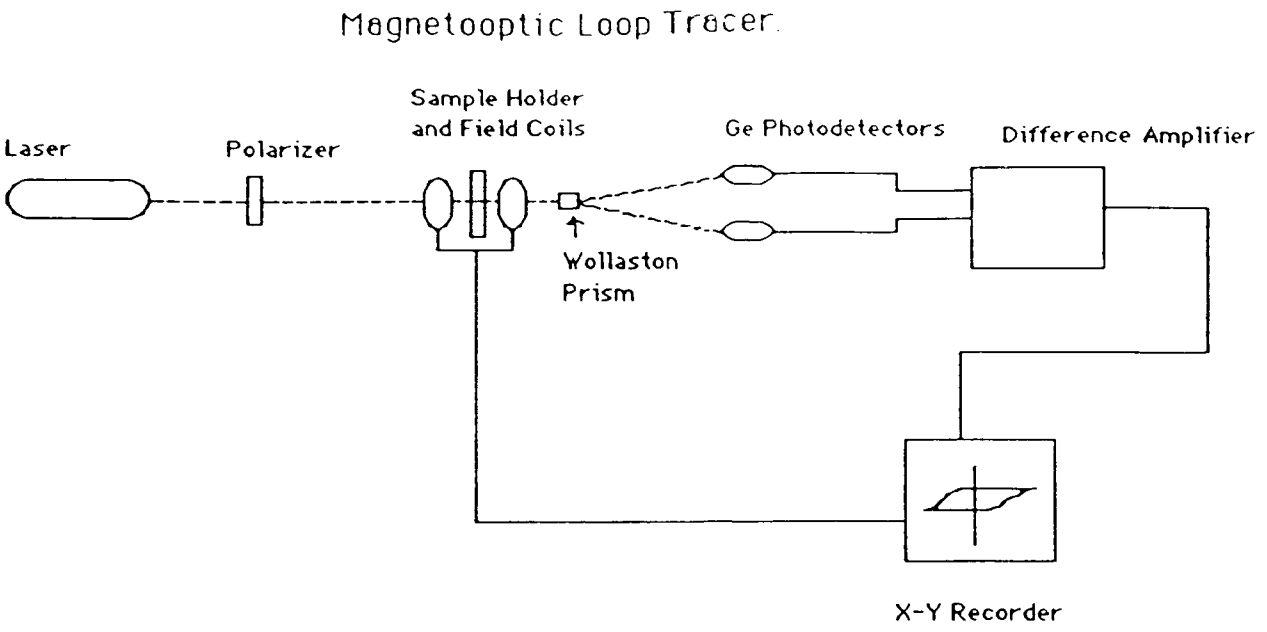

Figure 10. Diagram of magnetooptic loop tracer used to measure the Faraday rotation on (Bi,Lu)IG samples.

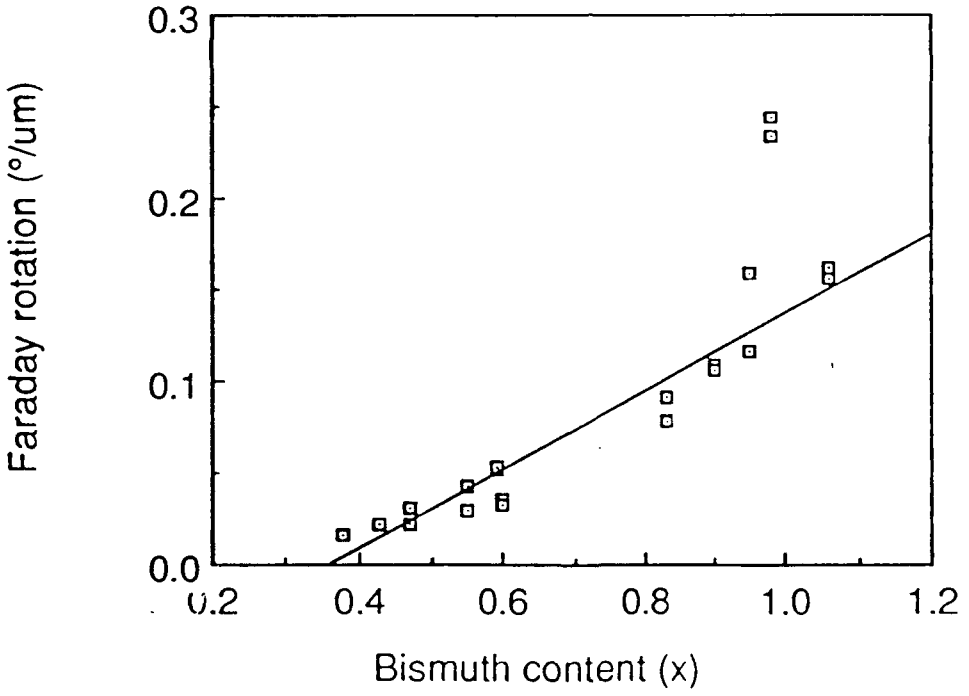

Figure 11. Faraday rotation measured at 1320 nm in (Bi,Lu)IG samples.

POLYCRYSTALLINE IRON GARNET THIN FILMS

Walter R. Eppler, *D. J. Rogers,
*D. E. Laughlin and Mark H. Kryder

Dept. of Electrical and Computer Engineering
*Dept. Metallurgical Engr. and Materials Science

ABSTRACT

The ferrimagnetic garnets are promising materials for a variety of integrated microwave, magneto-optic and optical guided wave devices. Sputtering and pyrolysis are two methods of depositing these materials in the polycrystalline form at temperatures significantly less than Liquid Phase Epitaxy on a variety of substrate materials. This report gives results on how the process parameters influence the bulk magnetic, microwave and magneto-optic properties. The incorporation of these materials in devices will depend on the ability to produce uniform finely grained films. We extensively investigated the crystallization of these films on glass substrates. We developed a simple and rapid method for analysis of the grain size and distribution and we have shown that the final microstructure is controlled by the initial nucleation density of the garnet phase.

Table of Contents

List of Figures

List of Tables

1 Introduction

Ferrites in both polycrystalline and single crystal form have been employed in microwave devices. Advantages of the polycrystalline form compared to the single crystal form are ease of ionic substitution to tailor the magnetic properties, the ability to make crystallographically isotropic materials and increased power handling capabilities[1]. Further miniaturization and integration with semiconductor devices require ferrites in the film (planar) form. Most work has centered around films grown by liquid phase epitaxy (LPE), a technique developed by researchers working on magnetic bubble memories, which produces high quality single crystal films. Many microwave and magneto-optic guided wave devices do not necessarily require the exceptional crystal quality of LPE grown films. Polycrystalline garnet films can be easily fabricated by simpler, less costly methods such as spin coating, sputtering, or spray coating. These methods not only have the inherent advantages of the polycrystalline form but also provide a wider choice of substrate materials, convenient chemical etchants and lower process temperatures. Control of the film microstructure (porosity, grain size, etc.) will be necessary to tailor their properties (line width, power handling capabilities, etc.). We studied the magnetic, microwave and magneto-optic properties of rf magnetron sputter deposited and thermally decomposed spin coated thin film iron garnets.

2 Sputtering

2.1 Film Preparation

Rf magnetron sputtering and ion beam sputter deposition were used to deposit films on Corning No. 7059 glass substrates. Sintered ceramic disks of composition $Gd_2Bi_1Fe_{4.6}Al_{0.2}Ga_{0.2}O_{12}$ (Target 1) (ion beam and rf) and $Gd_2Bi_{2.5}Fe_{3.5}Ga_{1.1}O_{12}$ (Target 2) (rf only) containing mostly the garnet phase were used as the targets. The deposition rate of rf magnetron sputtered films was 85 to 370 Å/min.. The deposition rate was 10 Å/min. for ion beam deposited films. The as-deposited films were amorphous and were crystallized by annealing at 670 $^{\circ}$C for four to five hours in an air atmosphere.

2.2 Rf Magnetron

Films were deposited varying one process parameter rf power, argon bleeding pressure, substrate bias voltage or oxygen partial pressure, while holding the other parameters constant. X-ray diffraction data indicates the annealed films are all randomly oriented single phase garnets (Fig. 1). The magneto-optic properties and coercivity were measured using a magneto-optic hysteresis loop tracer with a He-Ne laser ($\lambda = 633$ nm) as the light source. The films have room temperature coercivities greater than 1 kOe, Faraday rotations as large as 1.3 deg/μm and adjustable compensation and Curie temperatures.

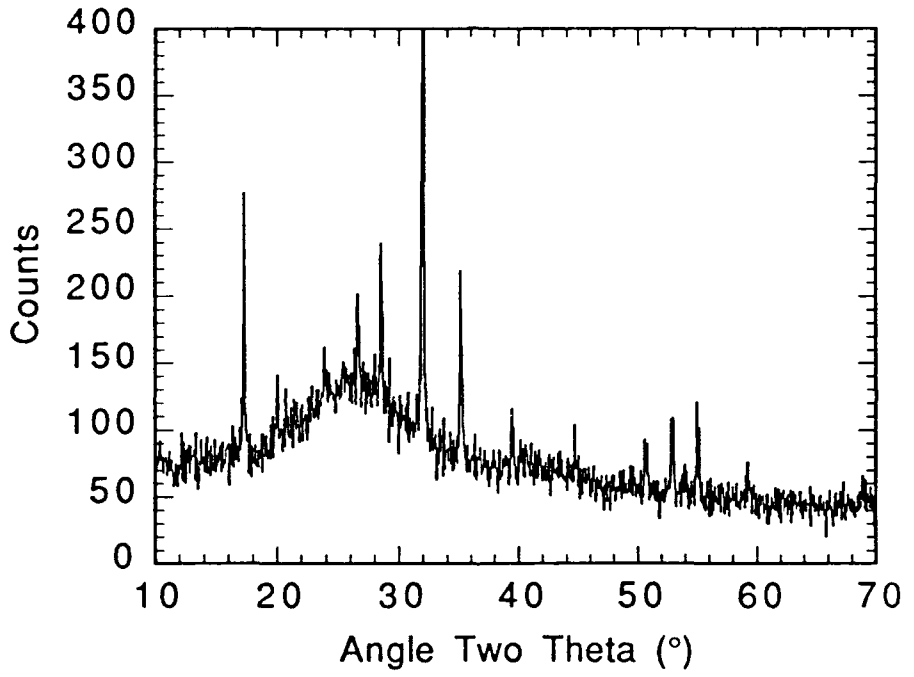

Figure 1: X-ray diffraction scan of 0.3 μm thick garnet film deposited at 5mTorr Argon Bleeding Pressure and 100 W rf power

2.2.1 Rf Power and Argon Bleeding Pressure

The coercivity as a function of temperature for films deposited from target 1 with different rf power is shown in Fig. 2. The compensation temperature of the film made at the lowest power (95 W) is approximately 10 °C and is increased to 80 °C at a power of 248 W. A similar change in the compensation temperature can be seen in the films deposited with different argon bleeding pressure (Fig. 3). The film made at 5 mTorr has a compensation temperature of approximately 0 °C while the film made at 25 mTorr has a compensation point of 45 °C.

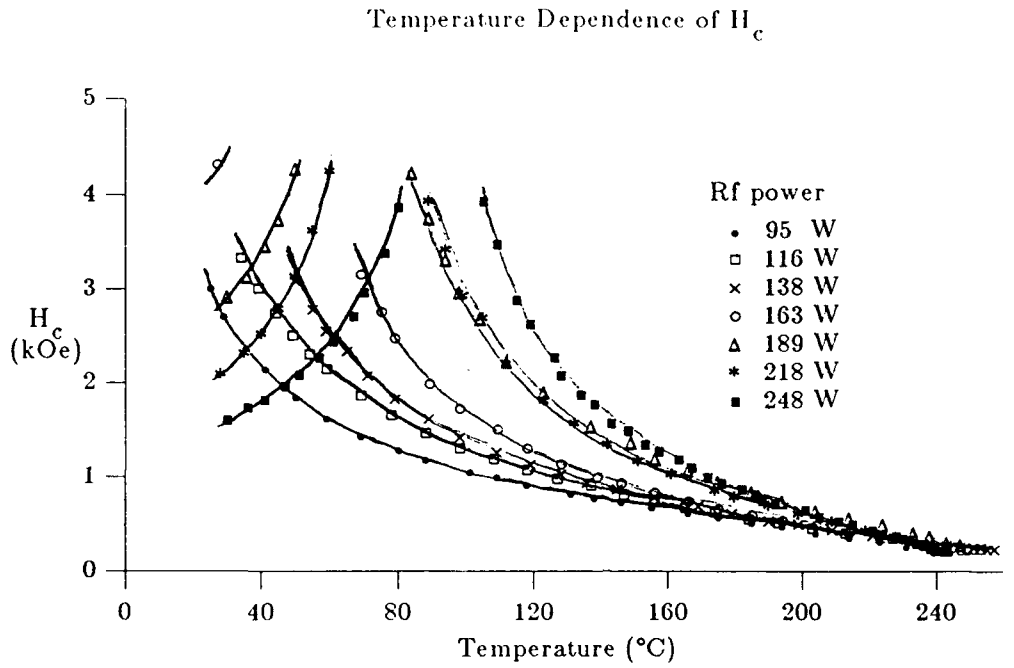

Figure 2: Plot of coercivity vs. temperature for films deposited at different rf powers and argon bleeding pressure of 10 mTorr

The composition of the series of films deposited at different rf powers was measured by x-ray fluorescence. The compositions of these films and the target are shown in Table 1. Oxygen's fluorescence yield is too low to be measured by x-ray fluorescence therefore the films were assumed to be completely oxidized with a cation to anion ratio of 8:12. The aluminum content could not be measured because the substrate, Corning 7059 glass, contains about 12% Al_2O_3. Since the sputtering yields of elemental aluminum and gallium are similar[2], and the atomic percentage of aluminum and gallium in the target is approximately the same, the aluminum content of the films was assumed to be the same as the gallium content. The value of $\frac{(Gd + Bi + Cu)}{(Fe + Ga + Al)}$ is less than that of the stoichiometric composition (i.e. 0.6). This suggests the existence of a second amorphous or micropolycrystalline phase undetected by x-ray diffraction consisting of the excess Fe, or that some of the dodecahedral sites of the garnet are vacant or occupied by some of the Fe.

Substitution of a diamagnetic or paramagnetic ion into the dodecahedral site ("c" site) will decrease the "c" sublattice magnetization lowering the compensation temperature. Mean field

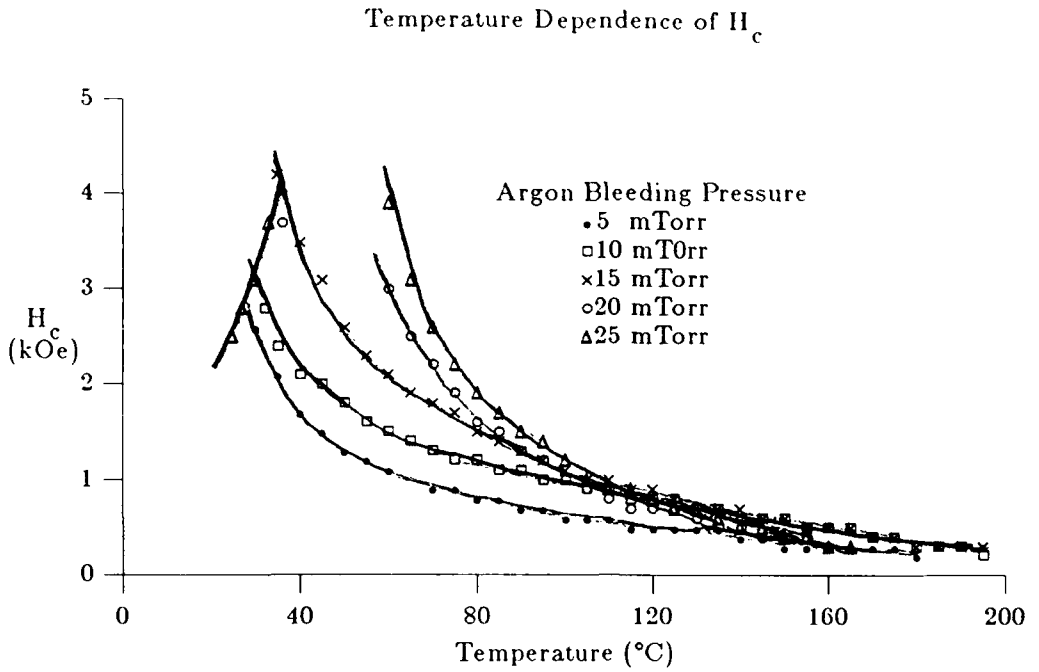

Figure 3: Plot of coercivity vs. temperature for films deposited at different argon bleeding pressures and 95 W rf power

Table 1: Composition of films deposited from Target 1

$(Gd_uBi_vCu_w)[Fe_xGa_yAl_z]O_{12}$							
	Gd (u)	Bi (v)	Cu (w)	Fe (x)	Ga (y)	Al (z)*	O**
Target	2.02	1.06	-	4.53	0.21	0.19	12
95 W	1.10	0.86	0.72	4.87	0.23	0.23	12
116 W	1.26	0.86	0.62	4.87	0.2	0.2	12
138 W	1.36	0.79	0.65	4.88	0.17	0.17	12
163 W	1.56	0.72	0.58	4.74	0.2	0.2	12
189 W	1.47	0.57	0.53	4.95	0.24	0.24	12
248 W	1.68	0.44	0.5	4.86	0.26	0.26	12

* Assumed to be the same as the gallium content

** Cation to anion ratio assumed to be 8 : 12

theory predicts for GdIG a decrease in T_{comp} of 124 °C/mole of substituent. The films contain significant amounts of copper (sputtered from the target backing plate) which will enter the dodecahedral site[3]. Thus both copper and bismuth will dilute the gadolinium lowering T_{comp}.

A plot of the measured compensation temperature versus the sum of the copper and bismuth content (Fig. 4) is a straight line with a slope of 153 °C/mole in reasonable agreement with mean field analysis.

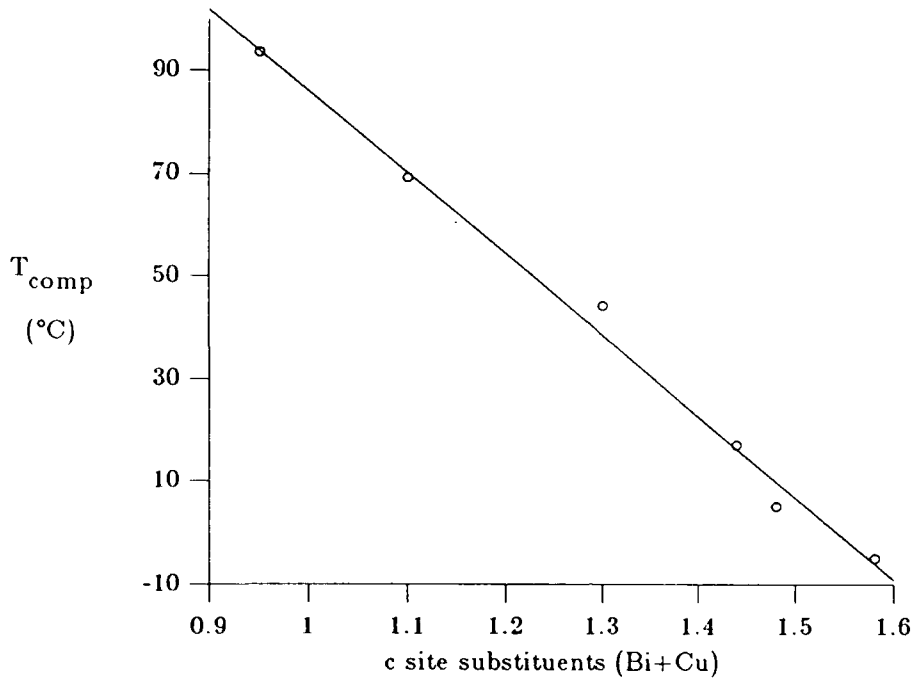

Figure 4: Decrease in T_{comp} with dodecahedral site substitution

The large size of the bismuth ion gives rise to an increase in the lattice constant of 0.05 Å/mole[4]. The lattice constant of the films, measured by x-ray diffraction, is plotted in Fig. 5 against the measured bismuth content and is a straight line with a slope of 0.051 Å/mole. These results are consistent with a decrease in bismuth content due to preferential resputtering of bismuth at higher power.

The measurement of the optical rotation was performed by placing a mirror behind the film to use the reflected beam. The magnitude of the optical rotation measured by this method is affected by changes in the reflection coefficient of the glass/air and glass/film interfaces. These reflection coefficients depend on the refractive index of the film and the thickness of the film and substrate. The optical rotation for films made with identical sputtering and annealing conditions but different sputtering times is shown in Fig. 6. Interference effects can be seen in the oscillatory behavior of the rotation with increasing film thickness. Variations in the optical

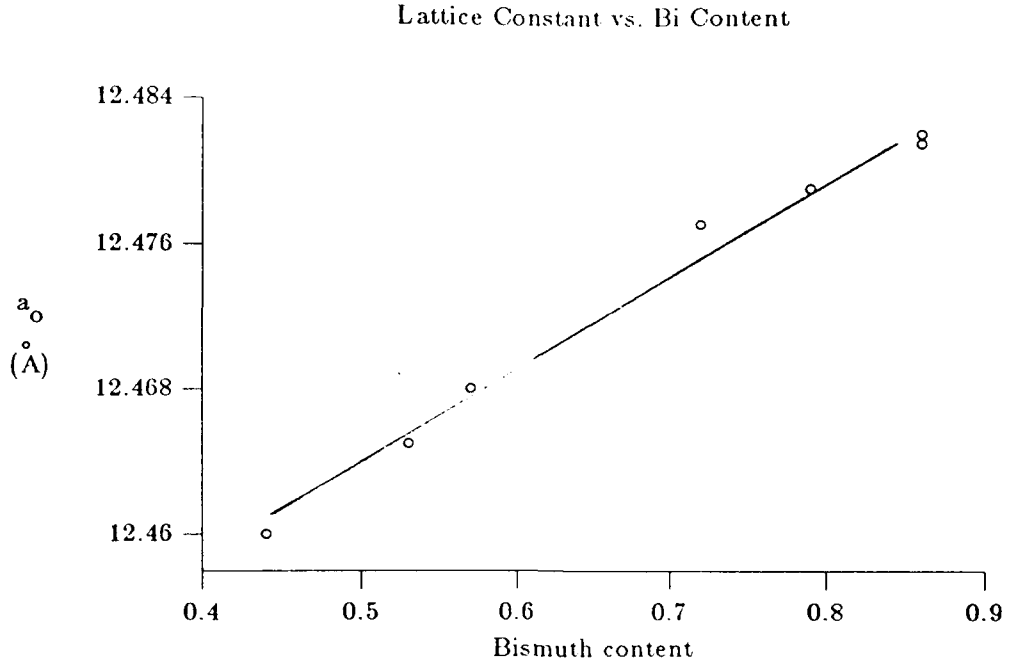

Figure 5: Increase in lattice parameter with bismuth content

rotation less than 50% can not be attributed to compositional changes unless the films are exactly the same thickness. The Faraday rotation for films made with different rf power and argon bleeding pressure of 95W are between 0.6 and 1.3 deg/μm as shown in Fig. 7. Due to variations in sample thickness, of the films deposited with different rf powers, it is difficult to determine if the variations in Faraday rotation are due to variations in composition or due to interference effects.

The Faraday rotation as a function of temperature was measured for these films and the Curie temperature obtained by linearly extrapolating the Faraday rotation to zero near the temperature at which the magneto-optic signal vanishes as shown in Fig. 7. A plot of the measured Curie Temperature as a function of the rf power in Fig. 8 shows a maximum of 260 $^\circ$C at 138 Watts. A decrease in the bismuth content would give rise to a decrease in the Curie temperature of about 17 $^\circ$C/mole through a reduction in the superexchange interaction[5]. The decrease in bismuth content cannot account for the peak in the Curie temperature. An increase in the tetrahedral site substituents (Al and Ga) will decrease T_{curie} through a reduction in the exchange constant between the two iron sublattices. It can clearly be seen from Fig. 8 that as the Ga content of the film decreases, the Curie temperature increases and as the Ga content increases, the Curie temperature decreases.

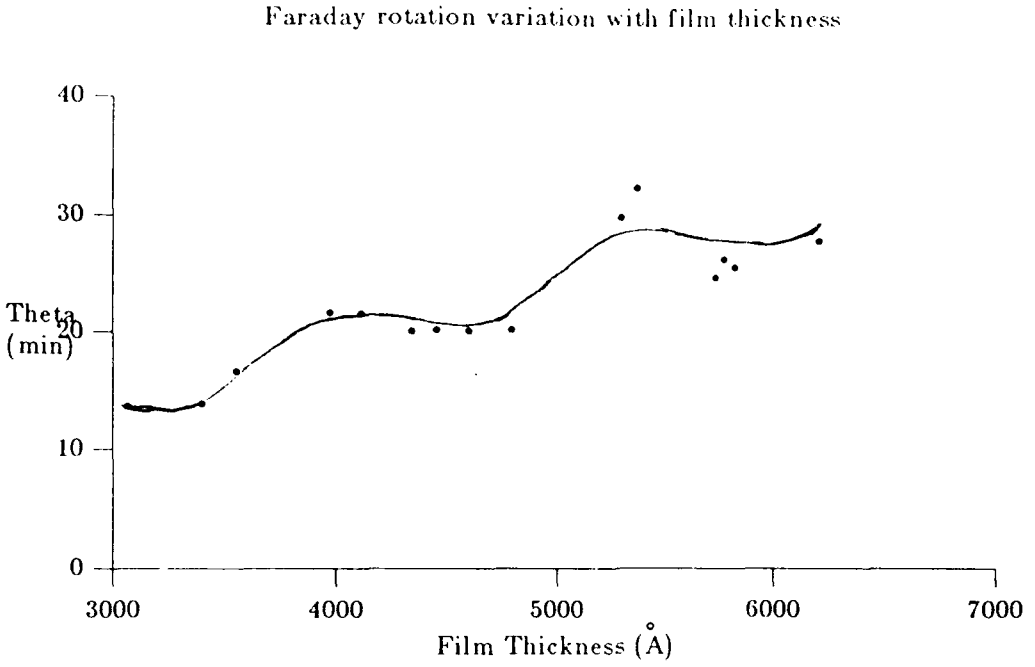

Figure 6: Variations in optical rotation for films of different thickness deposited with identical sputtering conditions

2.2.2 Substrate Bias

A negative substrate bias voltage is often used to modify the film microstructure and composition by increasing the bombardment of the growing film by energetic particles. A small negative substrate bias voltage drastically reduces the bismuth content of garnet films[6]. The temperature dependence of coercivity for a film made with 0 Volts substrate bias and a film made with -15 Volts Substrate bias are shown in Fig. 8. The film deposited at 0 Volts has a compensation temperature of 91 °C while the composition of the film made with -15 Volts of substrate bias has been altered enough that a compensation temperature no longer exists.

A decrease in the bismuth content will increase the crystallization temperature[7]. Films were deposited at 0 V, -15 V and -25 V substrate bias and then annealed at 675 °C. The structure of the films was examined by x-ray diffraction and magneto-optic hysteresis loop traces. An amorphous film will have no magneto-optic rotation and a partially crystallized film will have a smaller Faraday rotation and higher coercivity than a fully crystallized film. The films were annealed at increasing temperatures until no change was seen in the intensity of the most intense diffraction peak [4 2 0], the coercivity and the optical rotation. The change in

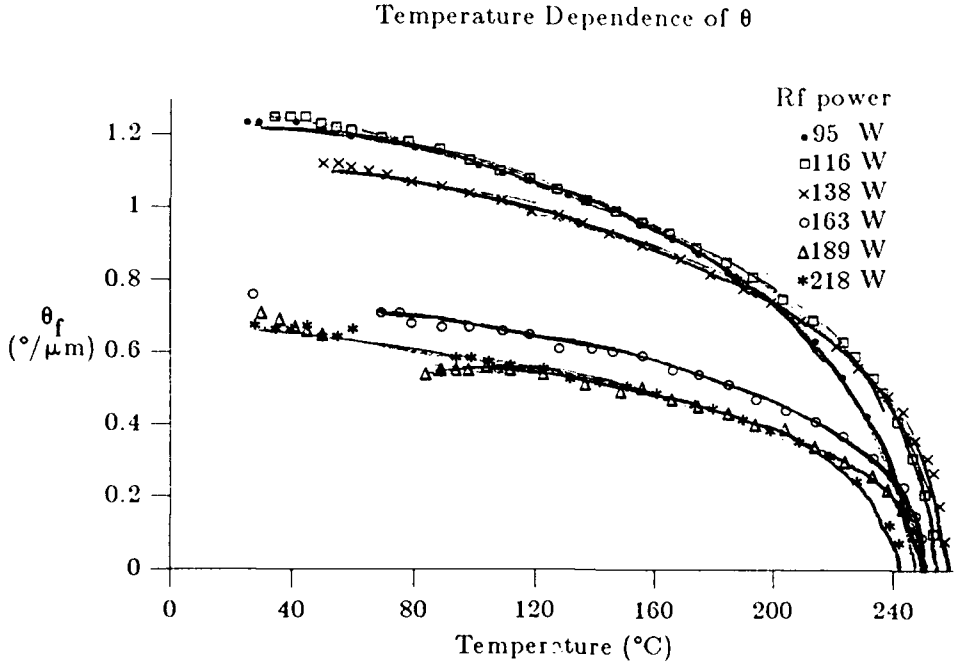

Figure 7: Temperature dependence of Faraday rotation for films deposited at rf powers between 95 W and 248 W and argon bleeding pressure of 10m Torr.

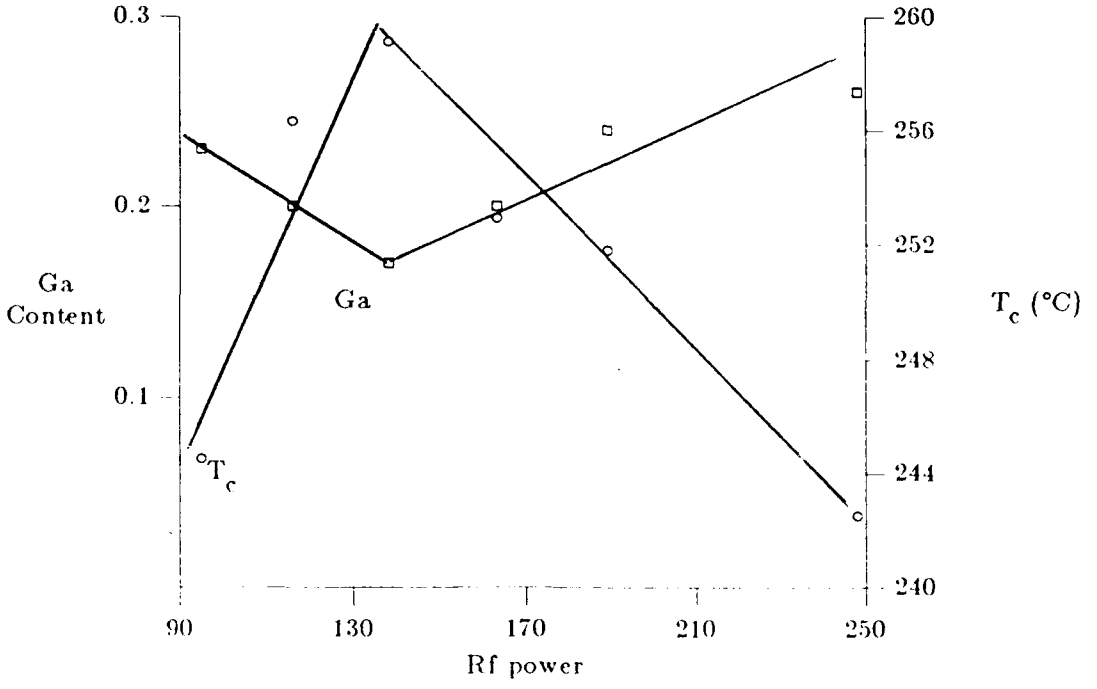

Figure 8: Curie temperature and Ga content of films deposited at different powers

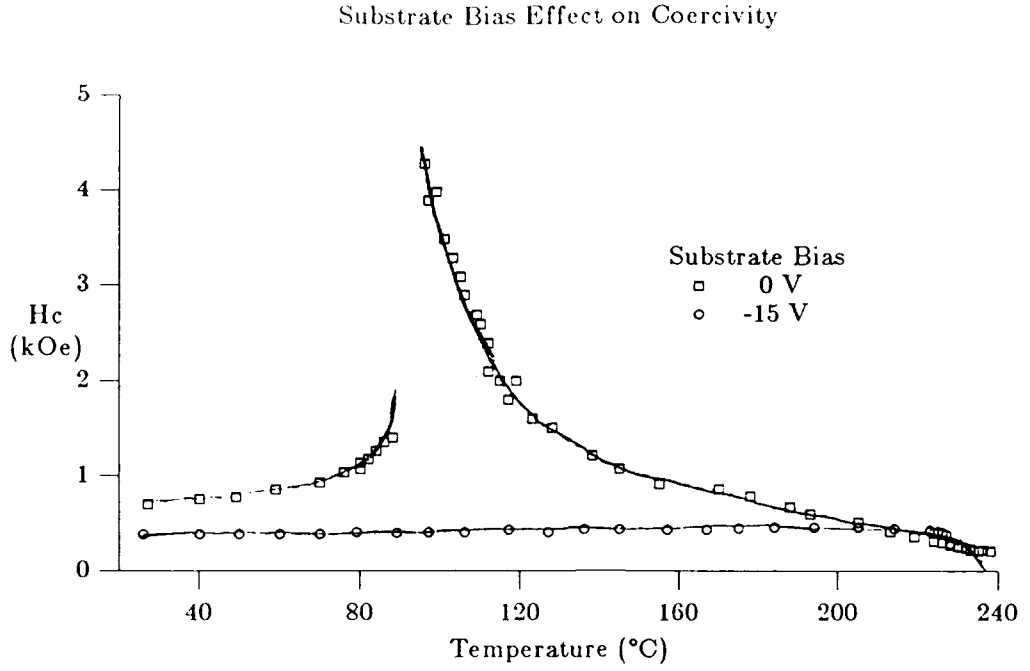

Figure 9: Change in compensation temperature with substrate bias

crystallization temperature with substrate bias, is shown in Fig. 10. As the substrate bias is made more negative increased the crystallization temperature is increased.

A reduction of the bismuth content of the films should result in a drastic reduction in the Faraday rotation and a small decrease in the Curie temperature. This can be seen in the plot of Faraday rotation as a function of temperature in Fig. 11 for films made at 0 V and -15 V substrate bias. The room temperature Faraday rotation has been reduced 80% and the Curie temperature decreased from 240 °C to 229 °C by -15 Volts substrate bias.

2.2.3 Oxygen Partial Pressure

Films were also deposited using different argon/oxygen mixtures at constant pressure as the sputtering gas. For low oxygen flow rates, as the flow rate of oxygen relative to the flow rate of argon is increased, the compensation temperature increases. The compensation temperature changes little at high oxygen flow rates as shown in Figs. 12 and 13. The increase in the compensation point at low oxygen flow rates is not likely due to a decrease in the bismuth content, because of the initial increase in the Curie temperature with oxygen flow rate. The changes in compensation temperature could possibly be explained by the oxidation of Fe^{2+} to

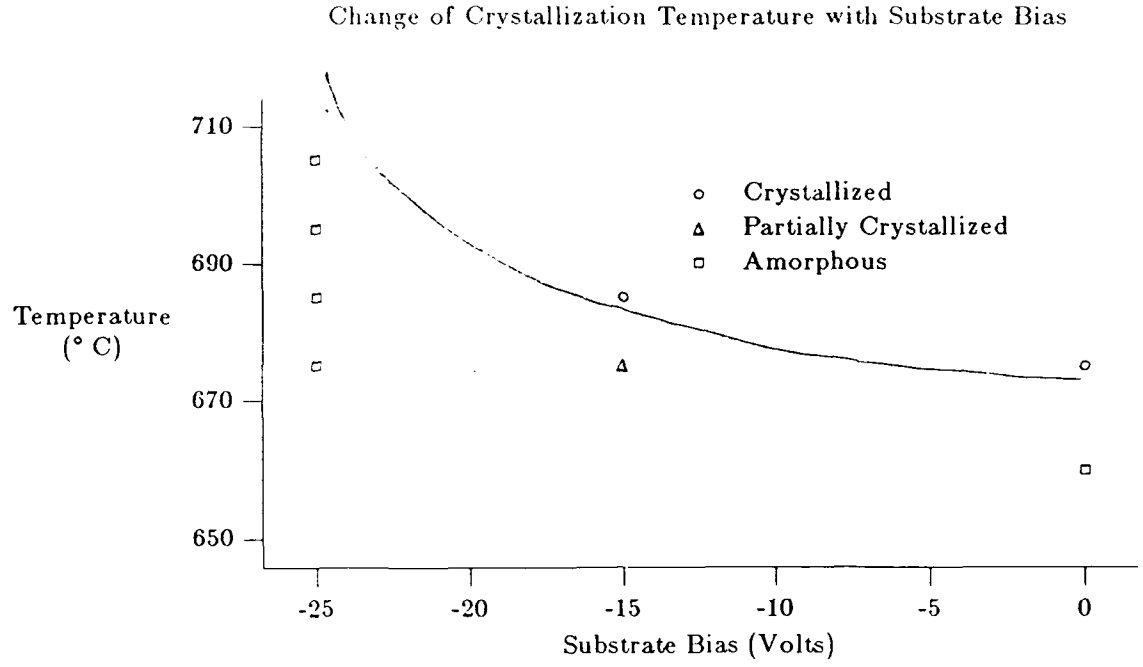

Figure 10: Increase in crystallization temperature with substrate bias

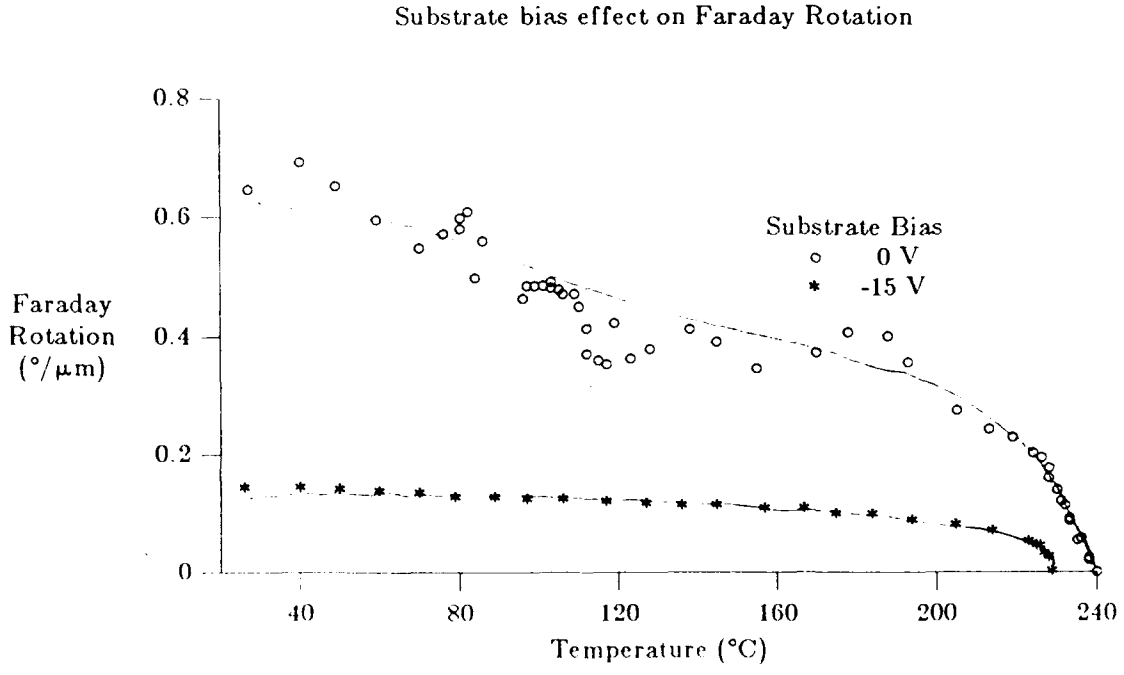

Figure 11: Faraday rotation vs. temperature for films made at 0 V and -15 V substrate bias

Fe^{3+} with increasing oxygen flow rate. If the Fe^{2+} were to preferentially occupy the octahedral site ("a" site), the magnetization of the "a" sublattice would be decreased, increasing the net magnetization and thus lowering the compensation temperature. The unit cell normally contains 160 atoms. If one of the 96 O^{2-} ions is missing, then 2 of the 40 Fe^{3+} ions must be Fe^{2+} and a 1 percent deficiency in O^{2-} requires 5 percent of the Fe^{3+} to be divalent. If the Fe^{2+} is located exclusively in the octahedral site, the mean field theory predicts a decrease in the compensation temperature of 3 °C for each percent of Fe^{2+} up to ten percent[8]. Thus a 2 percent deficiency in O^{2-} would decrease the compensation temperature 30 °C and once the film is completely oxidized no further change in the compensation temperature would occur with increases in the oxygen partial pressure. The dependence of compensation temperature on oxygen flow rate agrees well with these arguments. The Faraday rotation data in Fig. 14 is inconclusive because the changes in rotation are less than 20 percent and could be due to the difference in film thickness.

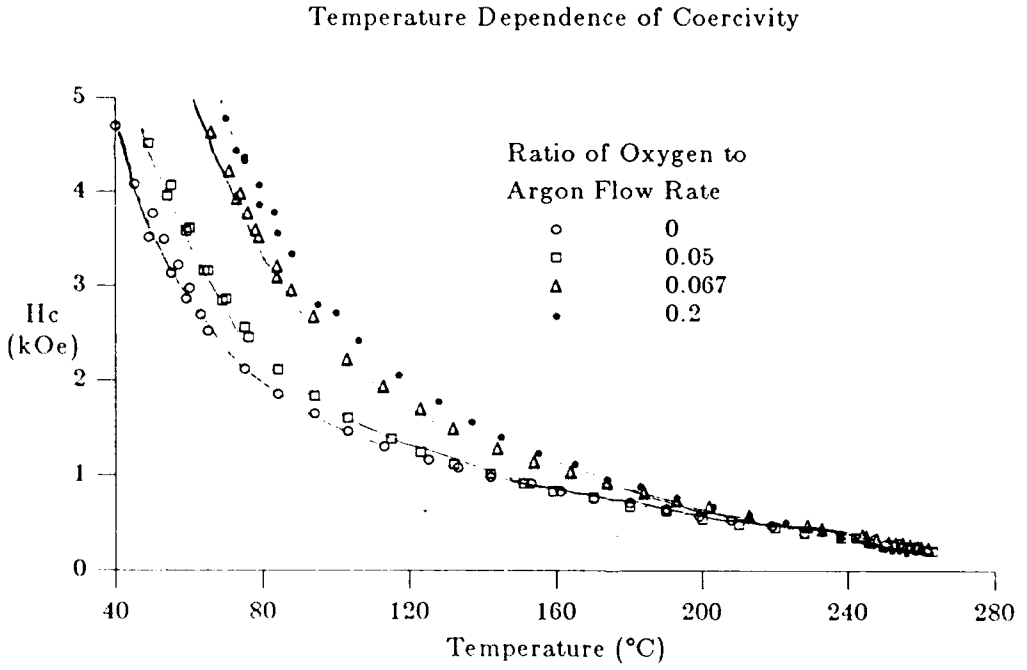

Figure 12: Temperature dependence of coercivity for films sputtered with different oxygen/argon mixtures

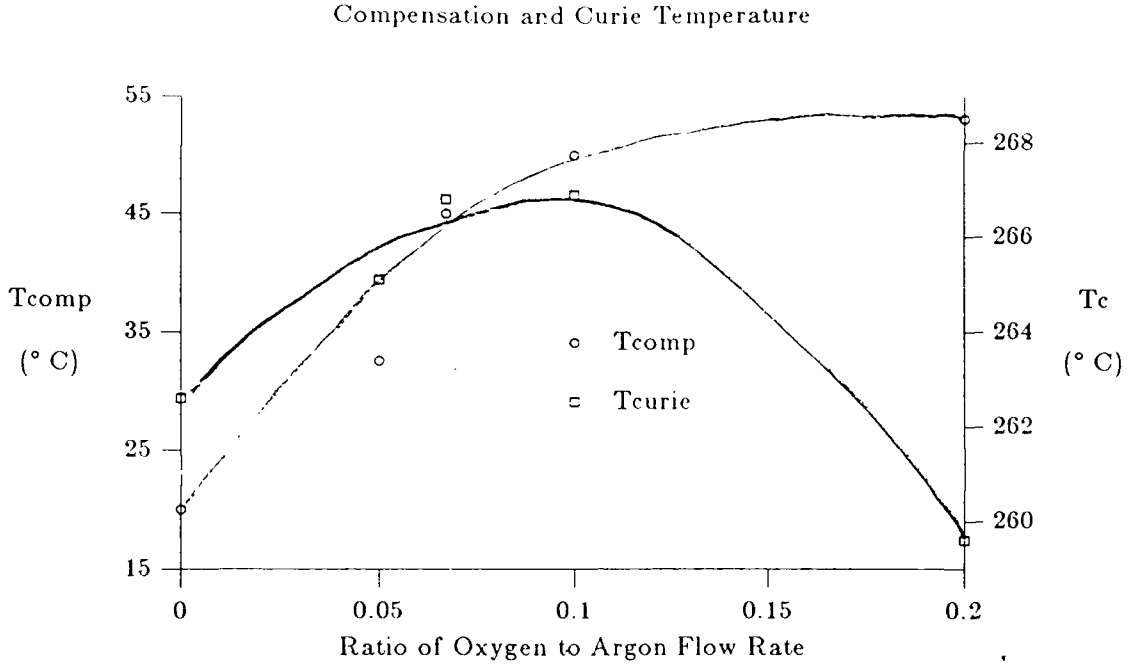

Figure 13: Changes in compensation and Curie temperature with different oxygen/argon mixtures

2.3 Ion Beam Deposition

Randomly oriented single phase garnet films have been deposited by ion beam sputter deposition. The films were deposited at 1 kV acceleration voltage and 100 mA beam current which was neutralized to avoid charging of the target and divergence of the beam. The deposition chamber atmosphere was 50/50 argon to oxygen at a pressure of 1.1 x 10^{-4} Torr. The films had a saturation magnetization of 385 G, uniaxial anisotropy constant of 1.5 x 10^{4} ergs/cc, Faraday rotation of 0.8 deg/μm, coercivity of 400 Oe and squareness of 0.7. The low coercivity and squareness compared to rf magnetron deposited films is due to the compensation temperatures (150 °C) being much further above room temperature. This could be due to the large oxygen partial pressure. Gomi et al.[9] reported a large decrease in the bismuth content with oxygen partial pressures over 50 percent in rf diode deposited films which would raise the compensation temperature.

A few films were deposited on GGG substrates. The as-deposited films are amorphous and were crystallized by annealing at 670 °C. X-ray diffraction indicates the films are single crystal

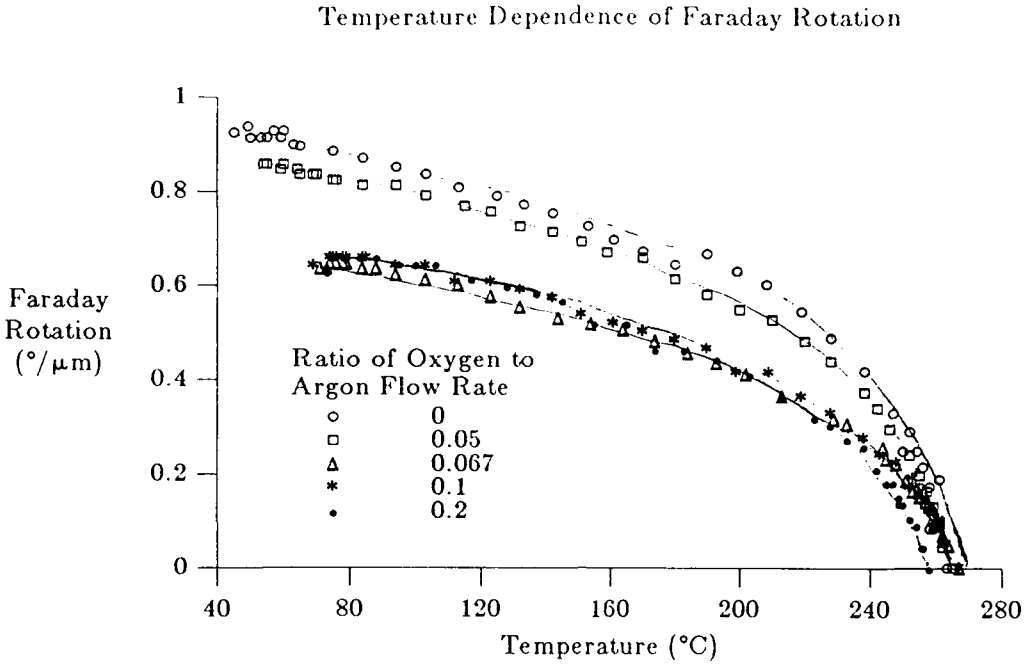

Figure 14: Faraday rotation as a function of temperature for films made with different oxygen/argon mixtures

or highly oriented since only the [4 4 4] diffraction line can be seen, as shown in Fig. 15. No grain boundaries can be seen with an optical microscope. The films have a large lattice misfit of 0.08 $\mathring{A}^{degr}$. This method of epitaxial growth could be advantageous to applications that require a high Fig. of merit but can not tolerate the dispersion of polycrystalline films.

3 Pyrolysis

3.1 Garnet Composition

Yttrium Iron Garnet (YIG), $Y_3Fe_5O_{12}$, is the basis of many ferrite microwave devices due to its low microwave losses, small g factor = 2.0 and small anisotropy field[10]. YIG is readily produced in bulk polycrystalline form by standard ceramic techniques, in bulk single crystal form by growth from solution or as high quality single crystal films by LPE[11]. LPE has drawbacks for fabrication of thin film devices or integration with semiconductor technology. The high temperatures required make integration with semiconductor materials difficult, the chemical similarity of the substrate to the film makes pattern definition difficult as all known etchants, etch both film and substrate. Growth of multiple layers and changes in film composition are

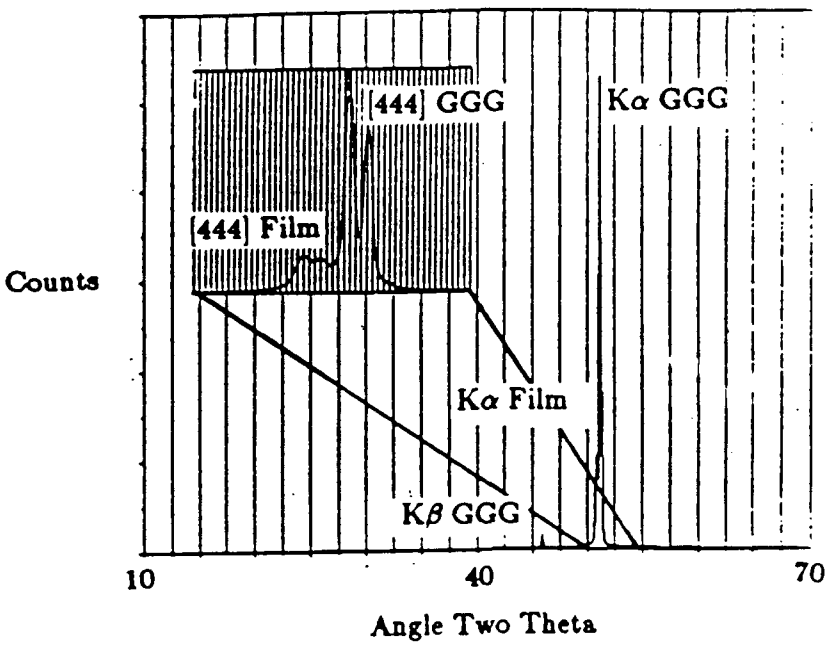

Figure 15: X-ray diffraction scan for ion beam deposited film on GGG.

difficult due to growth from the melt and lattice matching constraints. Deposition of polycrystalline films by sputtering or from solution eliminates many of these difficulties. Polycrystalline YIG is difficult to deposit due to the extremely high temperature necessary for crystallization (1100 °C), but, the addition of small amounts of bismuth reduces the crystallization temperature to 600 °C - 700 °C[12] greatly increasing the choice of substrate materials making deposition by spin coating/thermal decomposition or sputtering an attractive method for fabrication of thin film microwave devices.

3.2 Substrate

A substrate for thin film garnet microwave devices must be able to withstand the processing temperatures, have a thermal expansion coefficient which closely matches the garnet to reduce induced stresses, be able to be polished to a reasonably smooth surface and have low dielectric losses at the operating frequency of the devices. An amorphous or polycrystalline substrate will result in a polycrystalline film, while a lattice-matched single crystal is necessary to produce a single crystal or highly oriented polycrystalline film. Macor a glass ceramic produced by Corning can withstand temperatures up to 1000 °C, is machinable with standard metal working tools, has a thermal expansion coefficient of $9.4 \times 10^{-6}/^{\circ}$ C closely matching

that of garnet, and can be polished to a surface smoothness of two microinches. This material has been used extensively in our studies.

3.3 Film Preparation

3.3.1 Solution Preparation

Many garnets and ferrites can be obtained by the thermal decomposition (pyrolysis) of solutions containing stoichiometric amounts of the desired metal ions. Pure low melting point ($< 100\ ^\circ C$) hydrated nitrates ($Fe(NO_3)_3 \cdot 9H_2O$, $Bi(NO_3)_3 \cdot 5H_2O$) and water soluble nitrates ($Y(NO_3)_3 \cdot 4H_2O$, $Ce(NO_3)_3 \cdot 6H_2O$) or oxides are convenient sources of the desired metal ions. The materials are carefully weighed and combined in a covered beaker, the beaker is then slowly heated ($< 100\ ^\circ C$) and agitated to melt and dissolve the materials creating a super saturated solution. Care must be taken during heating not to drive off any water which can cause esterification when the solution is diluted with alcohol for coating. The solution is then slowly cooled and water and/or ethyl alcohol (solvents and dispersents) are added to stabilize the solution and lower the viscosity for coating. An appropriate coating technique is then used to obtain thick (spray coating, waterfall) or thin (spin coating) films.

3.3.2 Spin Coating and Decomposition

Thin garnet films ($< 1\ \mu m$) have been deposited by spin coating Macor substrates using a standard photoresist spinner. Spin coating of a 5 g solution diluted with 5 cc ethyl alcohol at 4000 rpm for two minutes produces a film with a final thickness of approximately 0.1 μm. The thickness of the film can be controlled through the solution viscosity and the angular velocity used during coating. The films are then decomposed (dried) by heating them at 400 $^\circ$C for ten minutes, driving off the volatile constituents and gasses, leaving an amorphous oxide film. Significant volume shrinkage occurs during this step and care must be taken (controlled heating and cooling rates, proper temperature, etc.) so the film does not crack. Thicker films can be obtained by repeating this process a number of times to build up a film of the desired thickness.

3.3.3 Annealing

The amorphous oxide films deposited are not ferrimagnetic and must be heat treated to crystallize them. Prior to heat treatment the amorphous films can be patterned by etching them in dilute nitric acid. This is a significant advantage over the LPE process for device fabrication because nitric acid does not etch the substrate, eliminating complicated mask steps. The films

are then annealed at 650 °C - 750 °C in an air atmosphere for three hours for crystallization. The heating rate of our furnace was 6 °C per minute. At the completion of the annealing cycle the furnace was shut off and allowed to cool naturally (about 2 hours) to room temperature.

3.4 Results

3.4.1 X-ray Diffraction

X-ray diffraction analysis of films deposited on Macor and Corning 7059 glass substrates show the films to be single phase randomly oriented polycrystalline garnets. Due to the thin nature of these films detection of other crystalline phase would be limited to those which compose at least 5 weight percent of the film[13]. Observation by TEM has also not detected any other crystalline phases. Earlier work using ion beam deposition to deposit the amorphous oxide on single crystal GGG substrates has demonstrated the possibility of obtaining single crystal or highly oriented polycrystalline films yielding a "solid phase epitaxy" process as can be seen by the absence of all diffraction peaks other than the [444] peak matching the orientation of substrate in Fig. 15. This technique offers the versatility of pyrolysis and the possibility of reduced line widths through improvement in the structure of the films for devices which can not tolerate the larger line widths or light scattering of polycrystalline films.

3.4.2 Differential Thermal Analysis

Differential Thermal Analysis is a technique that can measure heat of reactions. A thermocouple is embedded in the material under test and another in an inert material such as Al_2O_3. The thermocouples are connected in an opposing manner and this "differential" voltage monitored. An exothermic reaction will produce a positive voltage change and an endothermic reaction a negative voltage change. A plot of the differential temperature as a function of temperature of bulk amorphous samples of $Y_{2.6}Bi_{0.4}Fe_5O_{12}$ and $Gd_2Bi_1Fe_5O_{12}$ are shown in Figs. 16 and 17 respectively . Two distinct reactions can be seen in the first trace, an endothermic reaction at 500 °C associated with stress relief as the viscosity of the "glassy phase" passes through its annealing point[14], a strong exothermic reaction at 720 °C associated with the growth of the garnet phase. Three reactions can be seen in the second trace, an endothermic reaction at 500 °C associated with stress relief as the viscosity of the "glassy phase" passes through its annealing point[14], a strong exothermic reaction at 670 °C associated with the growth of the garnet phase and the beginnings of a endothermic reaction at approximately 1000 °C where this material begins to melt. This data shows the reduction of

the crystallization temperature from 720 °C to 670 °C as the bismuth content is increased from 2 to 5 atomic percent. This data also shows the optimal crystallization temperature for lightly bismuth doped YIG between 720 °C and 760 °C and the annealing point of the "glassy" phase between 450 °C and 550 °C[14].

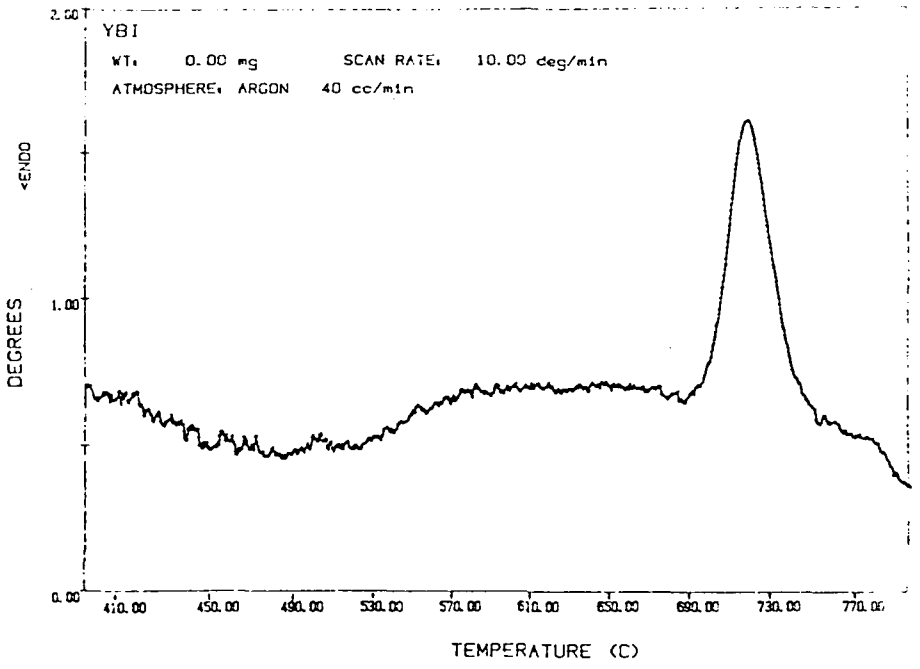

Figure 16: Differential thermal analysis trace for $Y_{2.6}Bi_{0.4}Fe_5O_{12}$

3.4.3 Ferromagnetic Resonance

A perpendicular FMR spectrum of a 0.4 μm thick $Y_2Bi_1Fe_5O_{12}$ using a minibox signal-coupler is shown in Fig. 18. The 5.5 GHz resonance at a field of 3.53 kOe has a signal strength comparable to those of thicker LPE grown garnet films. This spectrum also shows the film has a reasonably narrow resonant line width of 133 Oe.

A saturated garnet film in the perpendicular resonant mode with uniaxial perpendicular anisotropy should show a resonant frequency that varies linearly with the applied field as

$$\frac{f}{\gamma} = H_A + H_K - 4\pi M_S$$

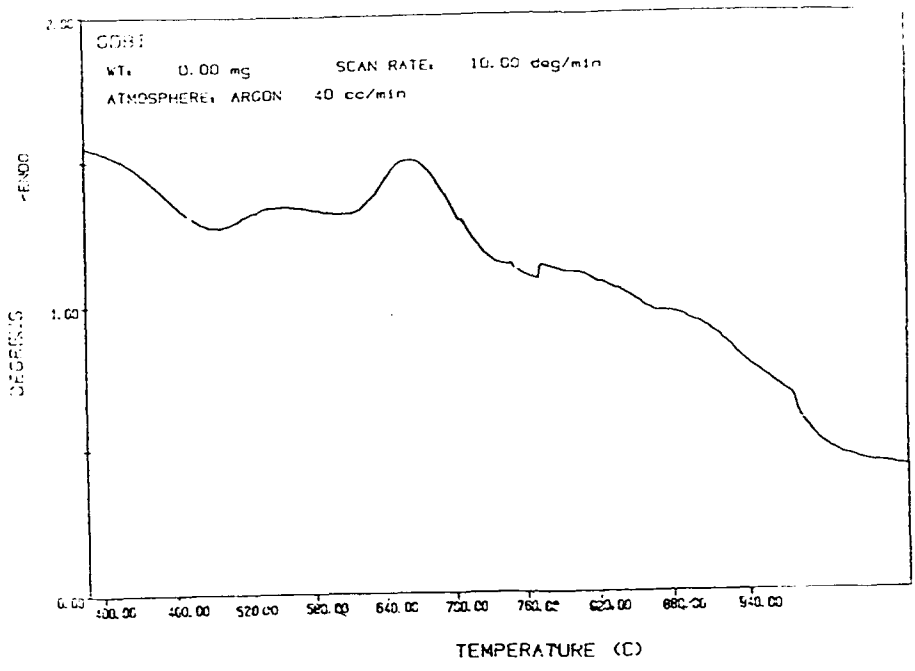

Figure 17: Differential thermal analysis trace for $Gd_2Bi_1Fe_5O_{12}$

where f is the resonant frequency, $\gamma = 2.8$ MHz / Oe is the gyromagnetic ratio, H_A is the applied field, H_K is the anisotropy field and M_S is the saturation magnetization. A plot of the resonant frequency versus the applied field in the perpendicular resonant mode is shown in Fig. 19 for three $Y_{3-x}Bi_xFe_5O_{12}$ garnets with different amounts of bismuth. Straight lines fitted through these data have slopes approximately equal to 2.8 MHz / Oe indicating almost complete crystallization of the garnet phase. All of these films had their easy axis of magnetization in the plane of the film determined by measurements using a vibrating sample magnetometer. The exact value of the anisotropy field can not be determined by extrapolation to zero field because of uncertainties in the measurement of the saturation magnetization. But it can clearly be seen that the addition of bismuth lowers the perpendicular anisotropy field since the saturation magnetization at room temperature varies little with bismuth substitution.

Substitution of other elements for either Y or Bi should have an effect on the anisotropy field through variations in the magnetostriction coefficient. By proper choice of the substituents, one with a positive influence on the anisotropy field and one with a negative influence, a composition with an anisotropy field identically equal to zero should be obtainable.

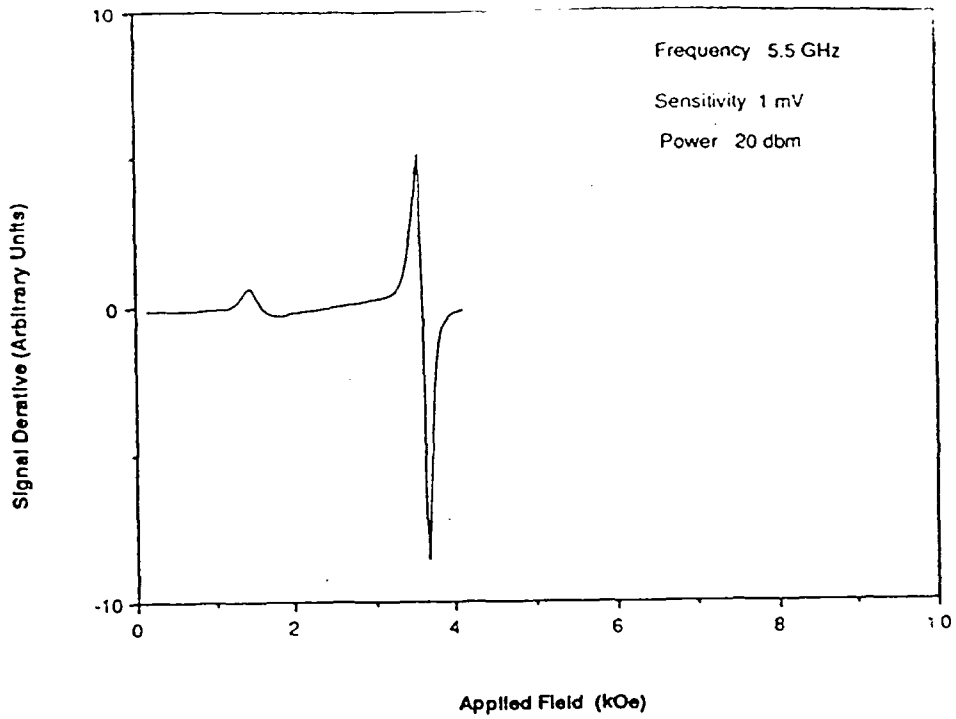

Figure 18: Perpendicular mode ferromagnetic spectrum at 5.5 Ghz for $Y_2Bi_1Fe_5O_{12}$

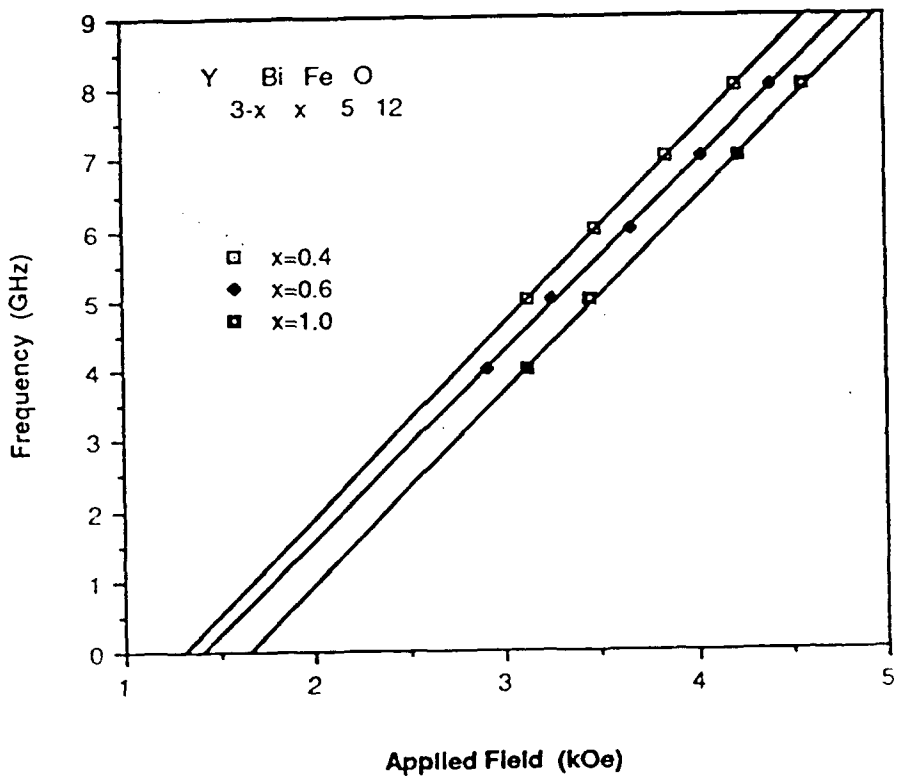

Figure 19: Perpendicular mode resonant frequency vs. applied field for $Y_{3-x}Bi_xFe_5O_{12}$

A saturated garnet film in the parallel resonant mode with a perpendicular uniaxial anisotropy should show a resonant frequency that varies as the square root of the applied field as

$$\frac{f}{\gamma} = \sqrt{H_A (H_A - H_K + 4\pi M_S)}$$

A plot of the resonant frequency versus the applied field in the parallel resonant mode for a 1 μm thick $Y_{2.4}Bi_{0.6}Fe_5O_{12}$is shown in Fig. 20. The data fits the model very well showing that the magnetization does not prefer any direction within the film plane (i.e. the resonant frequency will approach zero as the applied field approaches zero). For microwave devices it is desirable to operate with small bias fields, therefore it is necessary to be able to saturate the film in small fields to obtain a strong single mode resonance. The films deposited thus far are not sufficiently "soft"; fields over 300 Oe. are needed to saturate the films as can be seen from the B-H hysteresis loop for a 1 μm thick $Y_{2.6}Bi_{0.4}Fe_5O_{12}$ film in Fig. 21.

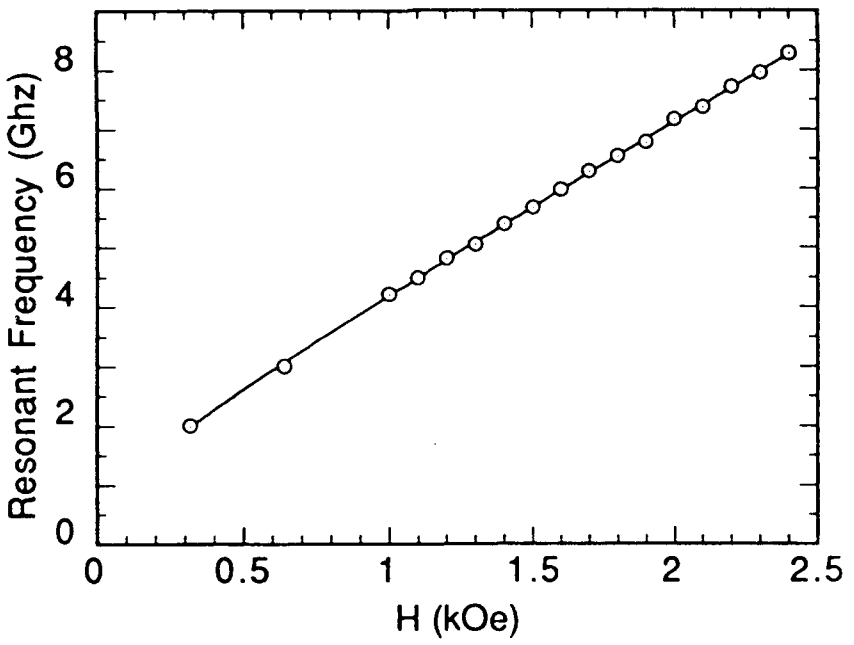

Figure 20: Parallel mode resonant frequency vs. applied field for $Y_{2.4}Bi_{0.6}Fe_5O_{12}$

The plane of the film is the easy axis but the coercivity of 30 Oe is rather large. The large in plane coercivity is due to the microstructure of the film. The grain boundaries act as pinning

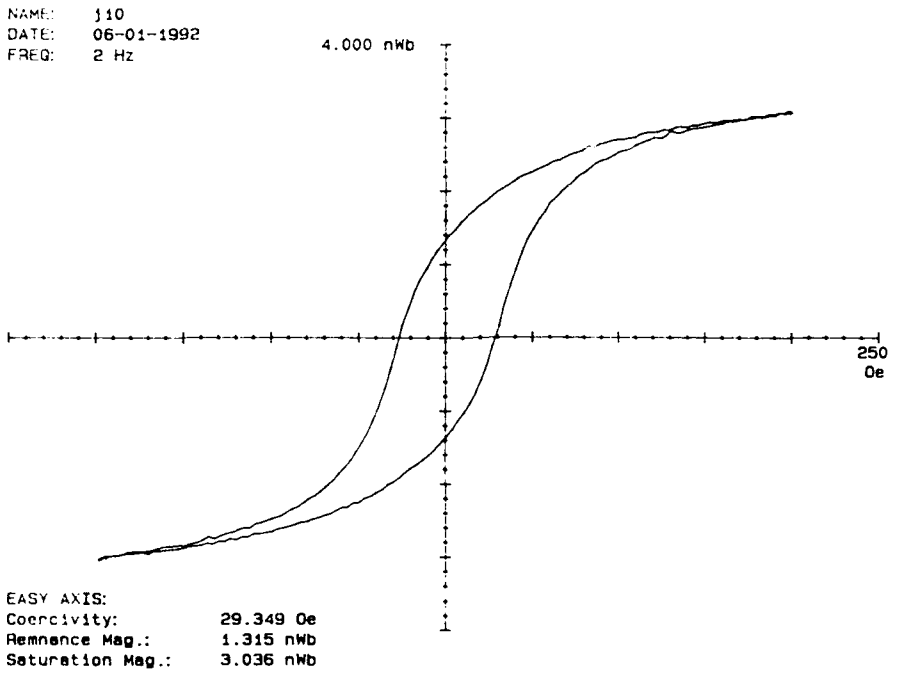

Figure 21: B-H hysteresis loop for 1 μm thick polycrystalline $Y_{2.4}Bi_{0.6}Fe_5O_{12}$ film

sites for domain walls and help to reduce the exchange between grains isolating each grain and increasing the coercivity. To obtain performance comparable with LPE grown films, the microstructure must be altered to produce "softer" films.

4 Microstructure

Although polycrystalline garnet films with bulk magnetic and magneto-optic properties suitable for optical guided wave devices or optical recording media can be deposited on a variety of substrates, and the magnetic properties controlled by choosing an appropriate composition, devices employing these films often exhibit severe degradation of performance compared to LPE grown films. This degradation of performance is related to the microstructure of the film. A magnetic domain written in a saturated film with a 3 μm circular laser spot is shown in Fig. 22. All the grains within the laser spot are magnetized in the reverse direction creating an irregularly shaped domain (i.e. the domain walls are located only along grain boundaries). In order to use these films for magneto-optic applications it will be necessary to produce uniform sized finely grained films to reduce light scattering and enable creation of controlled magnetization states.

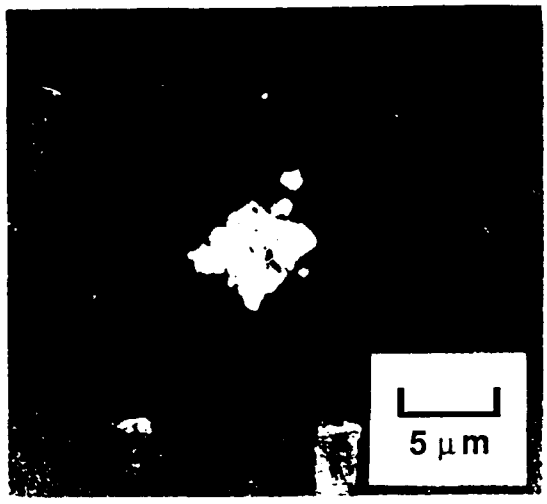

Figure 22: Domain written in garnet film with circular laser spot

4.1 Scanning Electron Microscopy

A $Gd_2Bi_1Fe_{4.6}Al_{0.2}Ga_{0.2}O_{12}$ film, 0.3 μm thick, annealed at 670 °C in air for 4.5 hours was coated with 10 nm of gold for observation in the SEM. An image using secondary electrons (SE), which are emitted from approximately the first 10 nm and provide mainly topographical contrast, showed no features, indicating that the surface of the film was smooth. The same film however, when imaged using backscattered electrons, which are emitted from depths of 0.1 to 1 μm and provide mainly atomic weight contrast, showed some features of the microstructure of this film as shown in Fig. 23. Grains approximately 1 μm in diameter can be seen separated by dark boundaries. The dark boundaries could possibly indicate that the grain boundaries are to a large extent voided; however, more detailed information is difficult to draw from the images due to the poor contrast and resolution of this technique.

Two films deposited under identical sputtering conditions as the film imaged previously,

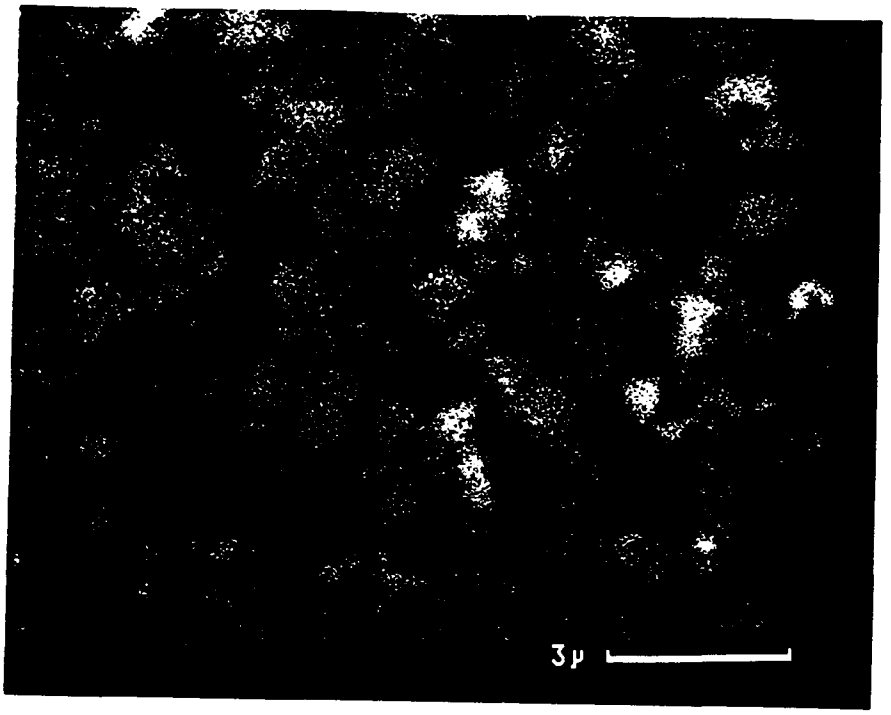

Figure 23: BE image of gold coated sputtered garnet film

one deposited on Corning No. 7059 glass and the other deposited on Corning No. 0317, were lightly etched for 15 seconds in H_3PO_4 at 120 ° C and then coated with 10 nm of gold. The acid etch, preferentially etches the grain boundaries revealing the microstructure using SE as shown in Figs. 24 and 25. This technique provides a simple means for rapid analysis of the grain size and distribution in polycrystalline garnet films. The film deposited on Corning No. 7059 glass has an average grain diameter of 2 μm while the film deposited on Corning No. 0317 has an average grain diameter of 1 μm. The etching also reveals a "radial spoke" substructure within individual grains, possibly due to a higher etching rate at crystal defects.

4.2 Transmission Electron Microscopy

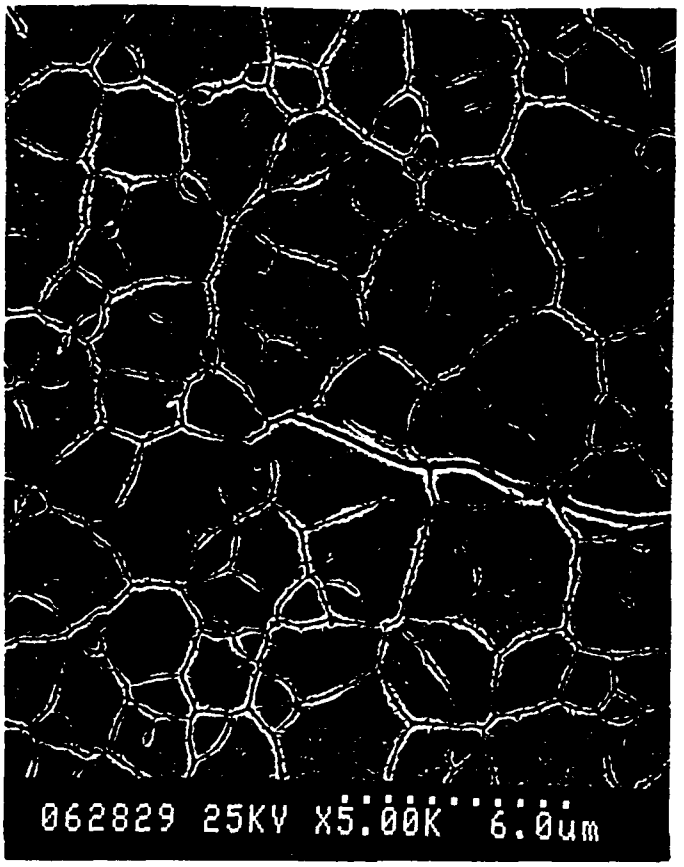

Figure 24: SE image of lightly etched sputtered garnet film deposited on Corning No. 7059 glass

4.2.1 Conventional TEM

In contrast to the scanning electron microscope where replication or etching techniques are used to observe topographical features indicative of the internal structure, direct observation of the microstructure of thin samples (< 1000 Å) is possible with the transmission electron microscope. Selected area electron diffraction (SAD) and dark field techniques can be used to distinguish between crystalline and glassy phases and for crystal structure identification. Selected area x-ray fluorescence (EDX) can be used to determine the composition of the phases present.

Mechanical polishing and ion milling was used to remove the substrate and thin a garnet film from both the top and bottom surfaces. It was necessary for the ion milling to be performed very slowly using a liquid nitrogen cooled substrate stage to avoid damaging the specimens. The

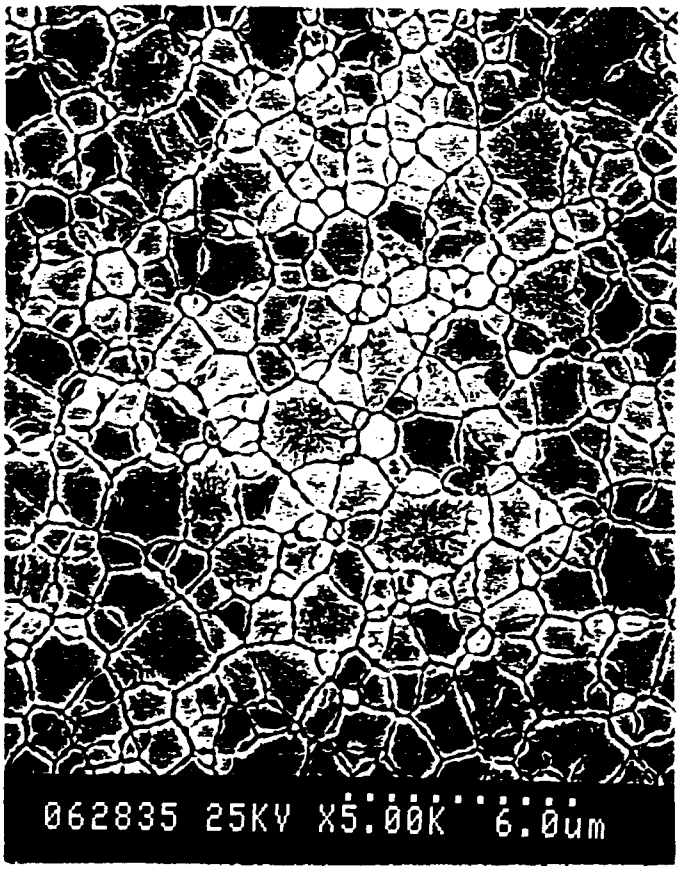

Figure 25: SE image of lightly etched sputtered garnet film deposited on Corning No. 0317 glass

bright field TEM (Philips 420T) micrograph in Fig. 26 clearly shows 0.5 - 1.0 μm sized grains and approximately 50 nm sized voids located primarily at the grain boundaries. The corresponding electron diffraction pattern in Fig. 27 shows the garnet phase, and a possible second phase although identification is difficult due to the multitude of diffraction rings. The corresponding dark field image in Fig. 28 shows these grains to be individual single crystals, as indicated by the three bright grains which changed contrast from the bright field image. Each grain is decorated with small ($<$ 50 nm) spherical "globules", uniformly distributed throughout as shown in Fig. 29.

Some experiments had pointed to segregation in these materials. A large increase in the Faraday rotation was observed when a sputter deposited film was quenched from 670 °C to room temperature rather than slowly cooled. No second phases were detectable by x-ray diffraction of these films. Due to these observations, and the solubility limit of Bi^{3+} in bulk

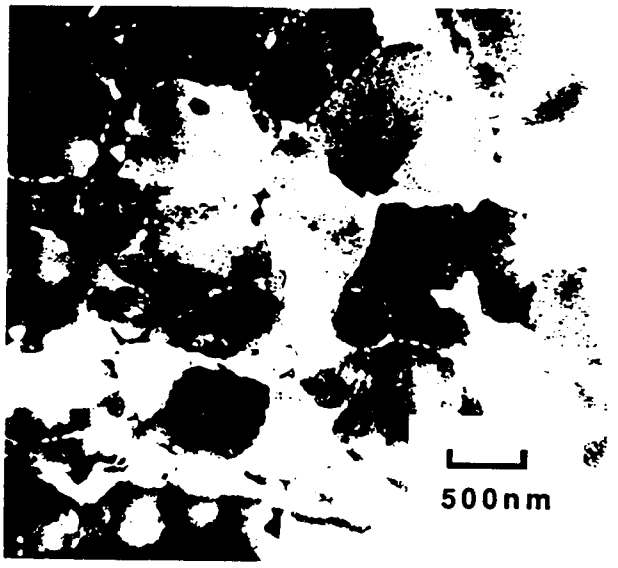

Figure 26: Bright field TEM image of garnet film

samples of rare earth iron garnets[4] bismuth segregation was suspected to be responsible for the difference in optical rotation. To add further evidence to the bismuth segregation argument two sets of films were prepared by pyrolysis $Gd_2Bi_1Fe_5O_{12}$ and $Gd_1Y_1Bi_1Fe_5O_{12}$, both slowly cooled and quenched. It was expected that a difference in rotation would be seen between the slow cooled and quenched samples for the first set, while the addition of the small dodecahedral site substituent (Yttrium) would help relieve the increase in strain energy associated with increasing bismuth substitution thereby reducing the tendency for bismuth segregation. The optical rotation increased when the $Gd_2Bi_1Fe_5O_{12}$ film was quenched while it did not increase for the $Gd_1Y_1B_1Fe_5O_{12}$ film. While this data does not conclusively prove bismuth segregation or determine its solubility limit in iron garnet thin films, it is otherwise difficult to explain and it does show a property of these materials which is very process dependent which will need to be reduced.

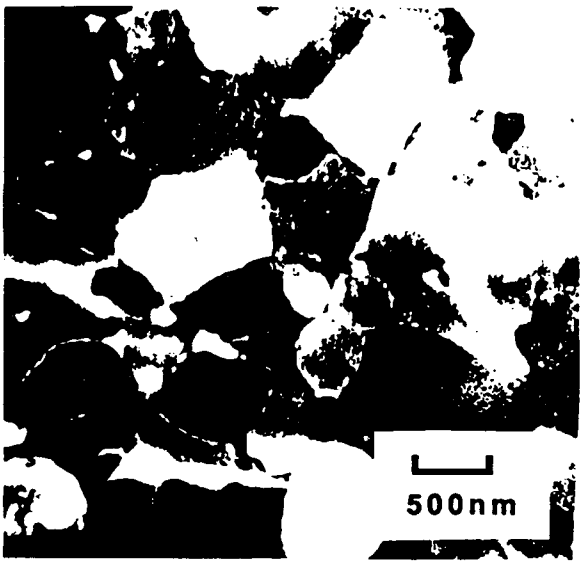

Figure 28: Dark field TEM image of garnet film

Selected area EDAX was done on the grain boundaries, "globules" and in the middle of the grains. The ratios of iron to gallium, iron to gadolinium and iron to bismuth peaks for each of these features and for large areas incorporating many of each type of feature are shown in Table 2. The iron to gallium and iron to gadolinium ratios are the same in all areas while the iron to bismuth ratio varies. The grain boundaries are slightly depleted in bismuth compared to grains while the "globules" are very bismuth rich. This is conclusive proof that bismuth segregation readily occurs in these materials. The size of these features are smaller than the available measurement apertures making quantitative analysis impossible as each spectrum contains some information from the surrounding regions. The segregation of bismuth will result in a smaller Faraday rotation than a comparable fully substituted film. Smaller dodecahedral site substituents such as Y or Lu should be employed in order to achieve large Faraday rotation (i.e. high Bi substitution).

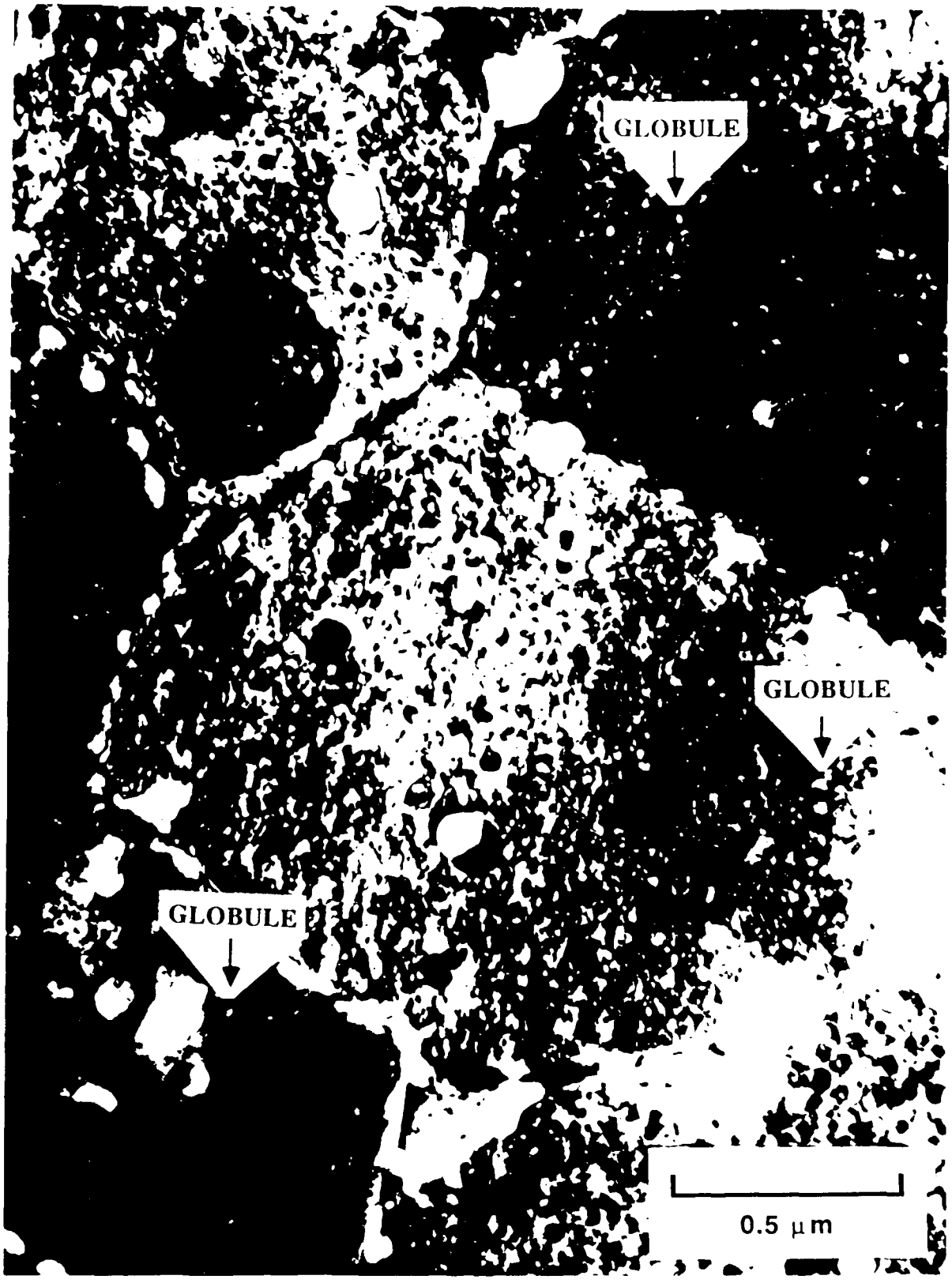

Figure 29: Bright field TEM image of garnet film showing "globules"

Table 2: Selected area EDAX ratio of elemental peaks

Feature	Fe/Ga	Fe/Gd	Fe/Bi
Area	3.40	1.74	2.27
Grain	3.43	1.72	2.35
Boundary	3.42	1.68	2.68
Globule	3.41	1.72	1.25

4.2.2 High Resolution TEM

Variations in the deposition and annealing process were observed to have little influence on the grain size and distribution, therefore the microstructure before and during annealing was investigated. Both x-ray diffraction and electron diffraction as shown in Fig. 30 revealed an amorphous type diffraction pattern for the as-deposited film. The TEM image, however, revealed small particles (10 nm) distributed across the film as seen in Fig. 31. The high resolution TEM (JEOL 4000EX) revealed these particles to be crystalline Bi (d 3.3 Å) with a spacing of about 20 nm as seen in Fig. 32.

4.2.3 In-situ Annealing

The annealing process was studied by performing in-situ annealing in the TEM (JEOL 120CX). The bismuth particles begin to grow producing diffraction rings at 400 °C and gradually transforms into βBi_2O_3 between 400 °C and 500 °C as shown in Figs. 33 and 34. At 650 °C the garnet phase begins to develop. The grains nucleate approximately 1 μm apart and rapidly grow until they impinge upon one another as shown in Fig. 35. The boundaries between the "glassy" phase and the garnet is blurred in this image due to grain growth during film exposure (exposure time 1 sec.). The rapid growth rate made it impossible to associate the nucleation sites with any particular microstructural features. No further growth occurs after the grains have grown together, therefore, the final grain size and distribution is determined by the initial density of garnet nuclei.

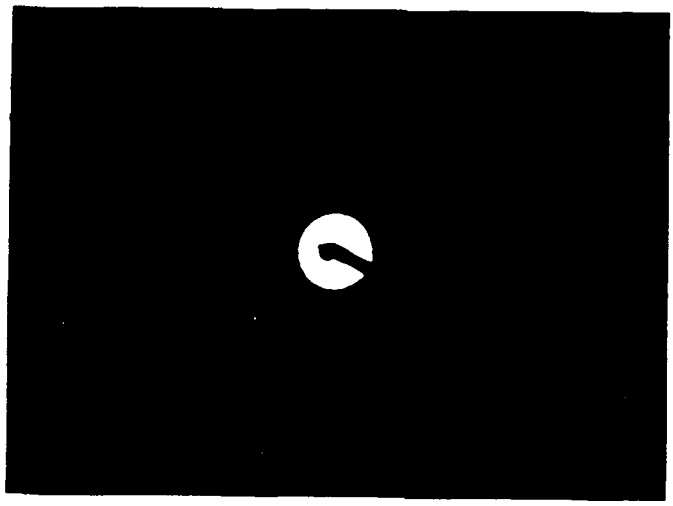

Figure 30: Electron diffraction pattern of as deposited film

5 Conclusion

The ferrimagnetic garnets are promising materials for integrated microwave and optical devices. Polycrystalline films offer many processing advantages over single crystal LPE grown films including, lower processing temperatures (670 °C), ease of ionic substitution, wider choice of substrate material, etc.. We have studied how the processing parameters affect the bulk magnetic microwave and magneto-optic propertice for rf magnetron sputter deposited films, ion beam sputter deposited films and spin coated / pyrolysis deposited bismuth doped iron garnet films. The chemical composition has a large influence on magnetic properties such as the compensation temperature and Curie temperature and through these controls other material parameters such as the coercivity. For sputter deposited films we have shown the composition can be controlled by the sputtering parameters and target composition. We have also shown that it is important to keep the resputtering of the growing film to a minimum to achieve high

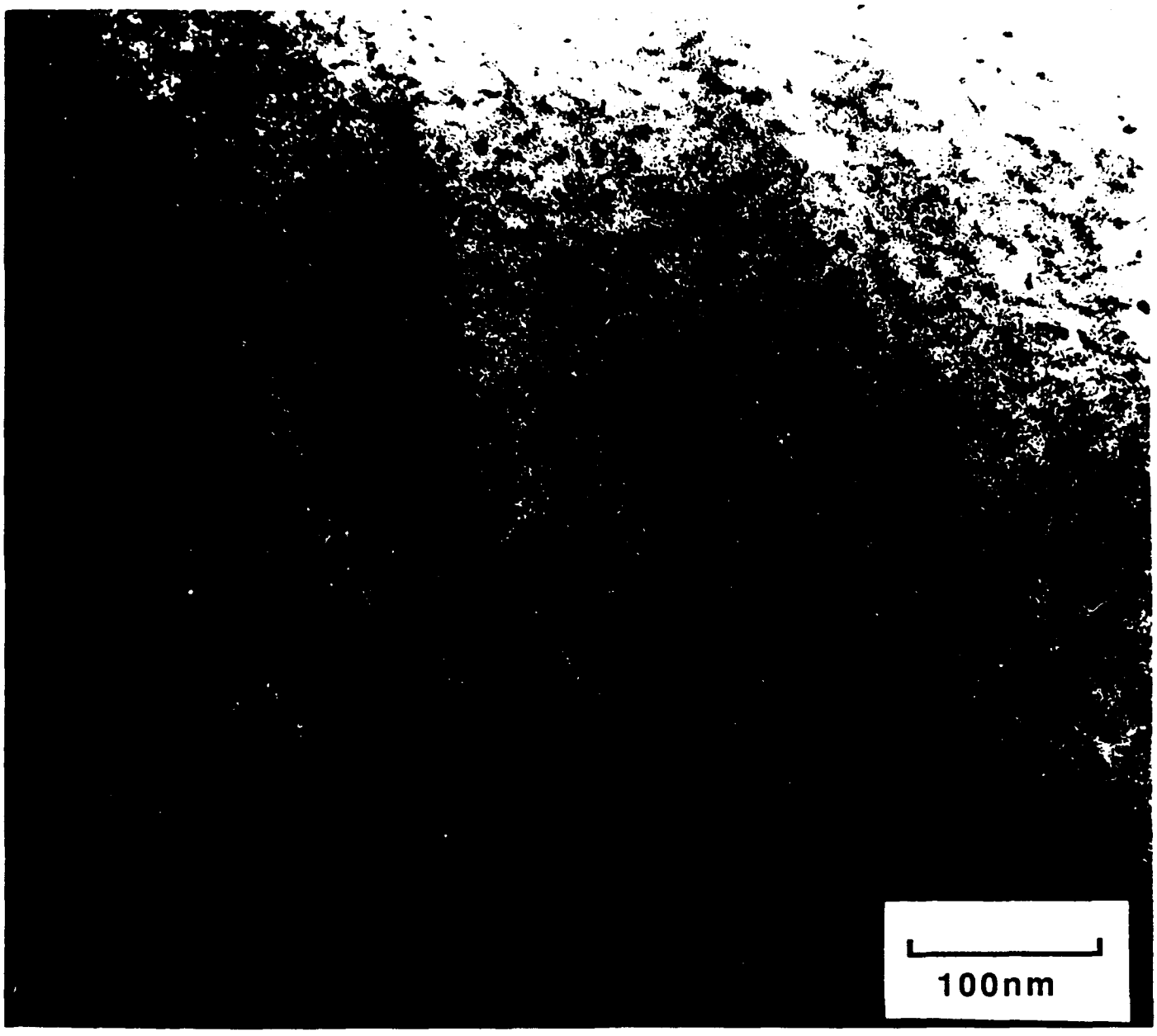

Figure 31: Bright field TEM image of as deposited garnet film

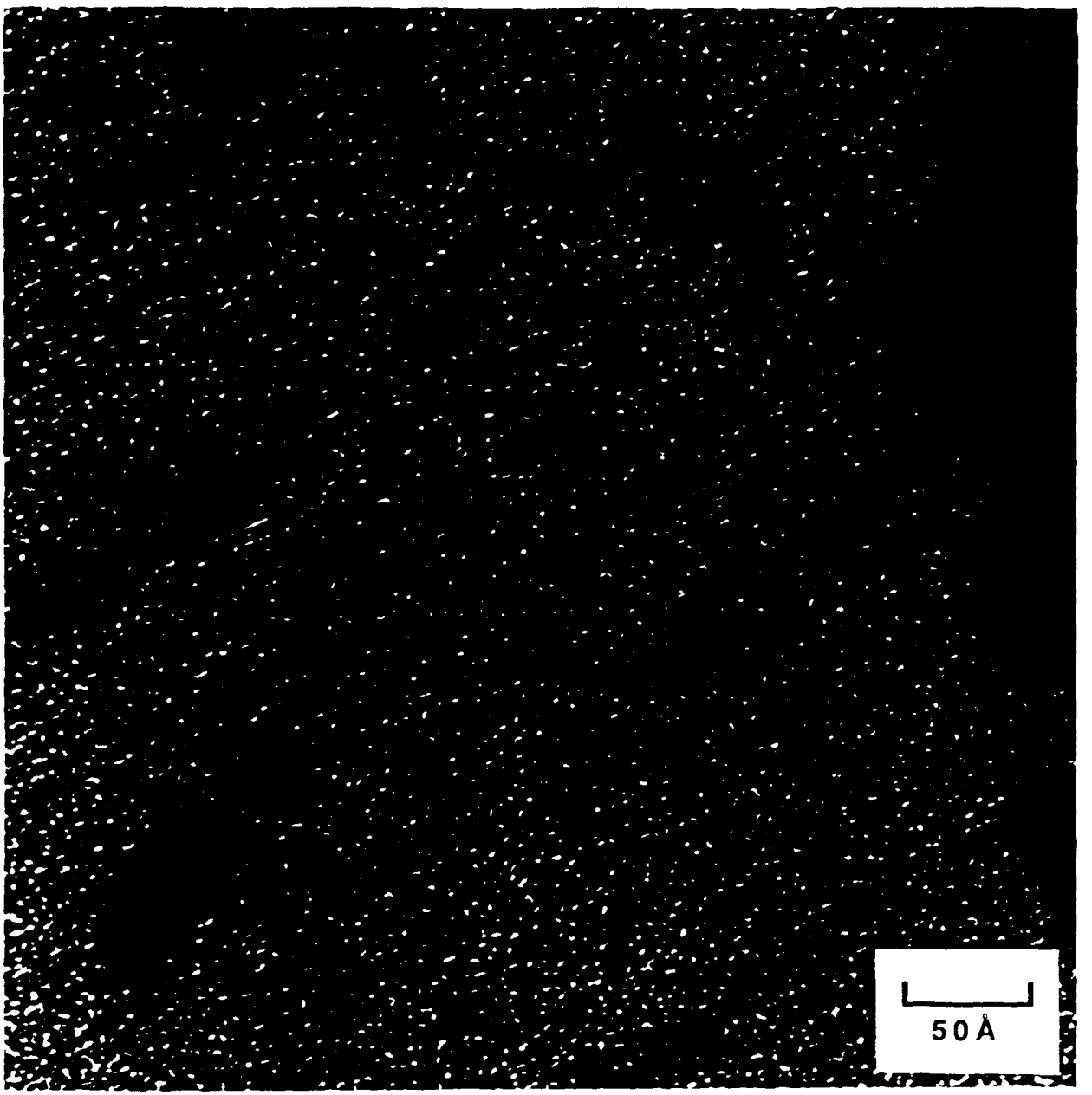

Figure 32: Bright field high resolution TEM micrograph of sputter deposited garnet film

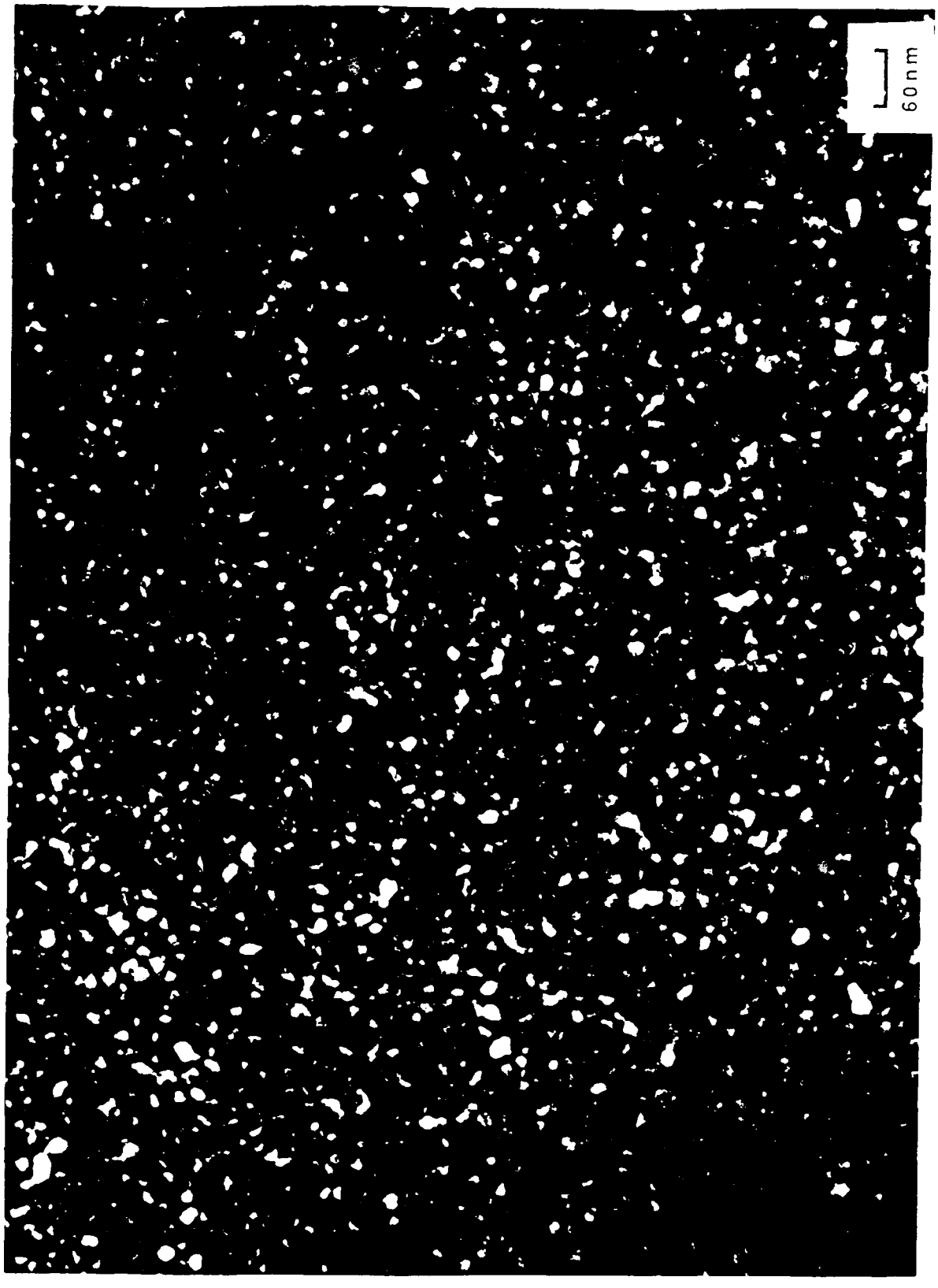

Figure 33: Bright field TEM image of [illegible] annealed for 500 °C for 30min

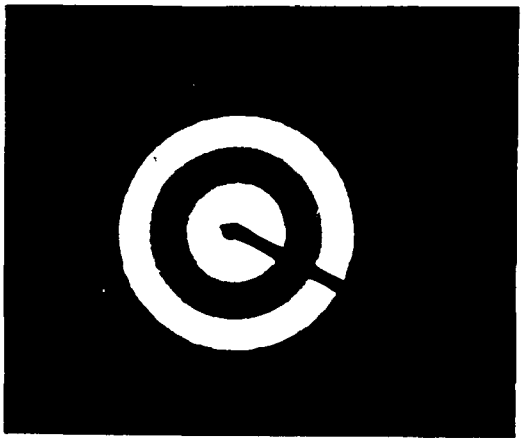

Figure 34: Electron diffraction pattern of film annealed at 500 $^{\circ}C$ for 30 min.

bismuth substitution. The composition for thermally decomposed films is controlled by the initial solution composition. The employment of these films in many types of devices will depend on the ability to produce uniform finely grained films. We have done extensive studies of the crystallization processes in these materials. We have developed a simple and rapid technique for the analysis of the grain size and distribution in these materials. We have shown that the large "c" site bismuth ion readily segregates to spherical regions distributed throughout the film in the as-deposited state, and as the film is heated, the bismuth transforms into βBi_2O_3. In-situ annealing in the TEM has shown that the microstructure of garnet films deposited on glass substrates is controlled by the initial nucleation density of the garnet phase. For these materials to be employed in devices it will be necessary to find a method to increase the nucleation density.

Figure 35: Bright field TEM image showing nucleation of garnet phase at 650 °C

References

1. T. Inui and N. Ogasawara, "Grain-Size Effects on Microwave Ferrite Magnetic Properties", *IEEE Trans. Mag.*, Vol. Mag-13, No. 6, 1977, pp. 1729-1744.

2. R. Behrisch, editor, *Topics in Applied Physics Sputtering by Particle Bombardment,* Springer-Veriag, Berlin, 1981.

3. S. Geller, "Garnets", *J. Appl. Phys.*, Vol. 31, No. 5, 1960, pp. 30S-37S.

4. K. Shinagawa and S. Taniguchi, "Solubility Limits of Bismuth in Rare-Earth Iron Garnets", *Japan. J. Appl. Phys.*, Vol. 13, No. 10, 1974, pp. 1663-1664.

5. P. Hansen and J.-P. Krumme, "Magnetic and Magneto-optical Properties of Garnet Films", *Thin Solid Films*, Vol. 114, 1984, pp. 69-107.

6. J. P. Krumme, V. Doormann and P. Willich, "Bismuth Iron Garnet Films Prepared by rf Magnetron Sputtering", *J. Appl. Phys.*, Vol. 57, No. 1, 1985, pp. 3885-3887.

7. M. Gomi, T. Okazaki and M. Abe, "Bi-Substituted Garnet Films Crystallized During Rf Sputtering for M-O Memory", *IEEE Trans. Mag.*, Vol. Mag-23, No. 5, 1987, pp. 2967-2969.

8. R. M. Josephs, "The Affect of Annealing on Sputtered GdIG Films", *IEEE Trans. Mag.*, Vol. Mag-6, 1970, pp. 553-558.

9. M. Gomi, K. Utsugi and M. Abe, "Rf Sputtered Films of Bi-Substituted Garnet for Magneto-optical Memory", *IEEE Trans. Mag.*, Vol. Mag-22, No. 5, 1986, pp. 1233-1235.

10. W. H. Aulock, editor, *Handbook of Microwave Ferrite Materials,* Academic Press, New York, 1965.

11. H. L. Glass, "Ferrite Films for Mirowave and Millimeter Wave Devices", *Proc. IEEE*, Vol. 76, No. 2, 1988, pp. 151-158.

12. S. Geller, H. J. Williams, G. P. Espinosa, R.C. Sherwood and M. A. Gilleo, "Reduction of the Preparation Temperature of Polycrystalline Garnets by Bismuth Substitution", *Appl. Phys. Lett.*, Vol. 3, No. 2, 1963, pp. 21-22.

13. H. P. Klug and L. E. Alexander, *X-ray Diffraction Procedures for Polycrystalline and Amorphous Materials,* Wiley, New York, 1954.

14. P. W. McMillan, *Glass-Ceramics*. Academic Press, London, 1964.

Magnetic Hexaferrite Films

X. Sui, W. Wang, M. Ramesh and M. H. Kryder

Data Storage Systems Center
Carnegie Mellon University
Pittsburgh, PA 15213

Abstract

Pure and substituted barium hexaferrites have been investigated for potential applications in magnetic/magneto-optic recording and microwave/millimeter wave technology. The goal of this investigation was to study the feasibility of preparing thin films of such ferrites, with good perpendicular c-axis texture, perpendicular anisotropy and large room temperature coercivities. The method of depositing such thin films was essentially rf sputtering and the effects of the various sputtering parameters on the magnetic properties were studied. The microstructure of these films was also studied and efforts were made to correlate the structural details to the sputtering conditions and in turn to the resulting magnetic properties. Pure barium hexaferrite films with high degrees of perpendicular c-axis texture, perpendicular anisotropy and desired coercivities have been obtained for low power sputter-deposition of around 20 watts, low argon pressure of 5 mTorr and a grounded substrate. A similar study was also conducted to determine the ideal sputtering conditions and their effects on stoichiometry in case of substituted hexaferrites. A number of substrates were investigated, as potential candidates for thin film growth. A variety of post-deposition annealing schemes was also studied. Attempts were also made to grow thick films using Liquid Phase Epitaxy (LPE).

1. Introduction

Barium hexaferrites, both substituted and unsubstituted, are being studied extensively for applications in the areas of magnetic, magneto-optical recording, as well as in the areas of microwave and millimeter wave technology.[1,2,3,4] This class of hexaferrites satisfies the requirements for various device applications, in that it has high permeability and saturation magnetization, good corrosion resistance, thermal stability, high room temperature coercivity and favorable magneto-optic and microwave properties. Another unique feature to this class of materials is that the unsubstituted barium hexaferrite has a very high uniaxial anisotropy, which can be systematically reduced over a large range by suitably substituting with Co ions (and Ti or Sn ions for charge compensation). Barium hexaferrite has attracted much interest as a high density perpendicular magnetic recording medium in part due to its large uniaxial anisotropy.

In magneto-optical recording, the presently favored recording media are rare-earth transition metal (RE-TM) alloys. A major drawback which exists with the RE-TM materials is that they are not corrosion resistant and have small magneto-optical effects. Among the materials which are currently being studied to resolve these problems are (besides Pt/Co multilayers [5,6,7]and oxides, such as Bi-substituted garnets[8,9]) substituted hexaferrites.[10] Barium hexaferrites have low Faraday rotation values. In order to improve the Faraday rotation, researchers have substituted Co-Ti for Fe in appropriate amounts, while still maintaining perpendicular magnetization. Since hexaferrites have large magnetocrystalline uniaxial anisotropy parallel to the c-axis, one can deposit polycrystalline films with perpendicular magnetization by simply obtaining high degrees of c-axis orientation.

Microwave and millimeter wave devices require materials with low magnetic losses and strong anisotropy fields.[3,4] The magnetic loss can be characterized by the resonance linewidths of the materials and narrow linewidths are indicative of low loss and thus increase the operating efficiency of the device. Barium hexaferrites have remarkably narrow linewidths. Also, materials with a high anisotropy field such as barium hexaferrite reduce the need for external high field magnets because the anisotropy enables the material to operate close to resonance at microwave and millimeter wave frequencies with small applied fields. The operating frequency can be changed by suitably altering the magnetic properties by Co-Ti substitution. By varying the anisotropy field through substitution,

devices can be fabricated in principle, to operate through a wide range of microwave and millimeter wave frequencies.

At present, these materials are grown as bulk crystals. This process produces near-perfect single crystals. However, single crystal bulk materials can be expensive. Also, many hybrid device configurations require that the magnetic materials be in thin film form. Thus considerable effort has been applied by various researchers to fabricate thin hexaferrite films.

The main objective of this project was to produce good quality thin films of substituted and pure barium hexaferrite suitable for device fabrication. In our study, the films were mostly deposited by rf sputtering, followed by a post-deposition annealing. This resulted in polycrystalline films, which were examined for composition, microstructure and magnetic properties. While these polycrystalline films may have good magnetic properties, it is usually not possible to grow thick enough films necessary for device applications by just sputtering. Hence attempts have also been made by various researchers[3] to grow hexaferrite films using the liquid phase epitaxy technique (LPE) which is so successful in producing single crystal garnet films. However, unlike the garnets, suitable lattice matched, inexpensive, non-magnetic substrates are not available commercially. A novel, modified LPE technique was suggested by Yuan et al[4] to grow thick, single crystal films. The first step of this technique involved sputter-depositing a layer of the hexaferrite on a substrate (such as polished sapphire crystals which are approximately lattice matched to the magnetic film). The sputtered film was then post-annealed to form a single crystal or large grain polycrystalline film. Even though the substrates belong to another class of crystal structure, the sputtered films were reported to have good hetero-epitaxy. The sputtered film was then used as a seed crystal for subsequent LPE dipping, using an appropriate melt system. Attempts were made by us to follow this scheme, but our initial results were not encouraging.

In the first part of this report, our work on pure barium hexaferrite is described. The details of the effects of various sputtering conditions on the resulting hexaferrite films are covered. Results on various substrates are also presented. In the second part, the Co-Ti substituted hexaferrites and our attempted LPE growth are described. FMR characteristics are also described.

2. Barium Hexaferrite

2.1 Experimental procedure

Three different choices of substrates were used for the barium hexaferrite films. (1) Vycor (Corning 7913 glass) (2) Single crystal sapphire and (3) thermally oxidized silicon (~5000 Å of thermal oxide). The films were deposited by rf magnetron sputtering in a Leybold Z-400 sputtering system. The target used was a three inch diameter sintered target of the constituent oxides of barium hexaferrites. The target composition was the same as the stoichiometric composition of barium hexaferrite. ($BaFe_{12}O_{19}$) The rf power and the argon pressure are the two sputtering parameters which were varied to determine the optimum sputtering conditions. The sputtered amorphous films were then crystallized by annealing in a tube furnace at 800°C for three hours in air.

The films were characterized by x-ray diffraction to determine the crystal structure of the thin films. Film composition was determined with a Tracor X-ray spectrace 5000 x-ray fluorescence spectrometer. A torque magnetometer was used to measure the effective perpendicular anisotropy. (The anisotropy of pure barium hexaferrite is too large to use any of the standard FMR cavity set-ups in our facility, all of which operate under 33 GHz) The coercivity and saturation magnetization were measured using vibrating sample magnetometer. The film thickness was measured with a Tencor alpha-step 200 profilometer.

2.2 Results

The x-ray diffraction patterns of films deposited on Vycor, sapphire and thermally oxidized silicon (at 25 watts rf power and 5 mTorr argon pressure) are shown on Fig. 1 (a), (b) and (c) respectively. The intensity peaks corresponding to the (006), (008), (00$\underline{14}$) planes of reflections of the magnetoplumbite phase of barium ferrite indicate the perpendicular c-axis orientation. These x-ray diffraction patterns indicate that all three substrates produced films with fairly high degrees of c-axis texture. The x-ray diffraction scans of the deposited films show that essentially only the magnetoplumbite phase is present. The thinness of the films (1000 Å to 5000Å) limits the x-ray detection of other phases to those which are at least five weight percent.[11]

Due to the large difference in thermal expansion of Vycor and barium ferrite, the crystallized films deposited on Vycor sometimes cracked and often the films peeled off fairly easily. The sapphire substrates produced crackless films since their thermal properties are similar to barium hexaferrites. Sapphire also had the closest lattice match with barium ferrite, with a lattice mismatch of approximately seven per cent. The films deposited onto the thermally oxidized silicon substrates were crackless only when the deposited film was less than about 2000Å thick. A good part of this study was done using thermally oxidized silicon as the substrate, since they were fairly inexpensive as compared to sapphire and still produced good quality films.

The reason that 800°C was chosen to be the annealing temperature is shown in hot stage x-ray diffraction data in Fig. 2. With the heating element in the x-ray diffractometer, high temperature x-ray diffraction pattern can be obtained. As shown in the figure, at temperatures below 700°C, sputtered films were in the amorphous state. However, at 800°C, films were very well crystallized with good c-axis orientation perpendicular to the film plane. This indicates that the crystallization temperature of sputtered barium hexaferrite films is within the range between 700°C and 800°C. For consistency, 800°C was chosen as the annealing temperature for the rest of the study described in this report.

Films were deposited with rf input power ranging from 25 watts to 150 watts at an argon pressure of 5 mTorr and with the substrate grounded. X-ray diffraction patterns as a function of rf power are shown in Fig. 3. These figures show that the c-axis texture decreases as the rf power is increased. Again, only the magnetoplumbite phase was detected. In order to estimate the degree of the c-axis orientation, a method proposed by F. K. Lotgering[12] was used. From the x-ray diffraction patterns, the integrated intensities of the (00l) reflections and the integrated intensities for all the (hkl) reflections including the (00l) reflections were calculated. The ratio of the two respective sums are determined for the oriented barium hexaferrite films (p) and for the randomly oriented barium hexaferrite (p_0). From these two values, a quality factor, f, for the orientation is calculated.

$$f = (p-p_0)/(1-p_0)$$

For increasing degree of orientation, f increases from 0.0 (random) to 1.0 (completely oriented) The results of these calculations for the sputtered films are shown in Fig. 4. The calculations indicate a good c-axis orientation at low rf powers.

Rocking curve measurements of the (008) crystal plane for the films are plotted in Fig. 5. The results compare favorably with the results of c-axis texture calculations in Fig. 4. From This figure, it can be seen that the films deposited with low rf power have low dispersion angles of about 6.0 degrees, while those deposited at higher rf power exhibit a broadening of the dispersion.

Using x-ray fluorescence, the barium content of the deposited films was determined. A plot of the barium content as a function of rf power is shown in Fig. 6. It was found that the rf power had very little influence on the barium content of the films.

The change in the effective anisotropy with rf power is shown in Fig. 7. The decrease in the perpendicular anisotropy with rf power was consistent with the results of the x-ray diffraction patterns, in that the degree of perpendicular orientation decreased with increasing power. The saturation magnetization and perpendicular coercivity plots as a function of increasing rf power are shown in Figs. 8 and 9, respectively. It can be seen from these plots that the magnetization decreased with rf power, while the coercivity increased with rf power. Films were deposited at argon pressures ranging from 5 mTorr to 25 mTorr at a constant rf power of 25 watts and with the substrate grounded. X-ray diffraction data of films deposited at various pressures are shown in Fig. 10. The diffraction patterns indicate a decrease in the c-axis texture with increasing argon pressure. The effects of increasing the argon pressure on the barium content is shown in Fig. 11. There was a noticeable increase in the barium content as compared to stoichiometry, as the argon pressure was increased.

The decrease in the c-axis texture with increasing argon pressure is also indicated by a decrease in the effective anisotropy constant as shown in Fig. 12. The changes in the magnetization and perpendicular coercivity are plotted in Figs. 13 and 14, respectively. These results are similar to those from films which were deposited at different rf powers.

2.3 Discussion

The crystal structure and magnetic properties are highly dependent on the composition of the deposited films. As shown in Figs. 4-6, barium content varies very little from that of the stoichiometric target composition when sputtered with different rf powers. However, the barium content increased when the argon pressure was increased (Figs. 4-

11). These results indicate that the deposition of films with target stoichiometry are highly sensitive to the argon pressure.

Increasing the rf power has the effect of increasing the number of ions and energetic electrons bombarding the substrates which in turn will increase the substrate temperature and resputtering of the deposited film. It is possible that such high substrate temperatures would result in the nucleation of small barium hexaferrite crystals, which could not be detected by standard x-ray diffraction procedure. During the post-deposition annealing process, these small randomly oriented crystals would grow, producing films with increasing randomness. Sophisticated techniques such as microdiffraction might be used to detect these microcrystals and verify this hypothesis.

As a measure of how well the c-axis texture is dispersed, a low $\Delta\theta_{50}$ of about 6.0 degrees was obtained for films deposited at low power. However, this is not as low as those reported by Morisako et al.[13,14] The trends in the coercivity and anisotropy correlated well with the crystal texture, in that as the degree of c-axis texture decreased, there was a corresponding decrease in the uniaxial anisotropy and an increase in coercivity.

The increase in the barium content of the deposited films at higher pressures could possibly be explained by the increase in the scattering of iron in the plasma. This resulted in films which have higher barium content. The issue of argon incorporation in the films was not significant since any argon trapped is released during the annealing process. The degree of c-axis texture of the films decreased with excess barium, which could be present in the form of amorphous phases of barium. This, in turn, resulted in the changes seen in the magnetization. However, this change in magnetization is not monotonic and at present we haven't been able to explain the trend observed in M_s (Fig. 13) due to changes in argon pressure.

By comparing with the M_s value for bulk barium hexaferrite, which is 380 emu/cc, the M_s for our initial thin films was about 250 emu/cc, almost 35% lower. Since saturation magnetization is an intrinsic property of a specific material, the low M_s indicates that films are not pure barium hexaferrite. Therefore, considerable efforts were made to diagnose this problem.

Saturation magnetization as a function of film thickness was measured and is shown in Fig. 15. All of the films were sputtered at an argon pressure of 5 mTorr and a

sputtering power of about 25 watts. Apparently, there is a problem in obtaining good barium hexaferrite in the initial layers of the film, because when the film is thin, even up to 1000Å, M_s is very low. For thick films, M_s reaches its highest value of about 250 emu/cc, which is still lower than the value for bulk material by almost 35%. Crystal anisotropy measurements show a similar behavior as shown in Fig. 16. X-ray diffraction patterns have already shown that only the magnetoplumbite phase is present in the film. What it doesn't show is whether the amorphous phase exists or not. We believe there is an amorphous phase present in the film because the amorphous phase for barium ferrite is non-magnetic. Thus, only part of the film, which is magnetic, contributes to the saturation magnetization and the magnetocrystalline anisotropy. This is why these two parameters are lower than for bulk material.

Film density and composition were also studied on the same films by using x-ray fluoresence. Results are shown in Figs. 17 and 18. The film density follows a very similar trend with thickness as the magnetization and anisotropy. Thin films exhibit low density, but even thick films have a lower density than bulk, which is 5.28 g/cc for barium hexaferrite single crystals. This low density could be caused by porosity, the presence of other phases or the existence of an amorphous phase in the film because, usually, the amorphous phase has a lower density than that of crystals, due to the fact that crystals have close-packed structure. Composition measurements indicate that these films do not have the correct composition to form single phase barium hexaferrite. The BaO content is about 2 mole% lower than the single phase region as shown in Fig. 18. This hinders the crystallization process of the film. This also suggests that the sputtering target composition needs to be further modified in order to maintain the correct single phase in the film.

A new target with composition of $Ba_{1.25}Fe_{12}O_{19}$ was then used in order to increase the barium content in the film. Sputtering parameters like argon pressure and rf power had very similar effects on film's magnetic properties as it did for the first target. Films deposited at an argon pressure of 5 mTorr and an rf power of 20 watts had the correct stoichiometric composition and very good c-axis orientation. Their M_s value reached 350 emu/cc, which is close to the bulk value. For comparison, the M_s vs sputtering power for the two different targets are plotted in Fig. 19. However, an interesting event arises. For the first target, when the film is thinner than 1000Å, it is seldomly crystallized. But, for the second target, even when the film is as thin as 500Å, it is still very well crystallized. The exact reason for this difference is not clear at present. Perhaps the crystallization process is very sensitive to the film composition. As shown in the standard

barium ferrite phase diagram (Fig. 20), M-type hexaferrite single phase can only be formed in the composition range between $BaFe_{12}O_{19}$ and $Ba_{1.20}Fe_{12}O_{19}$, noticing that barium content should be a little higher than or equal to its stoichiometry. The increasing of the M_s value is also, at least partially, due to the elimination of the initial layer problem existing in the film deposited from the first target.

Although the M_s value has been increased close to the bulk value, the magnetocrystalline anisotropy of the film measured by torque magnetometer (about $2.1x10^6$ erg/cc) was still lower than the bulk anisotropy which is reported as $3.3x10^6$ erg/cc in the literature. Imperfect crystal c-axis orientation might be the cause. Therefore, an alternate film crystallization approach was tried: an in-situ substrate heater was used during sputtering. It is expected that this will ultimately improve the crystallization of the films. Recently, a substrate heater with the capability of heating the substrate to a maximum temperature above 900°C was successfully installed in our Leybold z-400 sputtering system. An initial problem was bad thermal contact between the substrate and heater plate. This was solved by putting silver paste on back of the substrate. Sputtered films deposited onto SiO_2/Si substrates at a temperature of 800°C were crystallized as shown by x-ray diffraction measurement in Fig. 21. However, the spinel Fe_3O_4 phase with (111) direction perpendicular to the film plane was dominant. This indicates that oxygen might need to be mixed into the sputtering gas to reduce the amount of Fe^{2+} ions. When Ar/O_2 mixed sputtering gas was used, other phases appeared. X-ray fluoresence measurements showed that the barium content in these films deposited by reactive sputtering was significantly depleted. This is believed to be caused by re-sputtering effects due to the reactive sputtering gas. Therefore, the barium content in our target needs to be further increased.

2.4 Conclusion

Polycrystalline barium hexaferrite thin films have been successfully deposited by rf magnetron sputtering onto inexpensive, thermally oxidized silicon substrates. The effects of the sputtering conditions on the composition, crystal structure and magnetic properties have been determined. Increasing the rf power decreases the quality of c-axis texture with little effect on the composition of the deposited films. These films showed increasing perpendicular coercivity and decreasing magnetization with increasing rf power. Increasing the argon pressure had similar effects of reducing the c-axis texture, increasing the coercivity and decreasing the magnetization. However, the barium content increased with increasing argon pressure.

The low M_s value of our initial films is due to the composition deviation from its stoichiometry and poor crystallization of the initial film layer. A significant increase in M_s was achieved by using a new target with composition of $Ba_{1.25}Fe_{12}O_{19}$. The low magnetocrystalline anisotropy is believed to be caused by the imperfect crystal c-axis orientation. An 'in-situ' crystallization approach is being tried to solve this problem.

The films deposited at 20 watts and 5 mTorr argon pressure, possessed the best degree of c-axis texture perpendicular to the film surface and good c-axis orientation. The well textured films had large uniaxial anisotropies H_k of approximately 13 KOe. These films had saturation magnetization values ranging from 320 to 350 emu/cc and large room temperature coercivities ranging from 1 KOe to 3 KOe. These films are the most promising candidates for potential applications.

3. Co-Ti Substituted Barium Hexaferrite

One of the motivations for the study of substituted barium hexaferrites is to examine the change in uniaxial anisotropy, from about 18 KOe for pure barium hexaferrite to about zero for the substitution of about one formula unit of cobalt ions as shown in Fig. 22a. The magnetization, however, decreases only marginally,[16] as shown in Fig. 22b. Such altering of the Q value (defined as $H_k/4\pi M$) results in a wide range of operating frequencies for a microwave/millimeter wave device fabricated using these films. Studies of Domain Mode Ferromagnetic Resonance (DMFMR) were carried out on this class of materials.

Growth of substituted hexaferrites pose several challenges in addition to the difficulties associated with the growth of pure barium ferrites. For example, the uniaxial anisotropy is a very sensitive function of cobalt substitution and hence the stoichiometry has to be controlled very carefully. This in turn necessitates a careful study on the effect of sputtering parameters on the resulting stoichiometry.

The selection of a suitable substrate is even more of a problem in case of Co-hexaferrites. Unlike garnets, (which have cubic unit cells and thus only one dimension needs to be matched between the substrate and film) hexaferrites need to have substrates that are matched both along the basal dimension and along the hexagonal dimension. And, a small amount of substitution tends to vary the lattice constants considerably and thus specific substrates need to be found for specific compositions. Other researchers have used

substrates like specially tailored spinels and hexagallates, with mixed results. Recently, a novel technique was proposed by Yuan et al[4], where the authors first sputter-deposited a thin layer (~0.2μm) of ferrite on a suitable substrate and then annealed the sputtered films to achieve reasonable epitaxy. The sputtered ferrite layer was then used as a substrate for subsequent LPE dipping. This technique was used in our LPE study, and sapphire single crystal was chosen as the substrate.

3.1 Experimental Procedures and Results

The rf sputtering was done using a Leybold Z-400 sputtering machine and the composition of the target used was $BaCo_{1.0}Ti_{1.0}Fe_{10}O_{19}$. Like the pure barium hexaferrite target, this too was a sintered oxide target. The substrates used were polished sapphire and thermally oxidized silicon wafers. The composition was studied as a function of sputtering parameters such as rf power, argon pressure, DC bias voltage and partial pressure of other gases such as oxygen, when used. The resulting film compositions were determined using an x-ray fluorescence spectrometer and correlated to the sputtering parameters. The variation of the composition with respect to the sputtering parameters is shown in Figs. 23 through 26. It was found that changing some parameters such as the bias voltage can change the cobalt content in the film by as much as 1%.

The substituted films also showed a remarkably good c-axis texture as did the pure hexaferrites. The x-ray diffraction spectrum of a typical film deposited on sapphire at 25 watts and at 5 mTorr of argon pressure is shown in Fig. 27. Parameters such as rf power affected the c-axis orientation of the annealed film, much in the same fashion as for the unsubstituted films.

The annealing cycle of these sputtered films was studied systematically. The sputtered films were annealed by introducing them slowly into a furnace and holding them at the annealing temperature for a suitable period of time. The crystals start to nucleate at a temperature called the 'nucleation temperature', which is around 800°C for the substituted hexaferrite films depending on the composition. The nucleated grains start to grow in size at a higher temperature called the 'growth temperature'. In order to grow large sized crystal grains, we must nucleate as few grains as possible and let the few nucleated grains grow in size. Nucleation of a small number of grains was possible by quickly introducing the film to the nucleation temperature, by physically lowering it down a vertical furnace through a zone at the nucleation temperature. Then the grains are enlarged by keeping the film above

the growth temperature (at a temperature which we refer to as the annealing temperature) for a sufficient time. It was determined that a higher annealing temperature (875 degrees compared to 800 degrees in case of pure barium ferrite) was necessary to crystallize the substituted films.

The perpendicular ferromagnetic resonance spectra of these films were measured after each annealing cycle. Since the anisotropy fields of these films were smaller than pure hexaferrites, (on the order of 1500 Oe) perpendicular FMR signals were obtained at frequencies as low as 4 MHz using a mini-box FMR apparatus. This is the first time such low frequency FMR signals have been observed in hexaferrites. A typical signal is shown in Fig. 28 and a series of signals corresponding to a few frequencies are shown in Fig. 29. The FMR linewidth, which is related to the device losses, is required to be small. The extrinsic part of the FMR linewidth is in part due to the grain size of the polycrystalline films. The grain size in turn is affected by the annealing process. The effect of grain size on the ferromagnetic resonance linewidth can be seen by examining the FMR spectra taken after each annealing temperature. The narrowing of the FMR linewidth after repeated annealing is shown in Fig. 30. The FMR linewidths in these polycrystalline substituted hexaferrites are about 200 Oe.

3.2 LPE of hexaferrites

We also attempted to grow single crystal ferrite thin films using the modified LPE technique. As a first step, we only looked into the simplest system, namely the pure barium hexaferrite. Sputtered pure barium ferrites on single crystal sapphire, thermally oxidized silicon and glass were used as seed crystals. Two melt systems, one based on bismuth oxide and another melt based on boron oxide/barium carbonate were developed. While the bismuth oxide based melt attacked the substrate and the sputtered film, the boron oxide based melt seemed promising. In the latter melt, barium carbonate (which plays the dual role of film and flux constituent) was used instead of barium oxide due to its lower melting point. Additional problems arose when the melt went into solution, because the carbonate decomposed into oxide releasing carbon dioxide, which caused the melt to splatter. A barium temperature tried was around 930 degrees, which was much higher than the typical garnet growth temperatures. At higher temperatures, the sputtered seed film decomposed and at lower growth temperatures, poorer quality films resulted. The melt had the following nominal composition:

$BaCO_3$	351.10 gms
B_2O_3	70.75 gms
Fe_2O_3	84.41 gms

The LPE films, under the best of conditions, were not as good as sputtered films. Our biggest problems were (1) presence of other phases in the LPE films (2) very high growth rates, resulting in poor quality films and (3) flux adhesion. The thick films tended to peel off (together with the sputtered film). Some pieces of these peeled films were used to characterize the LPE growth. The films were usually over 100 microns thick for typical growth times of a few minutes and typically only about a third of this was magnetic. This was also confirmed by x-ray fluorescence data, where it was found that nearly 70% of the composition was due to barium oxide. Although dilute nitric acid has been reported in the literature as an agent to remove flux, we found it ineffective. The magnetic moment of one such piece was measured using a vibrating sample magnetometer (Fig. 31) and was found to be about ten times smaller than that of a typical barium hexaferrite film. This was further evidence of the presence of non-magnetic phases.

3.3 Discussion of LPE of hexaferrites

Although methods described in the literature were followed, attempts to grow high quality films by LPE were not successful. One major difference between our technique and the one we had been attempting to duplicate was that the substrate was heated to a high temperature during sputtering in the case of Yuan et al. This provision to heat the substrate was recently installed in our Z-400 sputtering system. Substrate heating results in 'in situ' crystallization, which in turn produces better c-axis texture.[17,18,19]

The role of grain size of the sputtered film in the subsequent LPE growth is not understood at present. While Yuan et al had described getting large grain sizes, some other researchers hold the opinion that even submicron sized grains can be suitable seeds, if the c-axis texture is excellent.[20]

3.4 Conclusion

Sputter-deposition of substituted barium hexaferrites was studied extensively and it was found that good quality sputtered films can be fabricated with suitable magnetic

properties. However, the deposition rate of sputtered films is low and, techniques such as LPE would be desirable to produce thicker films. Initial experiments with LPE have not been promising. Perfect c-axis orientation of the thin ferrite underlayer is desirable. Future studies of 'in-situ' crystallization processes during sputtering appear to hold promise for producing improved ferrite layers.

4. References

1. H. Machida, F. Ohmi, Y. Sawada, Y. Kaneko and H. Nakamura, "Magneto-optical Properties and Thermo-magnetic Recording of M-type Ba-ferrites", *J. Mag. and Mag. Materials.*, 54-57, 1986, 1399-1400.

2. A.Watada, Y. Kaneko, I. Miyamoto, F. Ohmi, Y. Sawada, H. Nakamura and H. Machida, "Multiple Reflection Effect on Co substituted Ba-ferrite for Magneto-optical Recording Media", *IEEE Trans. Mag.*, MAG-23, 1987, 2961-2962.

3. H. L. Glass and J. H. W. Liaw, "Growth and Characteristics of LPE Hexagonal Ferrites", *J. Appl. Phys.*, 49, 1978, 1578-1581.

4. M. S. Yuan, H. L. Glass and L. R. Adkins, "Epitaxial Barium Hexaferrite on Sapphire by Sputter Deposition', *Appl. Phys. Lett.*, 53, 1988, 340-341.

5. W. B. Zeper, F. J. A. M. Gredanus, P. F. Carcia and C. R. Fincher, *J. Appl. Phys.* 65, 1989, 4971.

6. Y. Ochiai, S. Hashimoto and K. Aso, *IEEE Trans. Magn.* 25, 1989, 3179.

7. W. B. Zeper, F. Greidanus and P. F. Carcia, *IEEE Trans. Magn.* 25, 1989, 3764.

8. M. Gomi, T. Tanida and M. Abe, "Rf Sputtering of Highly Bismuth Substituted Garnet Films on Glass Substrates for Magneto-optical Memory", *J. Appl. Phys.*, 57, 1985, 3888-3890.

9. W. Eppler and M. H. Kryder, "The Effect of Sputtering Conditions on Bismuth Doped Gadolinium Iron Garnet Films", *IEEE Trans. Mag.*, MAG-25, 1989,3743-3745.

10. L. Shono, M. Gomi and M. Abe, "Magneto-optical Properties of Magnetoplumbites $BaFe_{12}O_{19}$, $SrFe_{12-x}Al_xO_{19}$ and $PbFe_{12}O_{19}$", *Jap. J. Appl. Phys.*, 21, 1982, 1451-1454.

11. H. P. Klug and L. E. Alexander, X-ray Diffraction Procedures for Polycrystalline and Amorphous Materials, Wiley, New York, 1954.

12. F. K. Lotgering, "Topotactical Reactions with Ferrimagnetic Oxides Having Hexagonal Structure", *J. Inorg. Nucl. Chem.*, 9, 1959, 113-123.

13. A. Morisako, M. Matsumoto and M. Naoe, "C-axis Orientation of Hexagonal Ferrite Films Prepared by Rf Diode Sputtering", *J. Magn. Magn. Mats.*, 54-57, 1986, 1657-1658.

14. A. Morisako, M. Matsumoto and M. Naoe, "Ba-ferrite Thin Film Rigid Disk for High Density Perpendicular Magnetic Recording", *IEEE Trans. Mag.*, MAG-22, 1986, 1146-1148.

15. M. Matsuoka, Y. Hoshi, M. Naoe and S. Yamada, "Formation of Ba-ferrite Films with Perpendicular Magnetization by Target-facing Type of Sputtering", *IEEE Trans. Mag.*, MAG-18, 1982, 1119-1121.

16. D. J. De Bitetto, *J. Appl. Phys.*, 35, 1964, 3482.

17. P. Gerard, E. Lacroix, G. Marest, B. Blanchard, G. Rolland and B. Bechever, "Crystallization Phenomena in Thin Films of Amorphous Barium Hexaferrite", *Sol. State Comm.*, 71, 1989, 57-62.

18. P. Gerard, E. Lacroix, G. Marest, M. Dupuy, G. Rolland and B. Blanchard, "Annealing Effect on the Properties of Crystalline Barium Hexaferrite Films", *J. Mag. Mag. Mats.*, 1990, 13-14.

19. E. Lacroix, P. Gerard, G. Marest and M. Dupuy, " Substrate Effects on the Crystalline Orientation of Barium Hexaferrite Films", *To be published*

20. P. Gerard, *Private communication*

21. K. -H. Hellwege and A. M. Hellwege , editors, Landolt-Bornstein Numerical Data and Functional Relationships in Science and Technology, III/4b, "Magnetic Oxides and Related Compounds", Springer-Verlag Berlin, Heidelberg, New York, 1970.

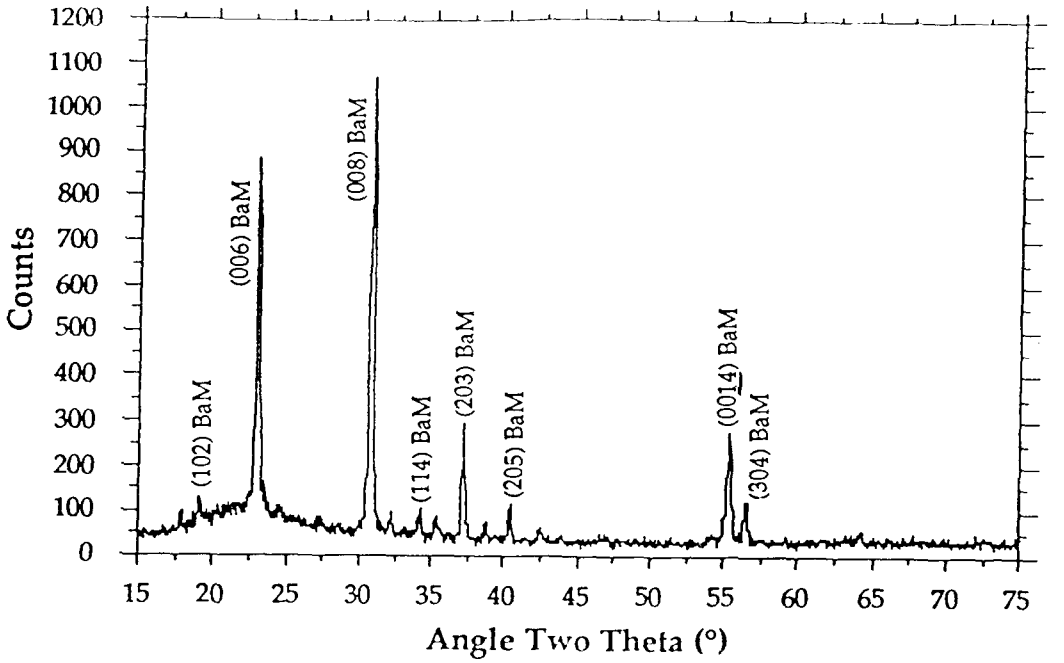

(a)

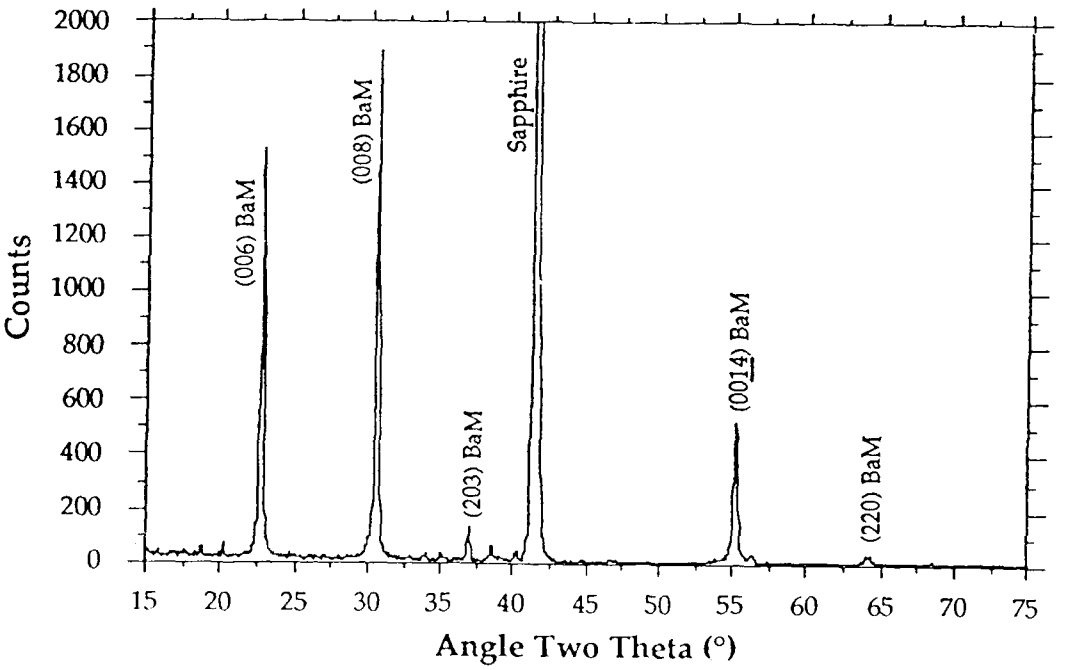

(b)

Figure 1: X-ray diffraction patterns of barium hexaferrite films deposited on (a) Vycor and (b) sapphire.

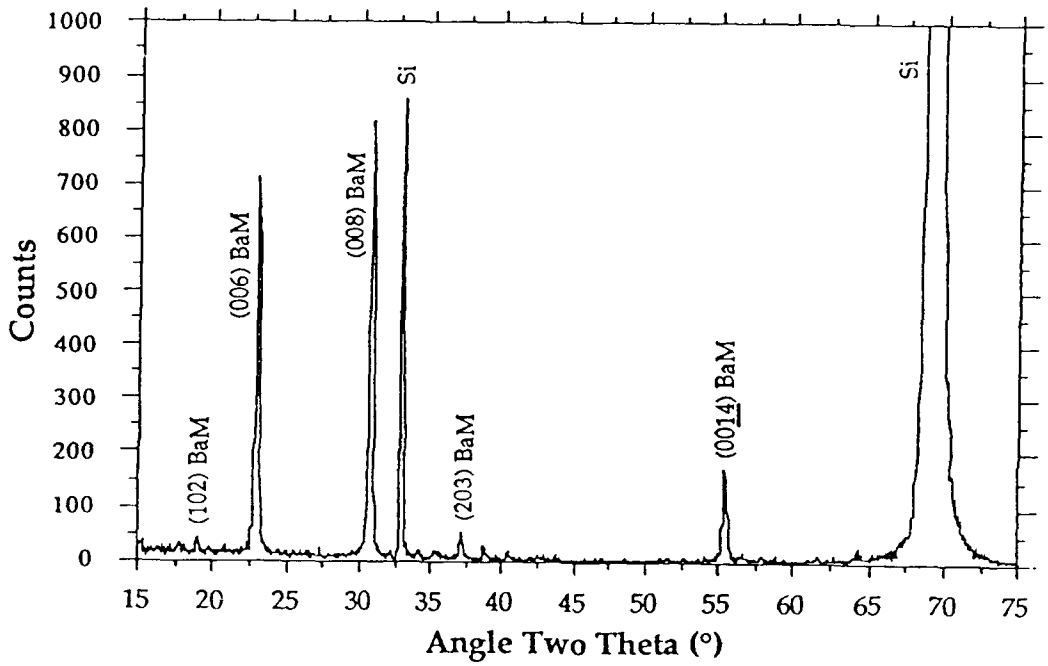

(c)

Figure 1: X-ray diffraction patterns of barium hexaferrite films deposited on (c) thermally oxidized silicon.

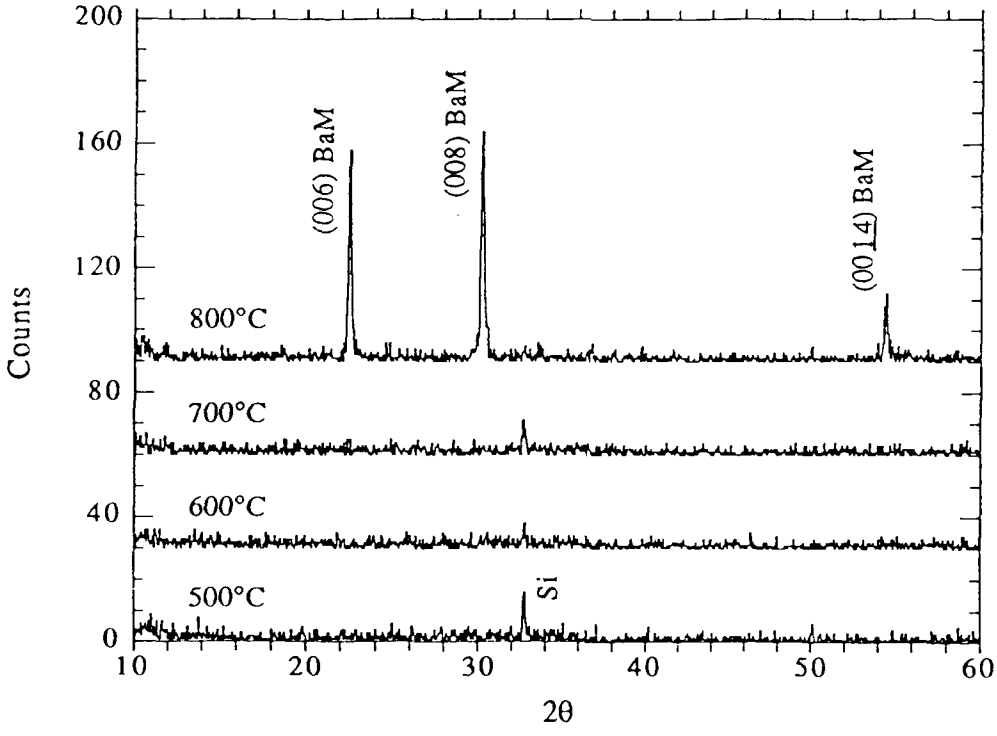

Figure 2: Hot stage x-ray diffraction patterns at different temperatures

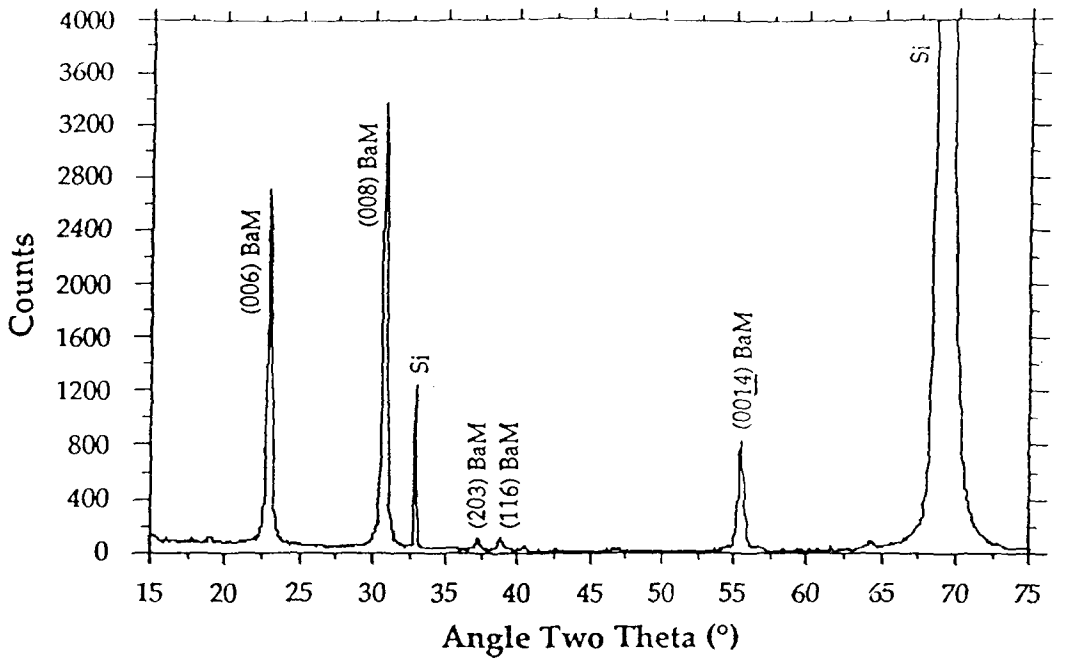

(a)

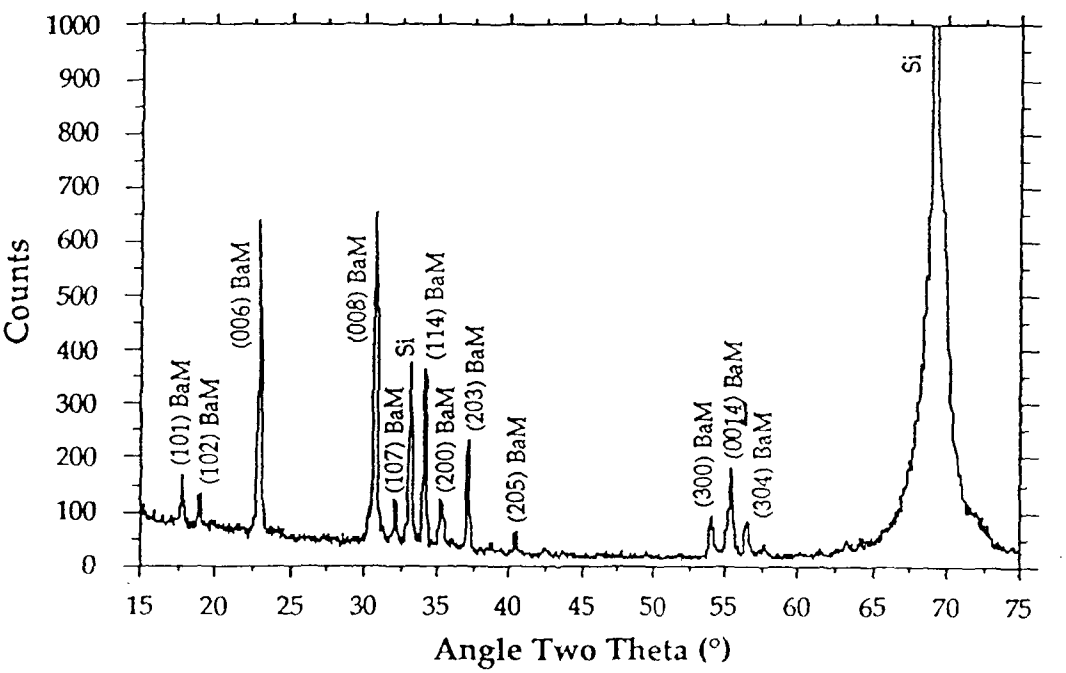

(b)

Figure 3: X-ray diffraction patterns for films deposited at rf powers of (a) 25 Watts and (b) 100 Watts.

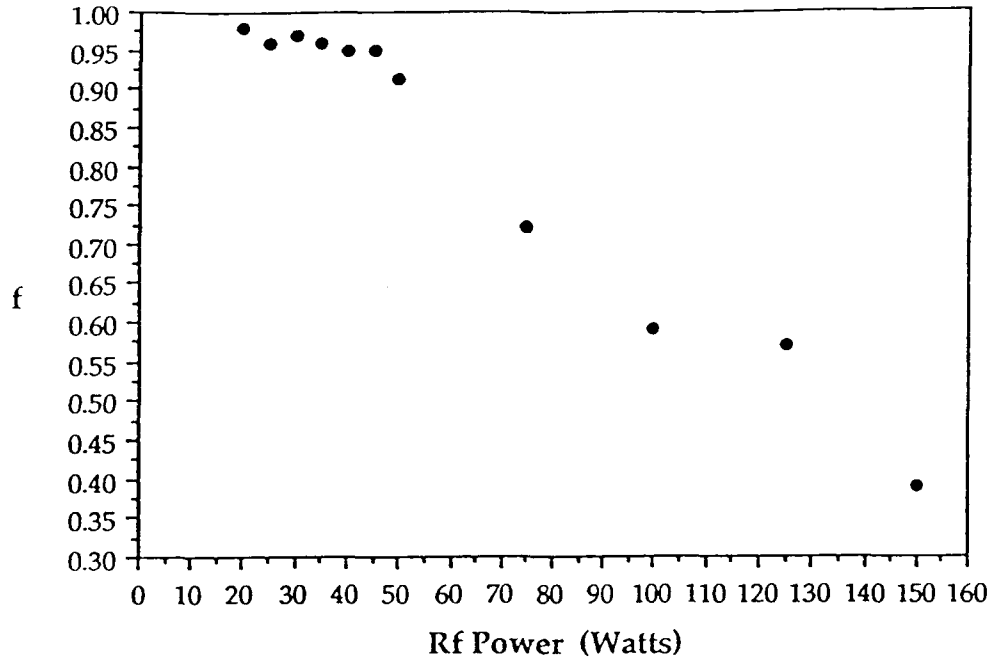

Figure 4: Changes in the degree of c-axis texture due to increased sputtering power.

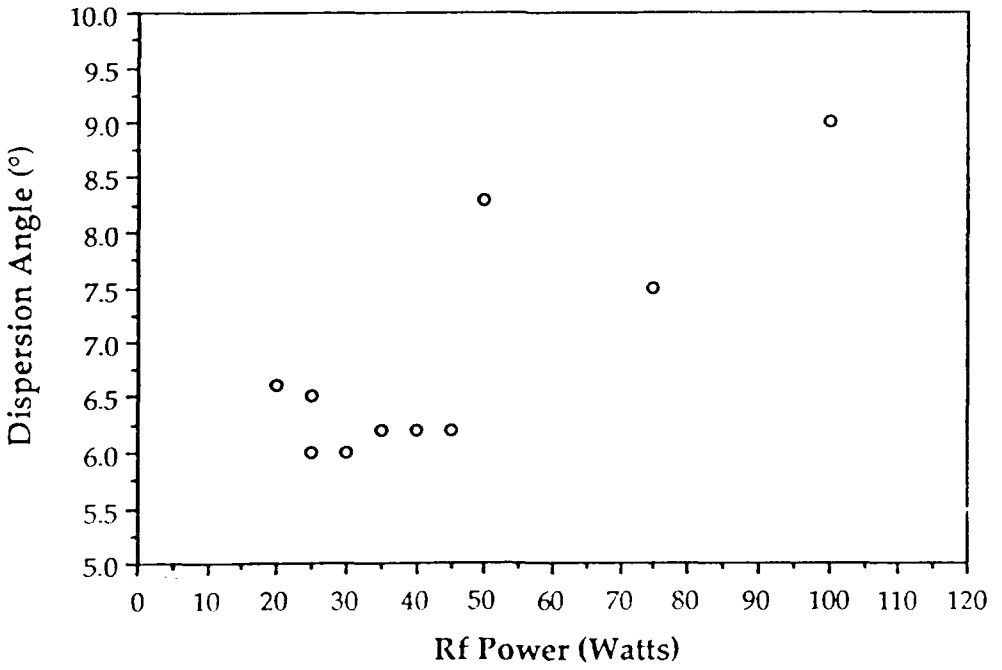

Figure 5: Rocking curve measurements for films deposited at different rf powers.

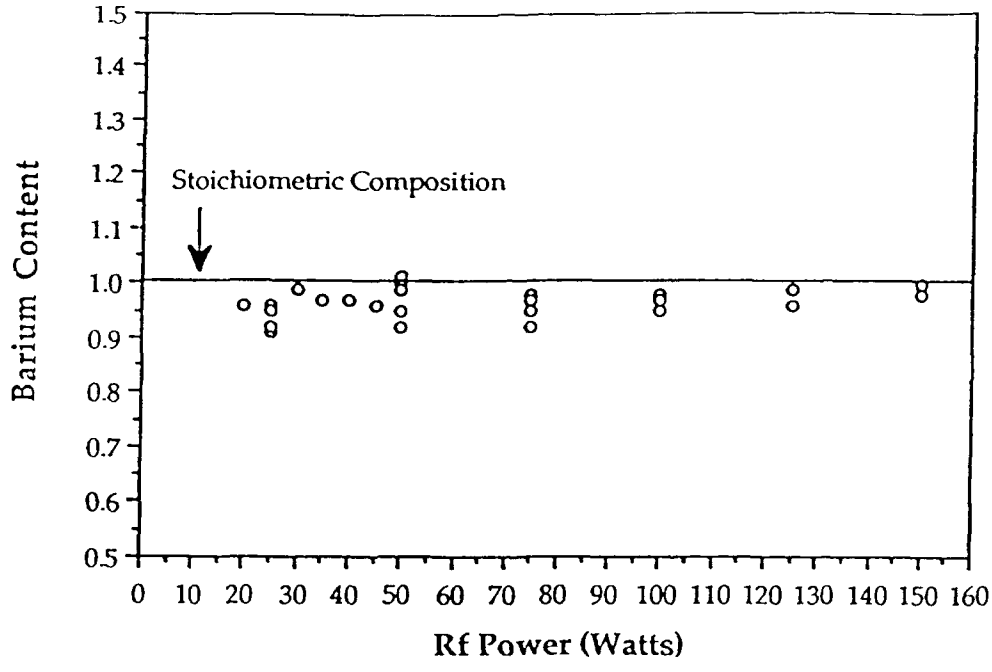

Figure 6: Barium content as a function of rf power.

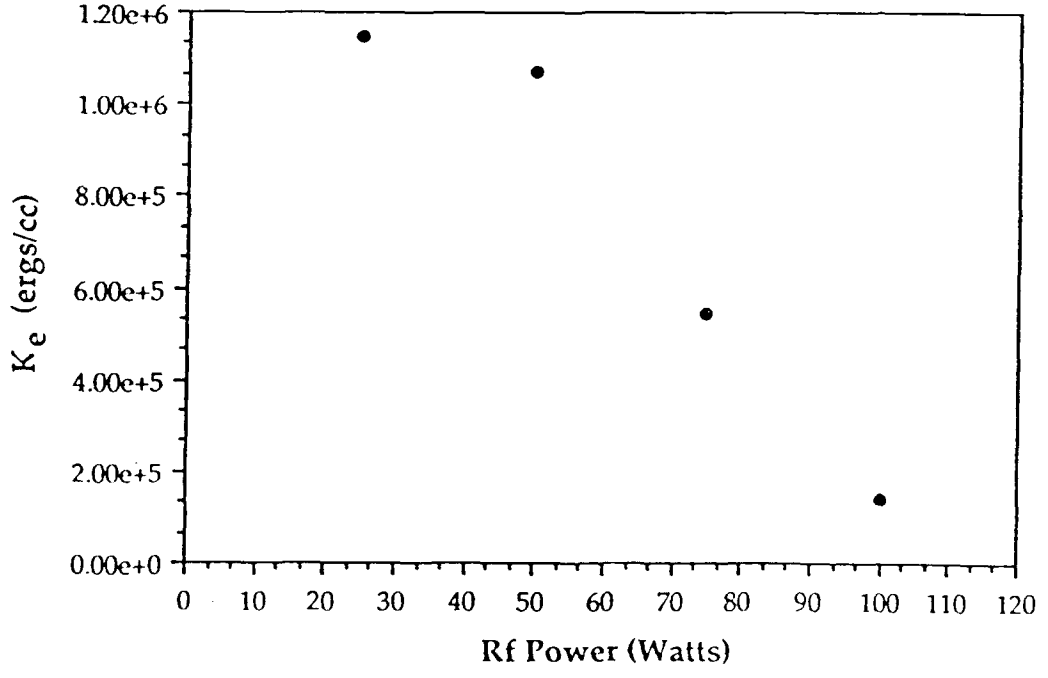

Figure 7: Effective perpendicular anisotropy constant as a function of rf power.

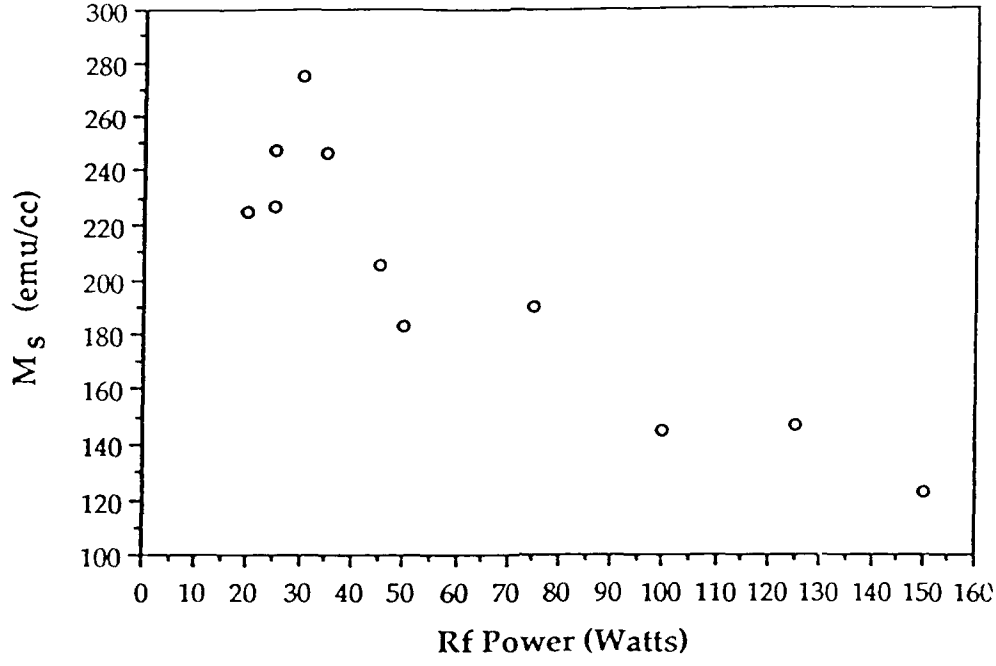

Figure 8: Saturation magnetization as a function of rf power.

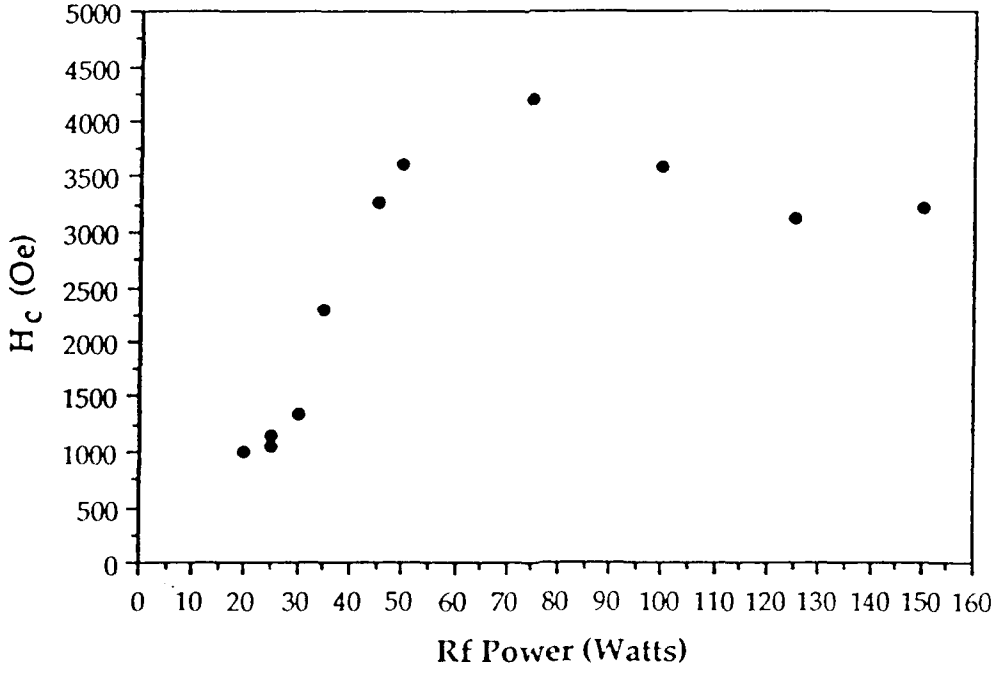

Figure 9: Perpendicular coercivity as a function of rf power.

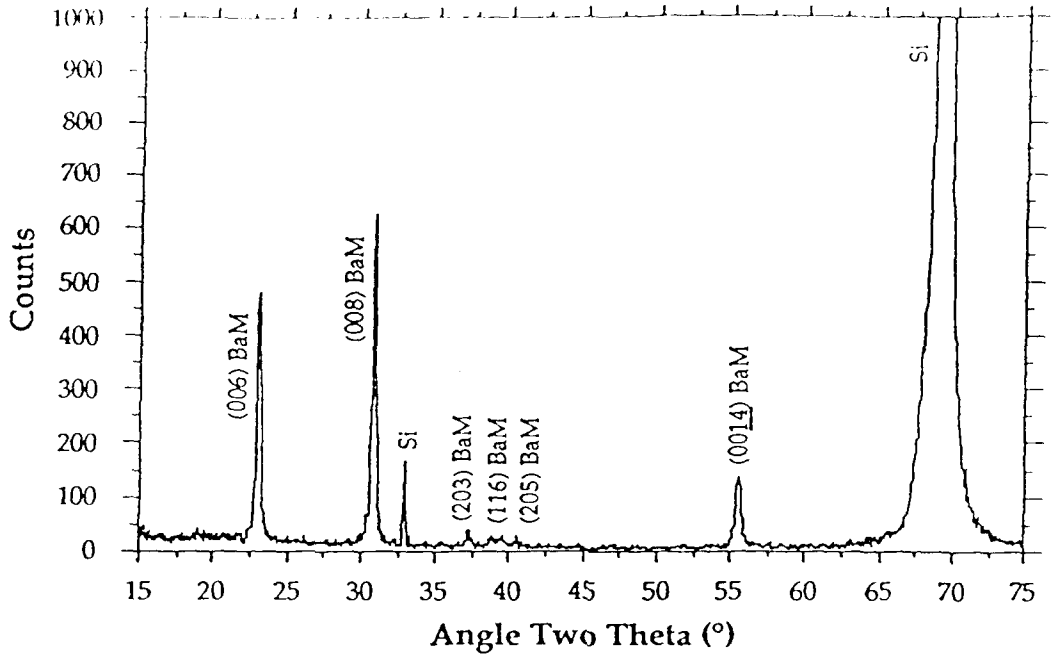

(a)

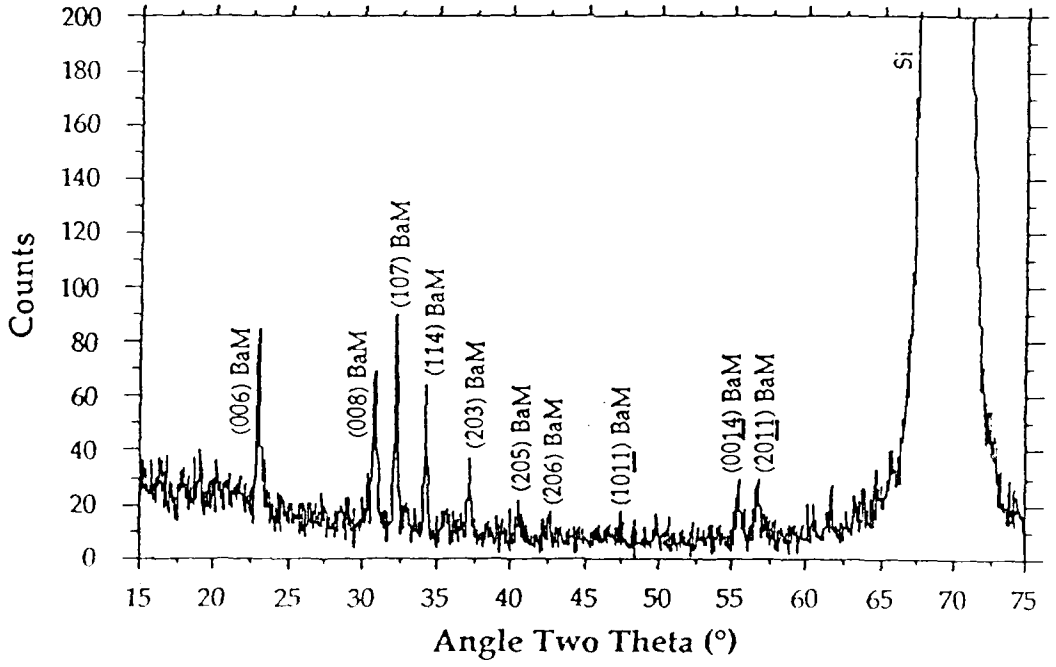

(b)

Figure 10: X-ray diffraction patterns of films deposited with argon pressures of (a) 5 mTorr and (b) 25 mTorr.

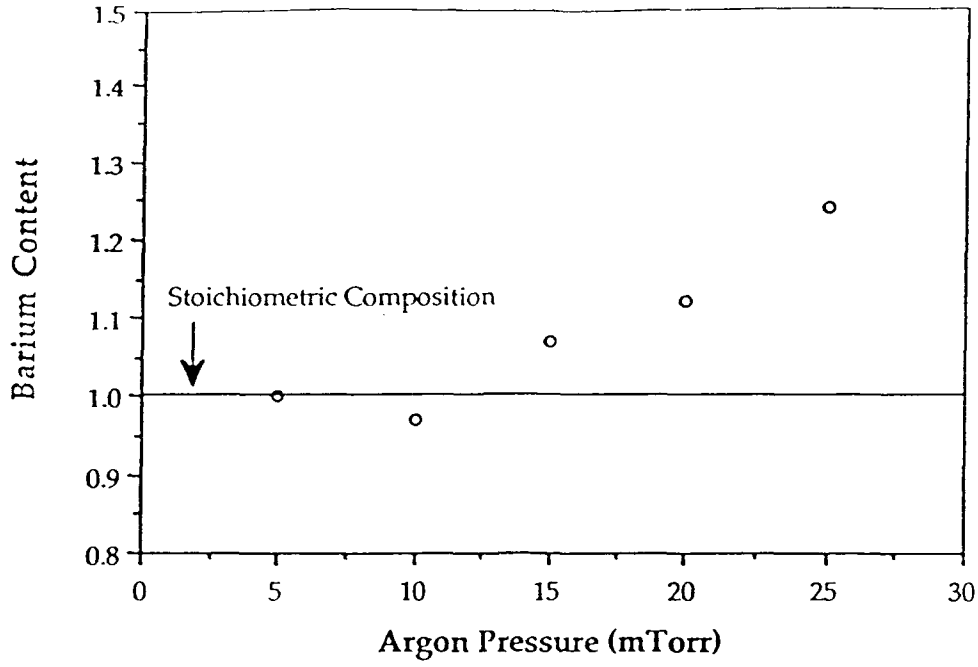

Figure 11: Changes in the barium content with argon pressure.

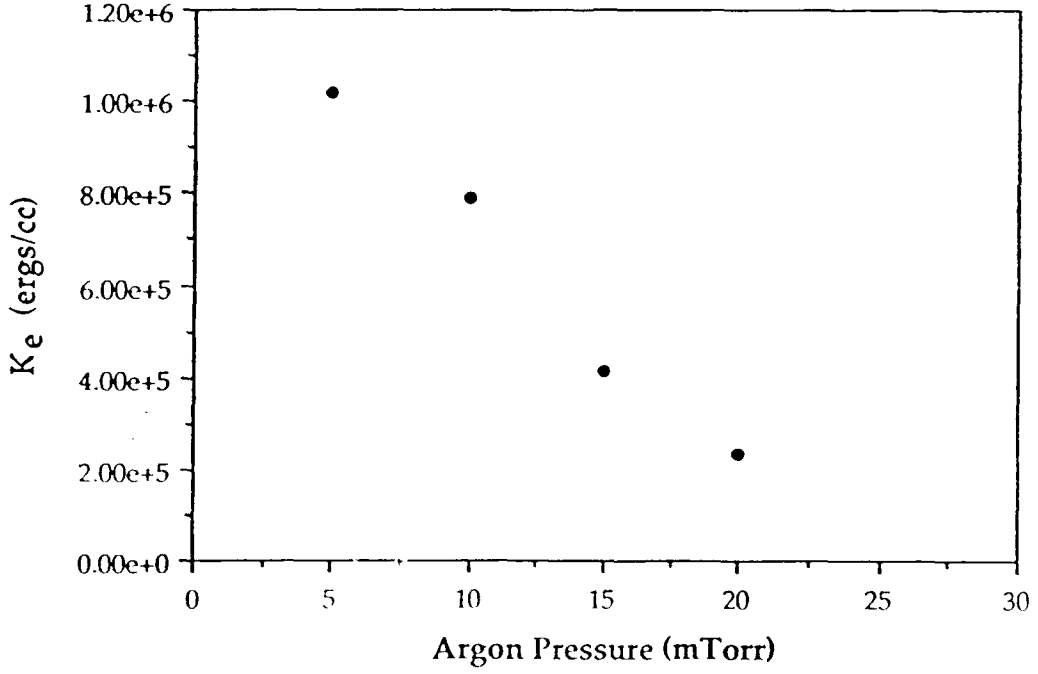

Figure 12 : Changes in the effective anisotropy constant with argon pressure

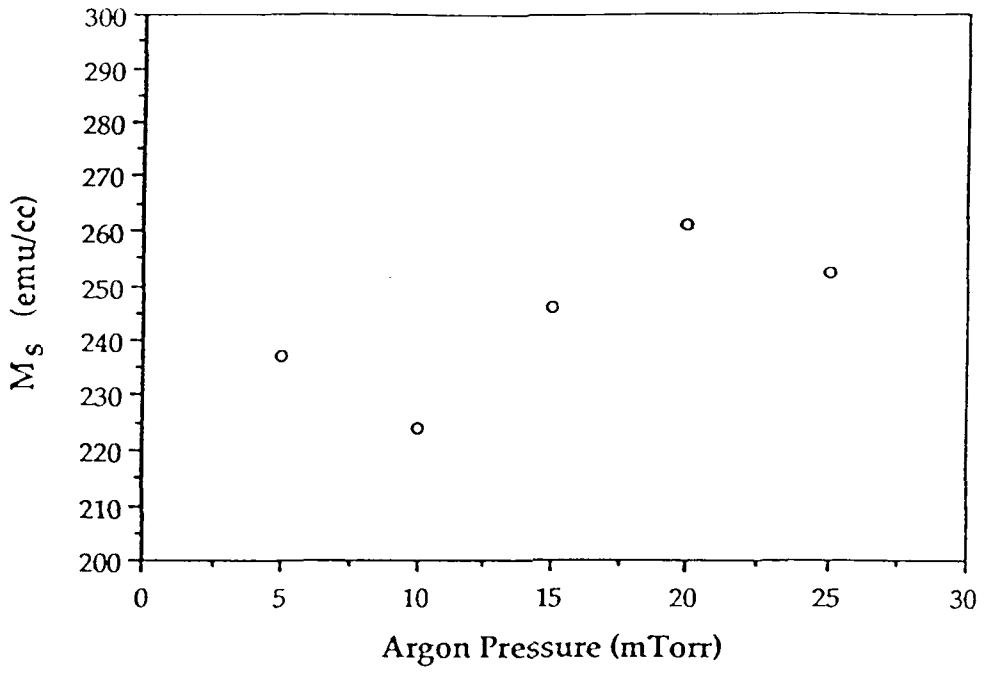

Figure 13: Changes in the magnetization as a function of argon pressure.

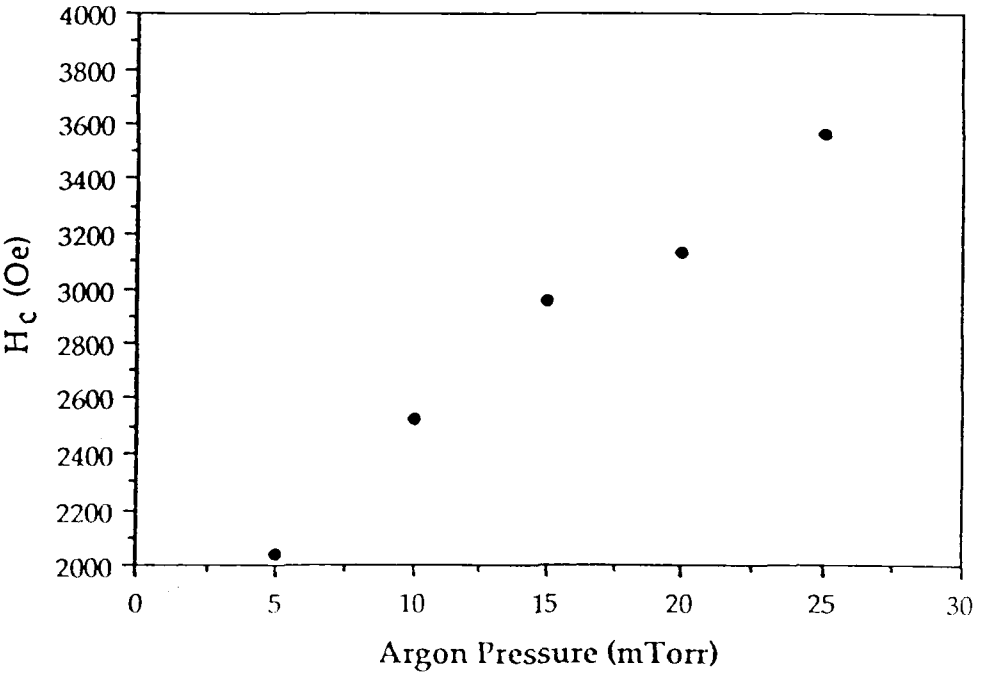

Figure 14: Changes in the perpendicular coercivity as a function of argon pressure.

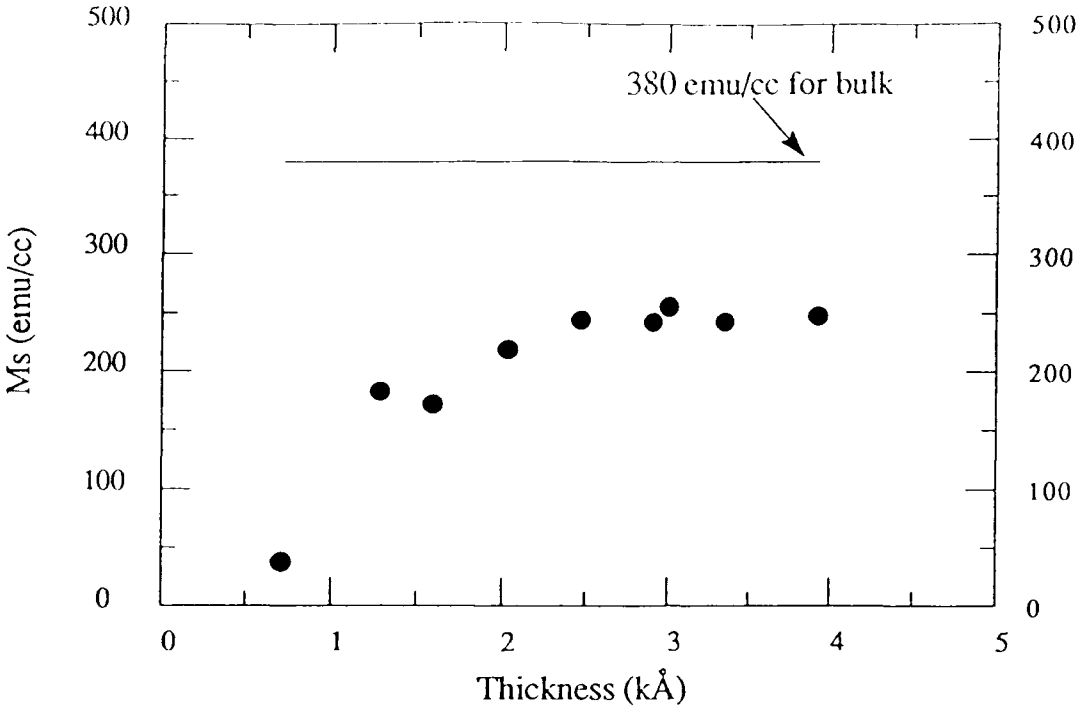

Figure 15: Saturation magnetization as a function of film thickness

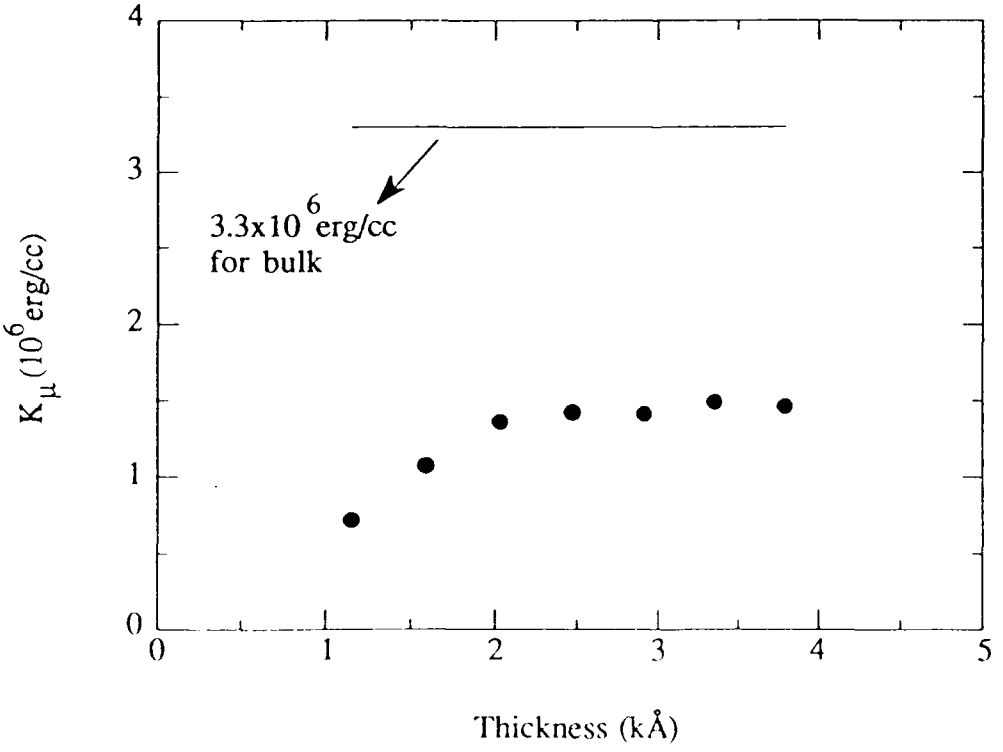

Figure 16: Crystal anisotropy as a function of film thickness

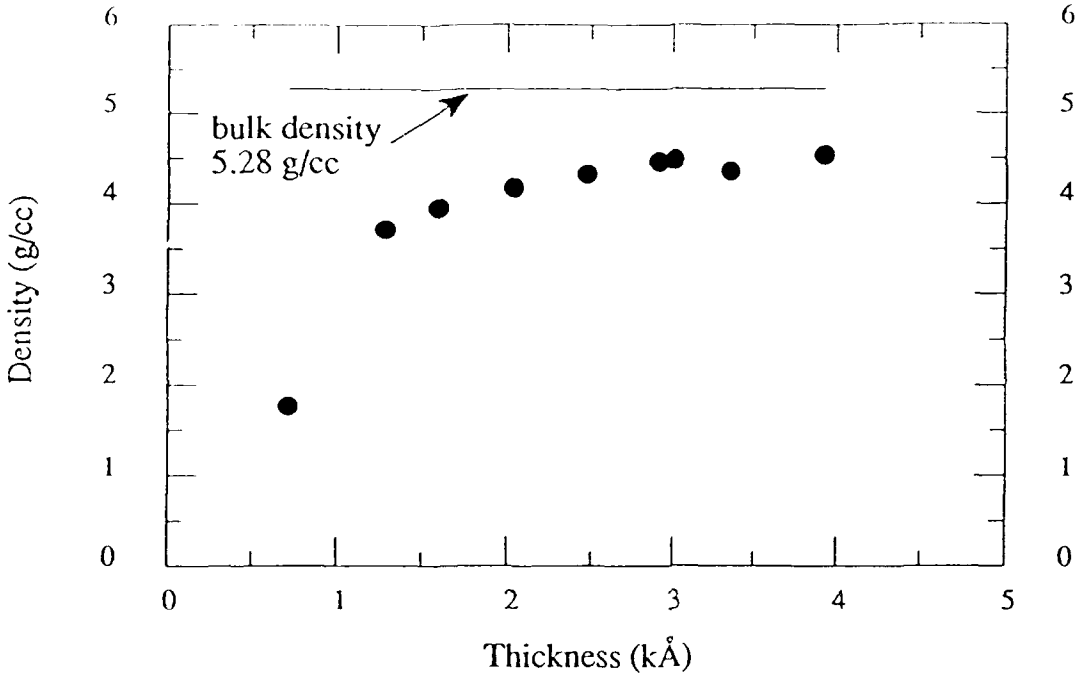

Figure 17: Film density as a function of film thickness

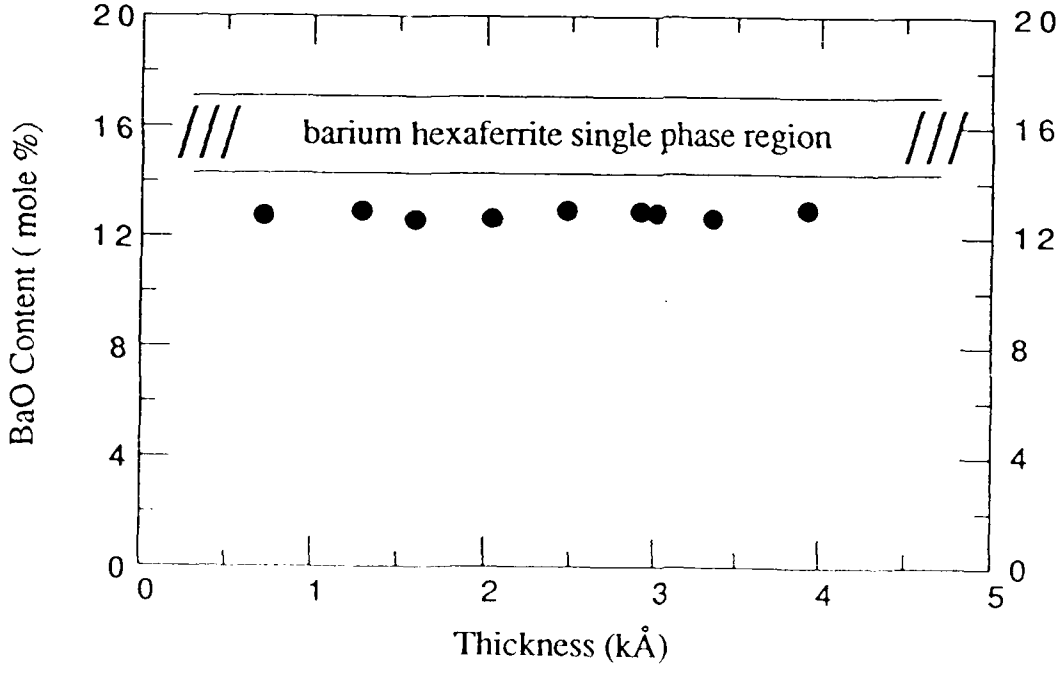

Figure 18: Film composition for various film thickness

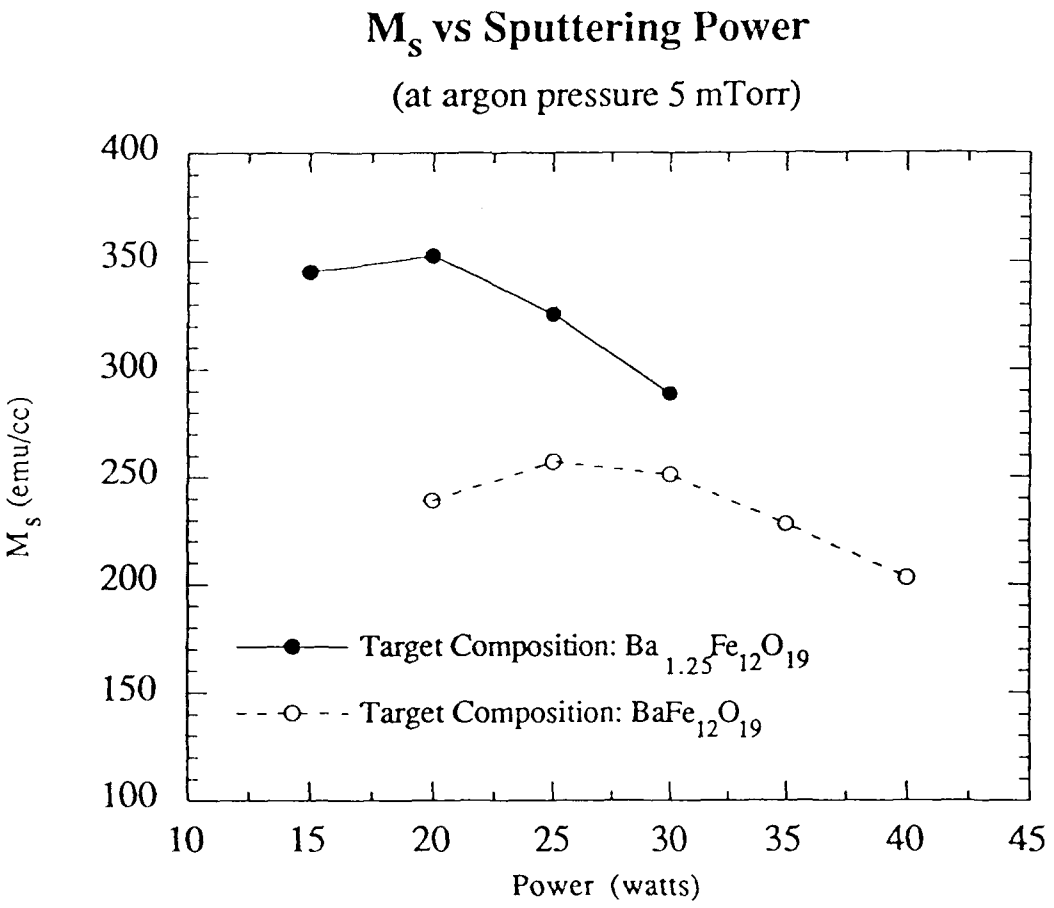

Figure 19: M_s vs sputtering power for two different targets

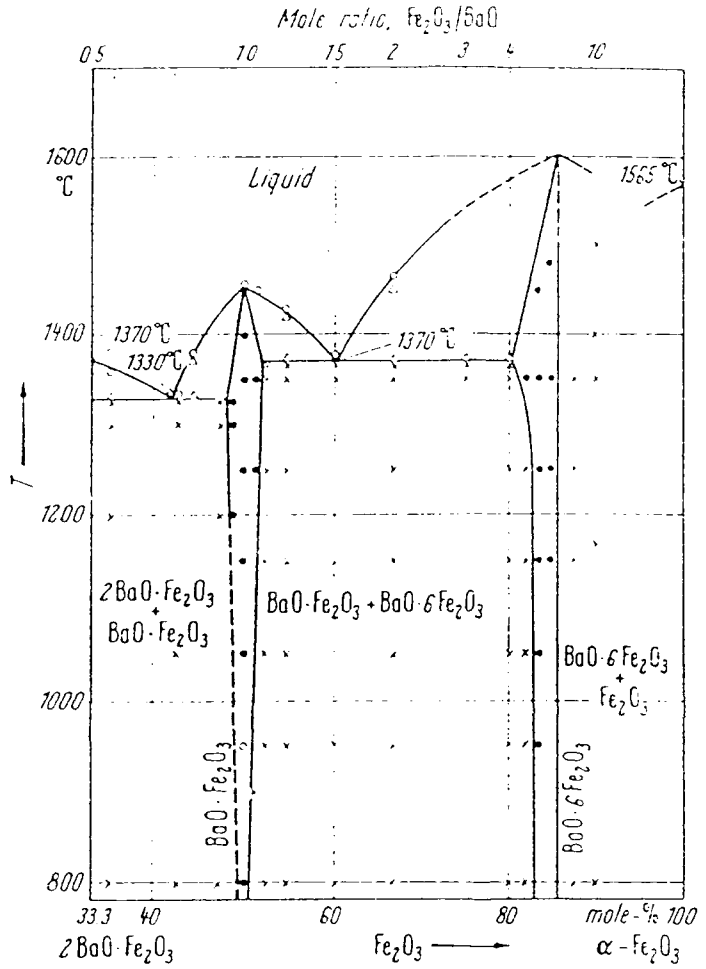

Fig. 5. BaO-Fe_2O_3 system. Phase diagram after [*60GT*]. For the system $BaFeO_{2.5...3.0}$ see e. g. also [*65GMCB*] and [*65MCPSW*].

× two solid phases
● one solid phase
△ liquid and solid phases coexisting
○ one liquid phase.

Figure 20: Barium ferrite phase diagram after Hellwege[21]

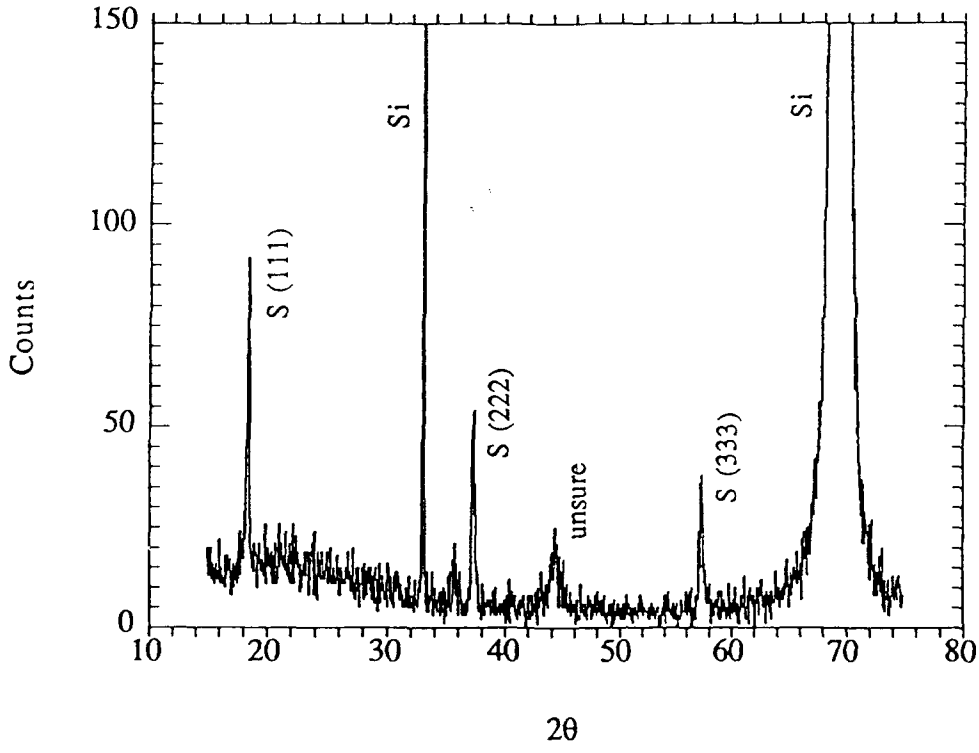

Figure 21: X-ray diffraction pattern for film sputtered at 800°C with pure argon

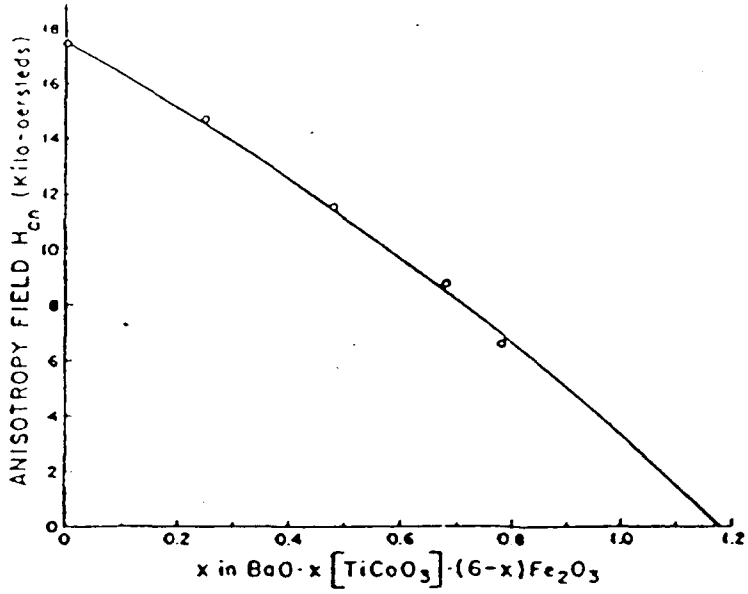

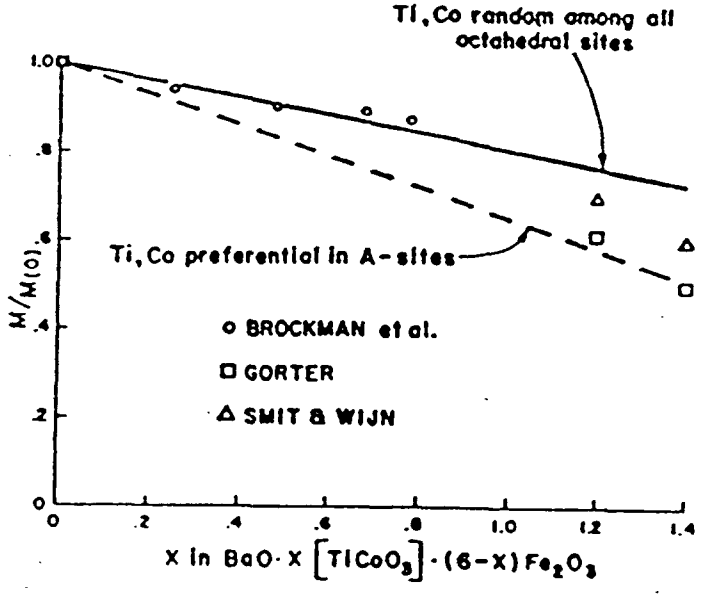

Figure 22: (a) Dependence of uniaxial anisotropy field, H_k and (b) saturation magnetization on composition in cobalt substituted hexaferrites.

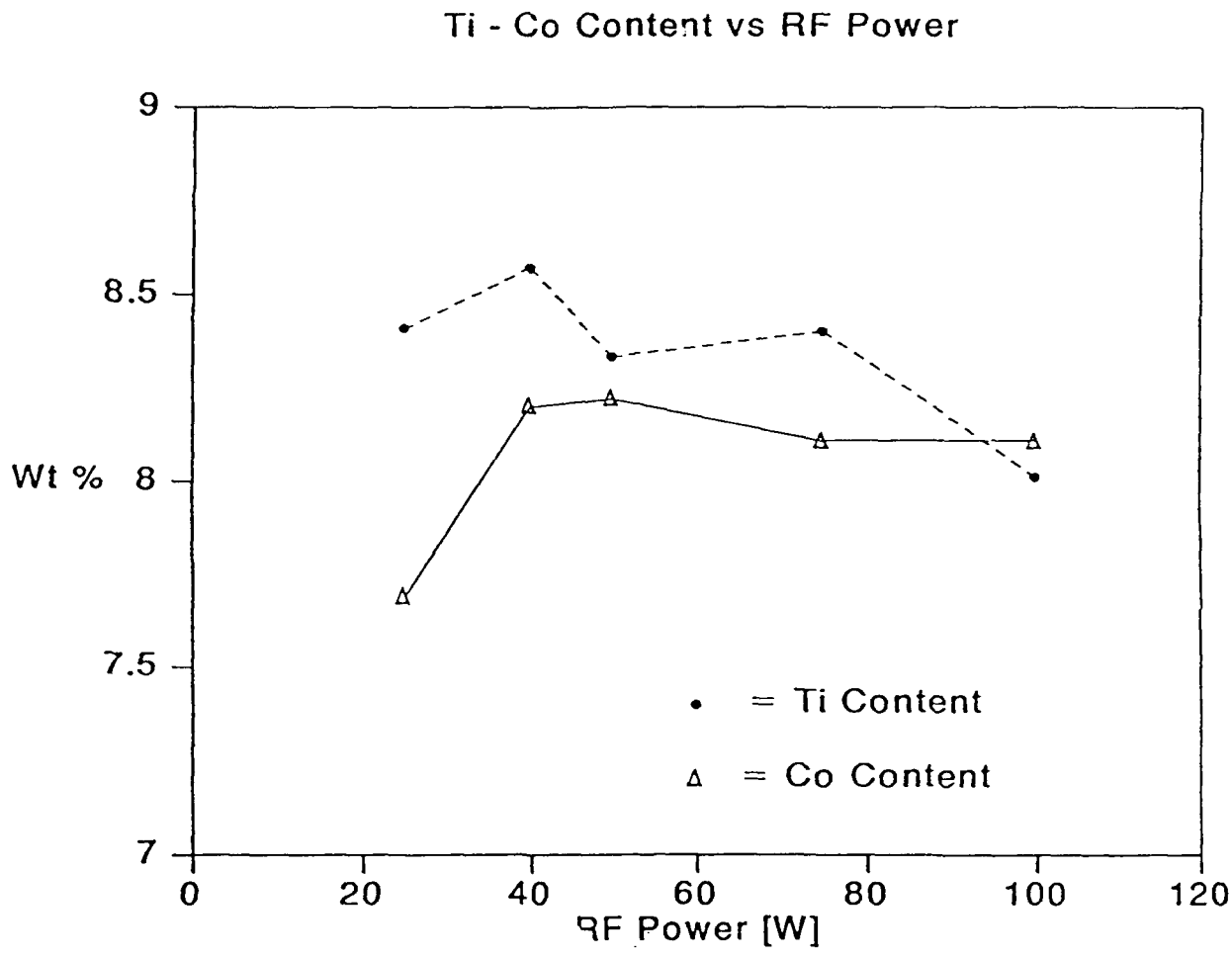

Figure 23: Co, Ti content vs sputtering RF power.

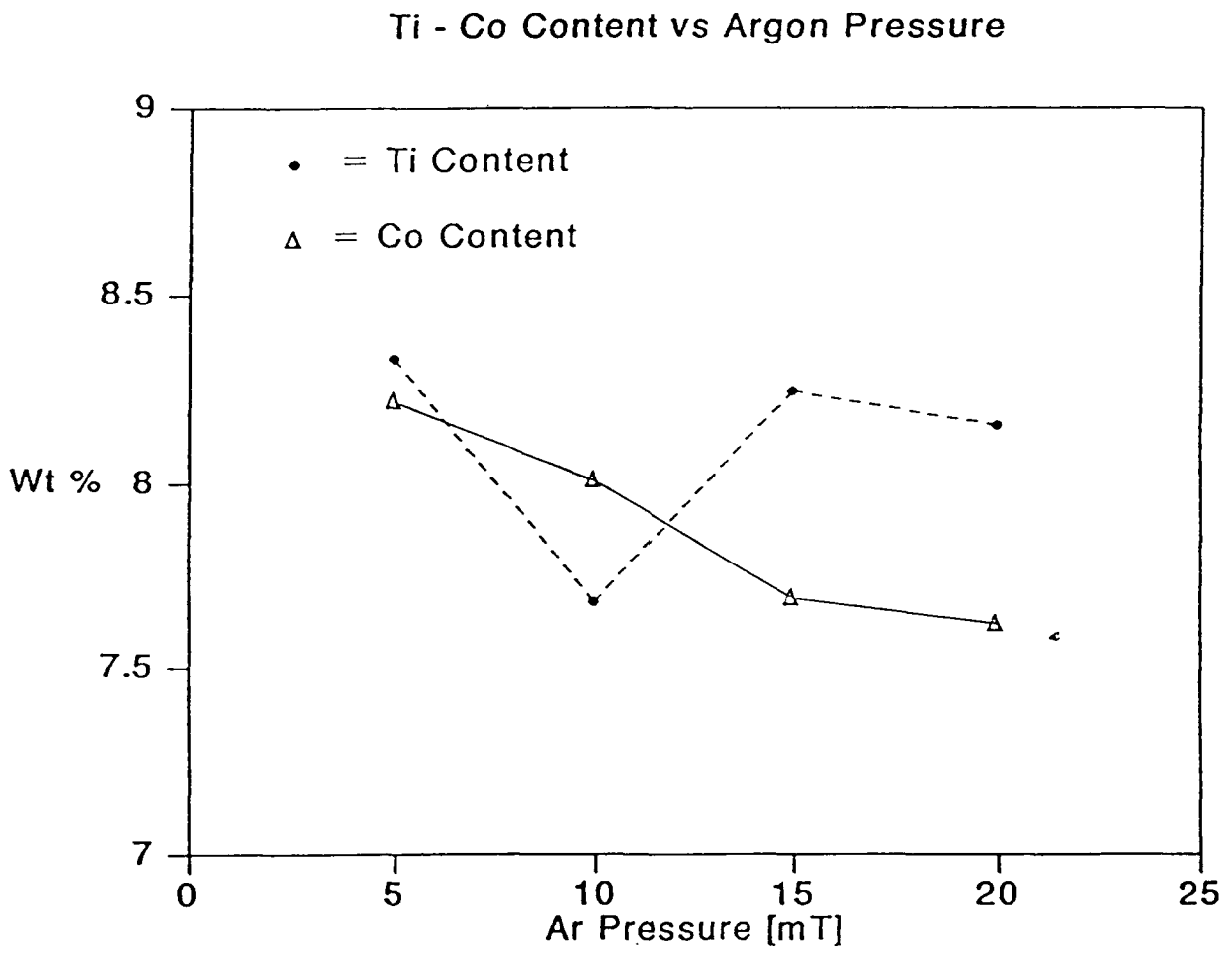

Figure 24: Co, Ti content vs argon pressure.

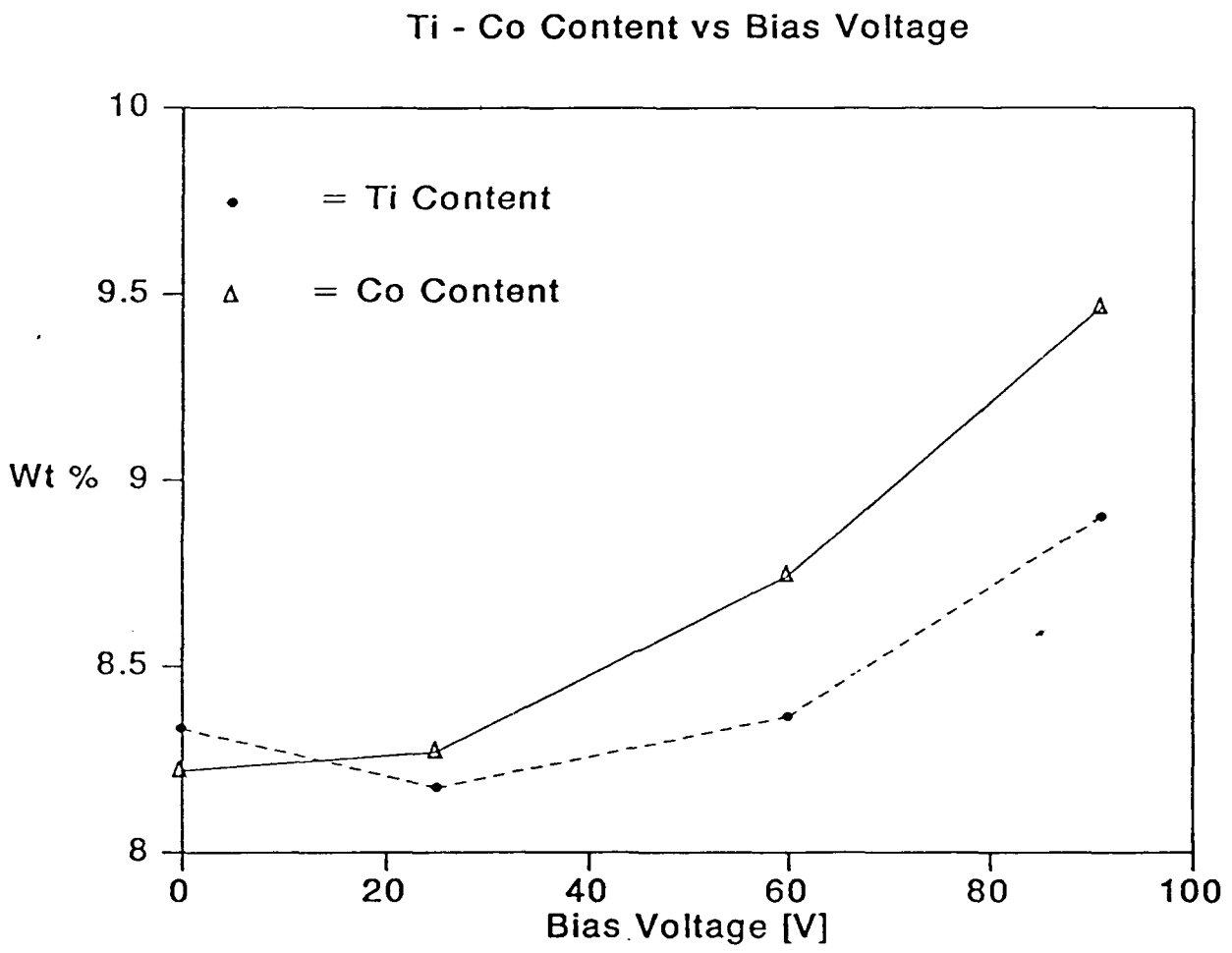

Figure 25: Co, Ti content vs bias voltage.

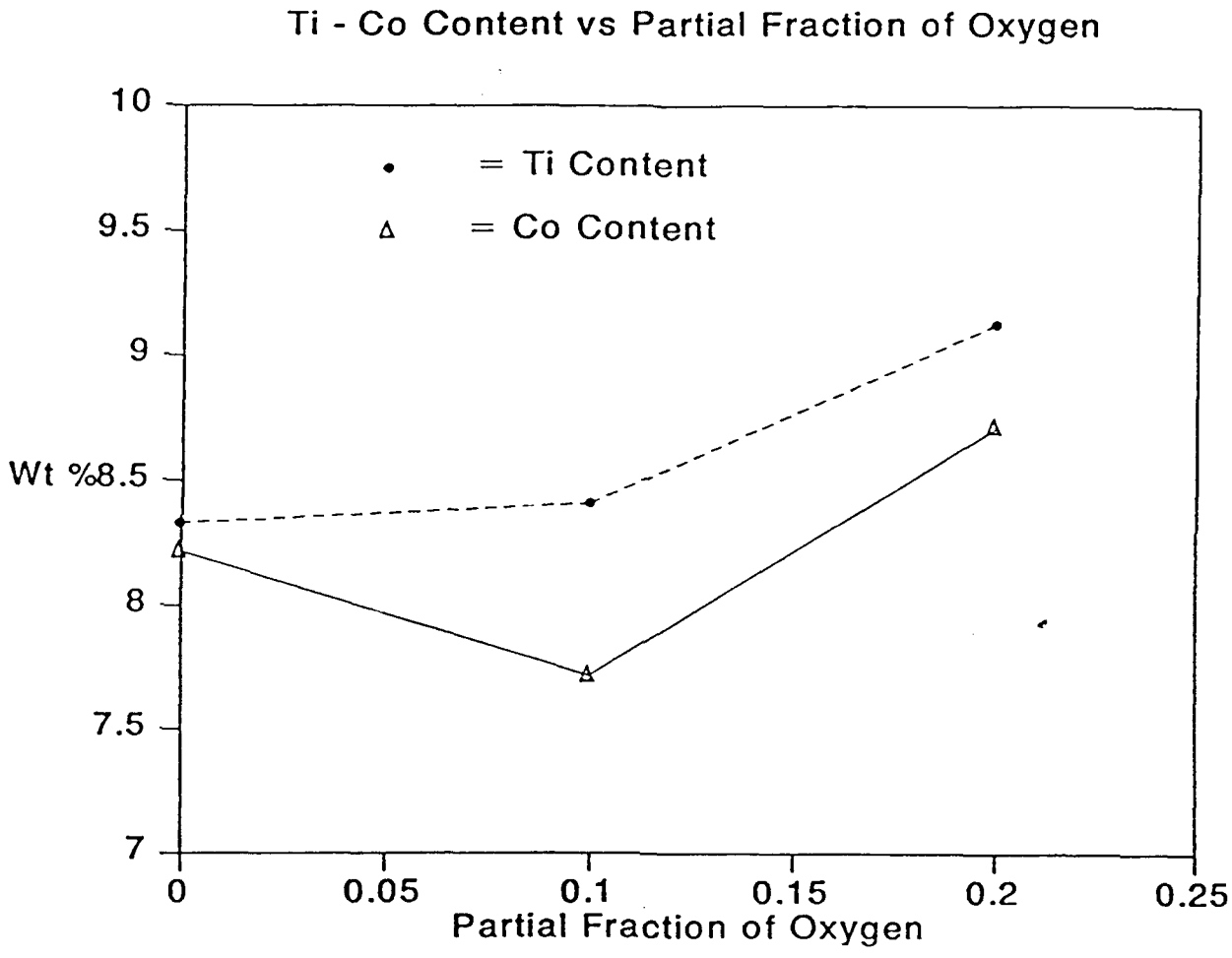

Figure 26: Co, Ti content vs partial fraction of oxygen.

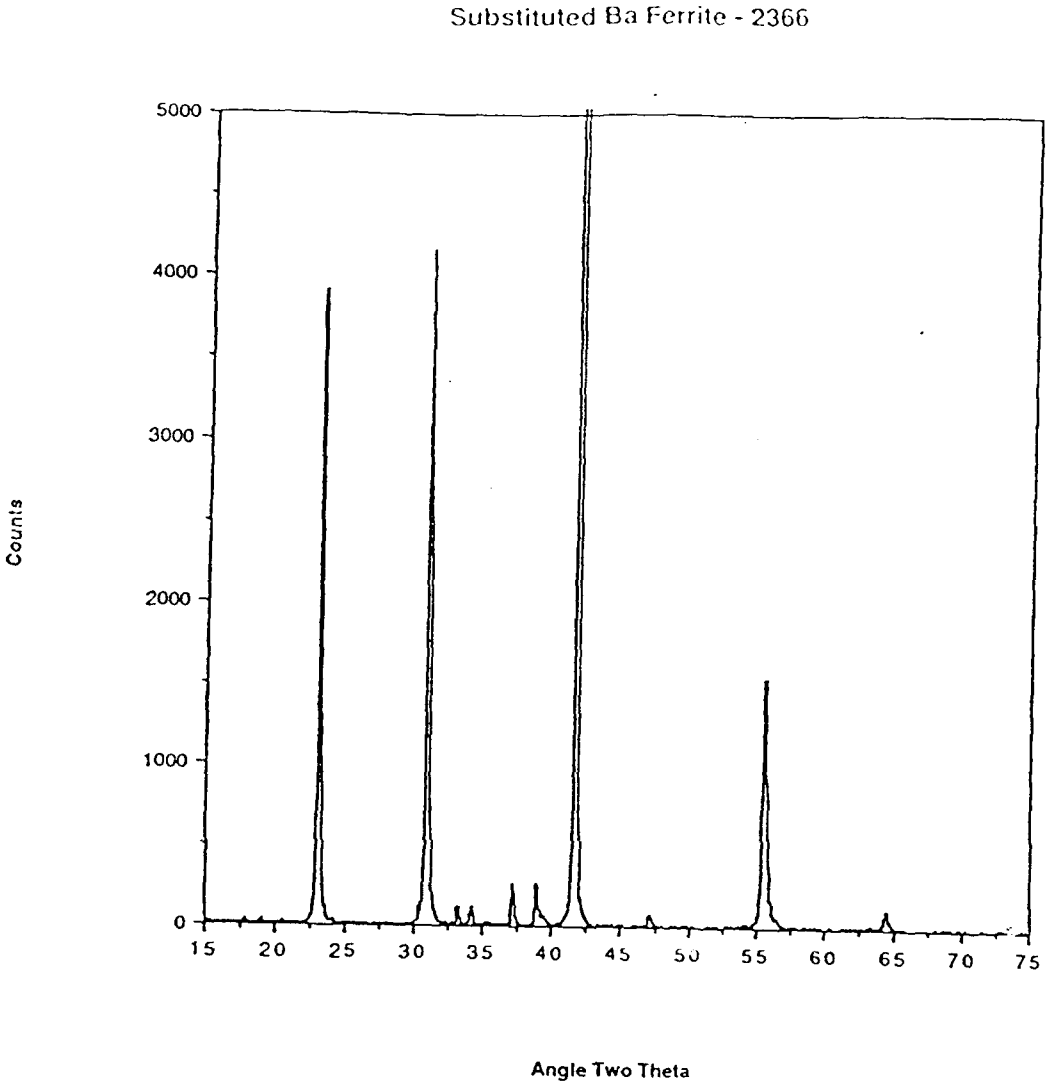

Figure 27: X-ray diffraction sweep of substituted barium hexaferrite.

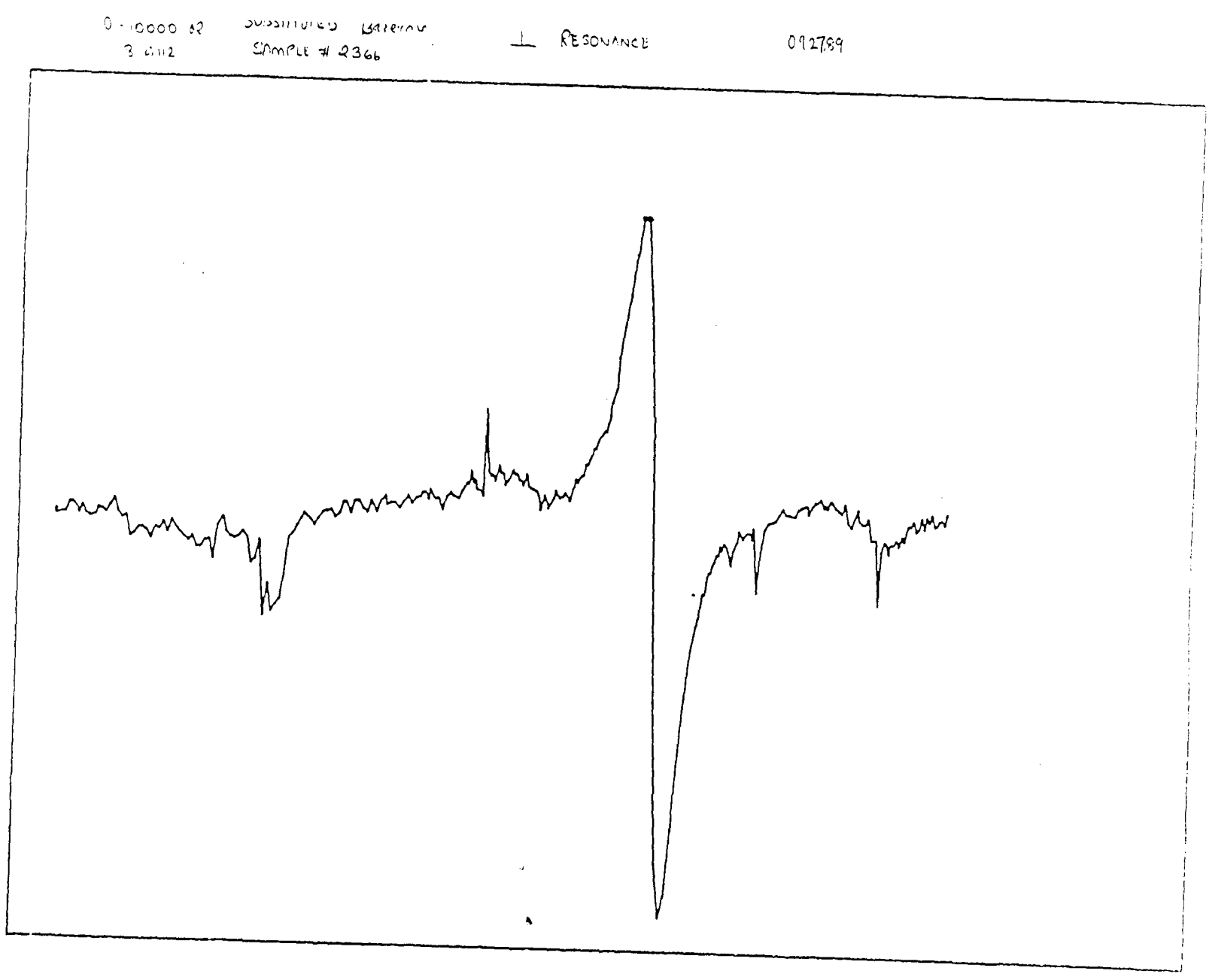

Figure 28: Perpendicular ferromagnetic resonance signal for Co-Ti barium hexaferrite at 8 GHz. (The horizontal axis represents a sweep of 10 KOe)

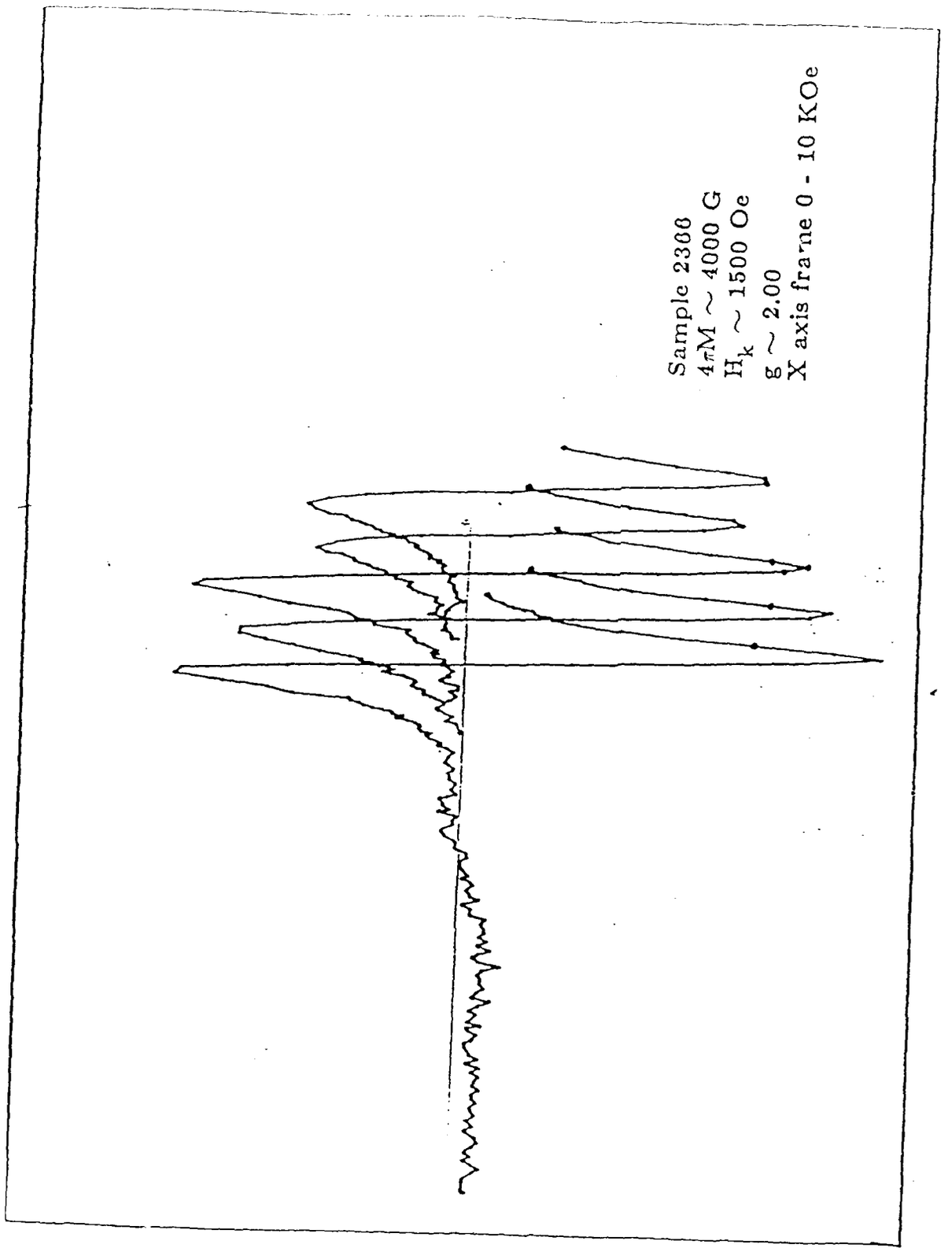

Figure 29: Perpendicular FMR spectra for Co-Ti barium hexaferrite at various microwave frequencies. (The horizontal axis represents a sweep of 10 KOe)

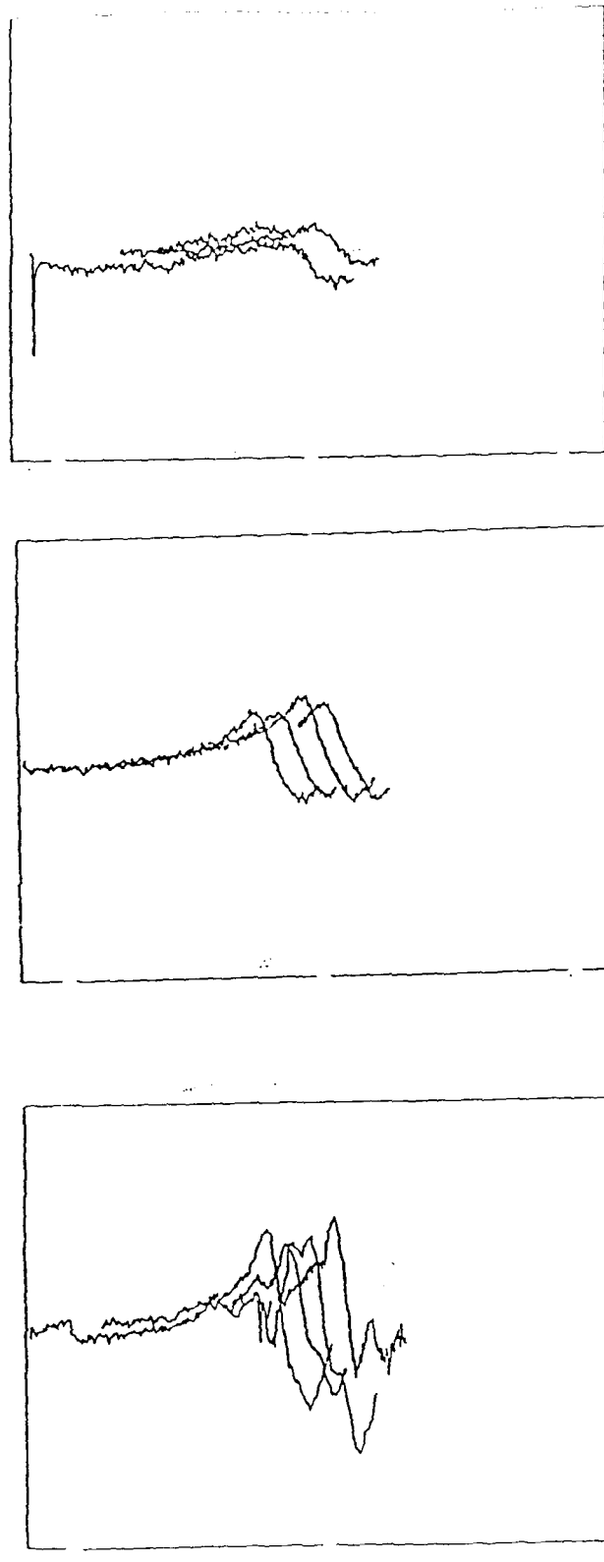

Figure 30: Narrowing of the FMR linewidth after successive annealing.

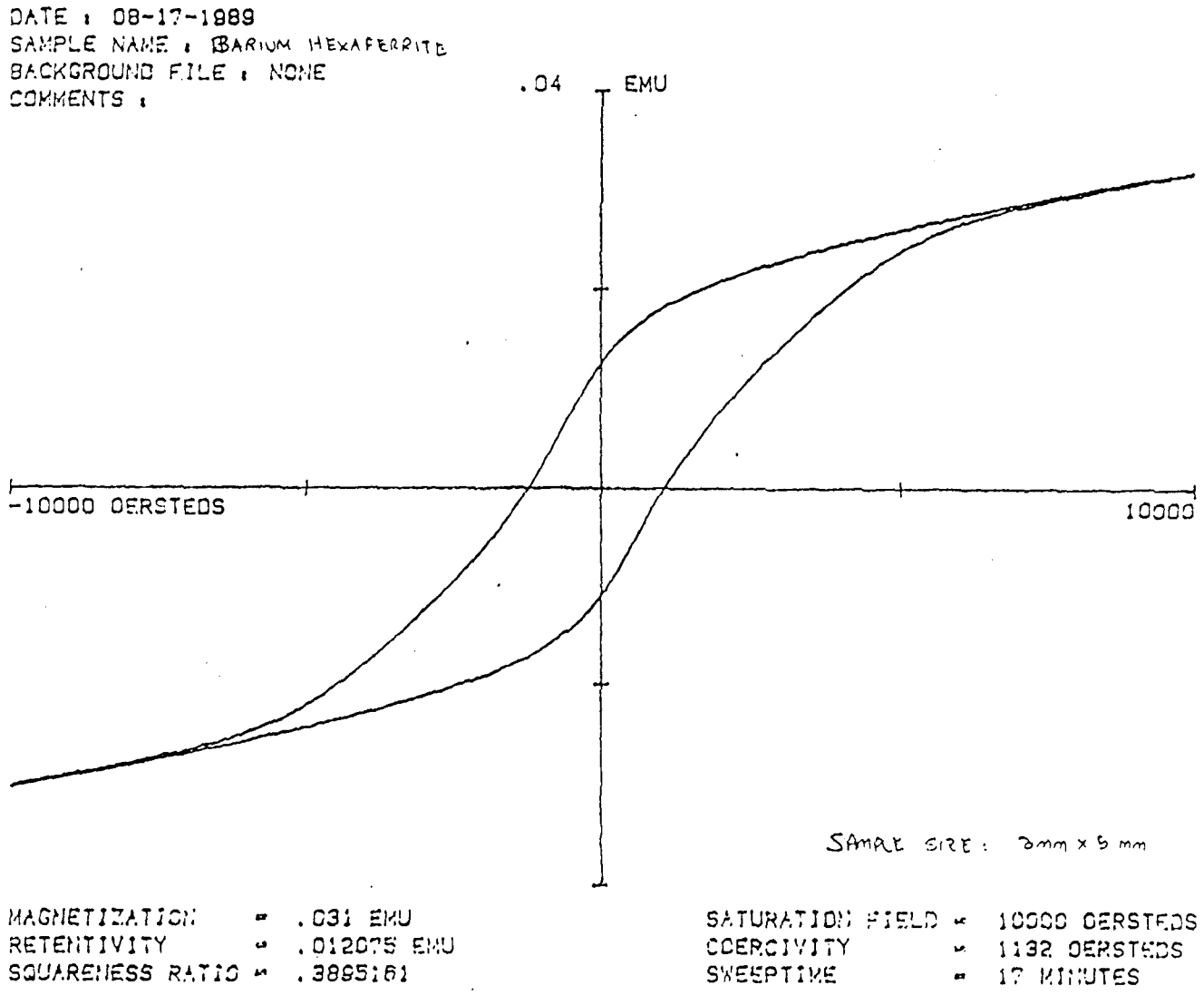

Figure 31: Magnetization curve for a 3 mm X 5 mm ferrite specimen grown by LPE.

Bismuth-doped lutetium iron garnet thin films for the MSW-Optical mode interaction

Project Report toward partial satisfaction of the requirements for the Master of Science degree in Electrical Engineering

Carnegie Mellon University,
Department of Electrical and Computer Engineering

Sherwood D. Silliman
May, 1992

Contents

Abstract

Bismuth-doped lutetium iron garnet thin films for the magnetostatic wave (MSW)-optical mode interaction were grown on paramagnetic gadolinium gallium garnet substrates from a PbO-based flux with varying amounts of MgO added. The ferromagnetic resonance (FMR) linewidth, optical waveguide absorption at 1320 nm wavelength, and magnetostatic wave passband were measured. The addition of magnesium drastically reduced the FMR linewidth, which reflects on the ability to excite magnetostatic waves in the film, as the divalent magnesium ion replaces the Pb^{2+} ion and charge compensates the Pb^{4+} ion. The optical absorption is only slightly increased due to creation of Fe^{4+} ions to compensate for the Mg^{2+}. The direct measurement of MSW passband showed a slight improvement in insertion loss at a low value of MgO doping, but it is still high and the passband shape is distorted. The higher than desired insertion loss is believed to occur as a result of inhomogeneities present in the films. The presence of inhomogeneities was confirmed by measured variations in absolute FMR resonance field across the wafer. However, if, as postulated, the MSW-optical interaction occurs close to the MSW launching antennas, the high insertion loss will not seriously degrade MSW-optical conversion efficiency. By incorporating Na_2O in the melt, it was shown to be possible to allow an adjustment of uniaxial anisotropy with subsequent annealing. Uniaxial anisotropy is an important parameter for the MSW-optical interaction.

These improvements coupled with future refinements of the growth techniques to

ensure homogeneity of the film composition suggest the potential for this material's applicability to magnetooptic signal processing devices based on the magnetostatic wave-optical mode interaction.

1. Introduction

Single crystal garnet thin films have been shown to be a good material for optical waveguides and devices [1]. Under certain conditions, microwave frequency magnetostatic waves can interact with the optical guided mode in these films, allowing optical modulation at microwave frequencies to be possible [2-5]. This modulation can be used to realize communications and signal processing devices, and with better properties than acousto-optic or electrooptic modulators in some cases [6].

Applications for the MSW-optical mode interaction exploit this modulation of the optical mode at the high microwave frequencies of the magnetostatic wave. Both optical and microwave device possibilities can be envisioned. In the optical domain, the primary application would be modulation of the optical signal through the waveguide at microwave frequencies, encoding microwave frequency density information on an optical carrier [2,3]. This could be extended to the digital regime, using the interaction as a switch, capable of up to gigahertz range speeds. The optical mode itself can also be shifted in frequency, allowing fine tuning of the light wave [7]. Filtering would be another area of application for this technology, as the band of the filter could be easily and quickly tunable by the administration of the magnetostatic wave [8].

The microwave domain would benefit from maturation of this technology also, as specific optical modes could be used to analyze the spectrum of a conglomerate microwave signal [9]. Filtering could also be done.

The basic component upon which these applications are based is the optical mode converter. This device may also be used to measure the efficiency of the interaction [4,5,10]. In the absence of the magnetostatic wave, the k-vectors of the two orthogonally-polarized optical modes are sufficiently different to prevent efficient mode conversion. The interaction of the magnetostatic wave and the incident optical mode results in the algebraic addition of the k-vector of the magnetostatic wave to that of the optical mode. The k-vector addition is sufficient to bridge the small k-vector gap between the two polarizations. This results in the input polarization of the optical mode being converted to the other polarization at the output.

These devices require the garnet film material to exhibit properties suitable for the propagation of both microwave-frequency MSW's as well as optical laser modes. The optimal parameters for the two regimes may be quite different, as with film thickness, or difficult to obtain together, as with high Faraday rotation and low optical absorption. This requires compromise in the grown film which degrades efficiency of the interaction. Future studies might incorporate a multi-layer format, with one layer optimized for microwave-MSW properties and another for optical waveguiding. It has been shown theoretically that the MSW-optical mode interaction could take place with maximum efficiency in such a heterostructure format [6].

The garnet material system is also promising for other device applications exploiting the magnetooptic effect. The possibility for other devices has been demonstrated, including a temperature-independent optical isolator, useful for eliminating feedback from laser optical systems. This device was realized from a

bismuth-lutetium-gadolinium: bismuth-gadolinium iron garnet composite film [11]. A novel magneto-optical wheel rotation rate sensor was fabricated from a bismuth-doped, multi-rare earth, silicon-doped iron garnet [12]. The magnetooptic properties also can lend themselves to the realization of printing or display devices, with small pixels of the material at different polarizations, changeable with laser light [13,14].

The first garnet studied with regard to the MSW-optical mode interaction was yttrium iron garnet, $Y_3Fe_5O_{12}$, also called YIG [2]. Certain problems arise in the use of pure YIG with the interaction. The fairly low magnetooptic effect, for example, in the form of Faraday rotation, degrades the efficiency of the interaction. Luckily the garnet system is well suited to fine tuning properties by way of varying composition [15]. The rare earth elements prove to be ideal for substitution into the crystal sites usually occupied by the yttrium. Bismuth can also substitute into these sites [16]. Bismuth is used to drastically increase the Faraday effect, and lutetium, with its smaller atomic size, can balance out the lattice mismatch that occurs with simple bismuth doped YIG [17].

The single crystal garnet thin films are grown by liquid phase epitaxy (LPE) [18]. A transparent, paramagnetic garnet substrate, gadolinium gallium garnet, is used as it has a very good lattice match to the rest of the system [19]. The substrate is dipped into the heated, though supersaturated, solution of the garnet component oxides in a flux, and the film grows [20]. YIG is usually grown from a lead oxide-based flux, but problems such as increased optical absorption arise from lead substitution into the

films [21]. Experimental work has been done by other researchers with a bismuth oxide-only flux to eliminate some of the lead substitution problems [5, 22]. Difficulties with this system include high melt viscosity [23]. Sodium addition is suggested to eliminate the problem [24]. However, in earlier work at CMU, lingering viscosity difficulties degrading the surface, prohibitively high optical attenuation in the films grown, and a greater dependence on temperature accuracies for the bismuth oxide flux pointed back to the original PbO-based flux system.

Magnesium oxide (MgO) was used by Tamada, et. al. as a dopant of the bismuth-only melt to improve both optical and magnetostatic wave attenuation in the waveguide [5]. Also, Nelson and Harvey have shown that magnesium can reduce the optical transmission attenuation of BiLu iron garnets grown from PbO-based melts perpendicular to the film [25], but the MSW-optical interaction requires examination of attenuation in the film as a waveguide.

In this study it is shown that the FMR linewidth reduction from MgO can be achieved in the PbO-based melt, without significant increase in optical absorption.

2. Thin Film Garnets

2.1. Garnet Material System

The base crystal system for the single crystal garnet technology is yttrium iron garnet, or YIG [15]. The garnet is characterized by a complex, but basically cubic, crystal structure with three main lattice site categories plus oxygen atoms (See Figure 1). In the YIG system, the dodecahedral sites, or c-sites, are occupied by the yttrium ion with a valence of +3. For more complex garnets it is these sites that contain the rare earth or bismuth ions. There are three dodecahedral sites per formula unit, and each site is surrounded by eight oxygen atoms. The octahedral and tetrahedral sites are both occupied by iron ions, also with +3 valence. There are 2 octahedral sites, surrounded by 6 oxygen atoms, and 3 tetrahedral sites, surrounded by 4 oxygen atoms, resulting in a total of 5 iron sites per formula unit. Nonmagnetic ions such as Ga^{3+} can also be substituted into these sites to dilute the saturation magnetization. This is undesirable in the application to the MSW-optical interaction, and so only iron atoms are required here.

The yttrium ion is nonmagnetic, as is lutetium, due to filled outer electron shells. Bismuth is also nonmagnetic [16]. This results in the iron ions being the only contributor to the magnetization of these films. The two iron sublattices, the 2 octahedral and 3 tetrahedral sites, oppose each other in magnetization due to

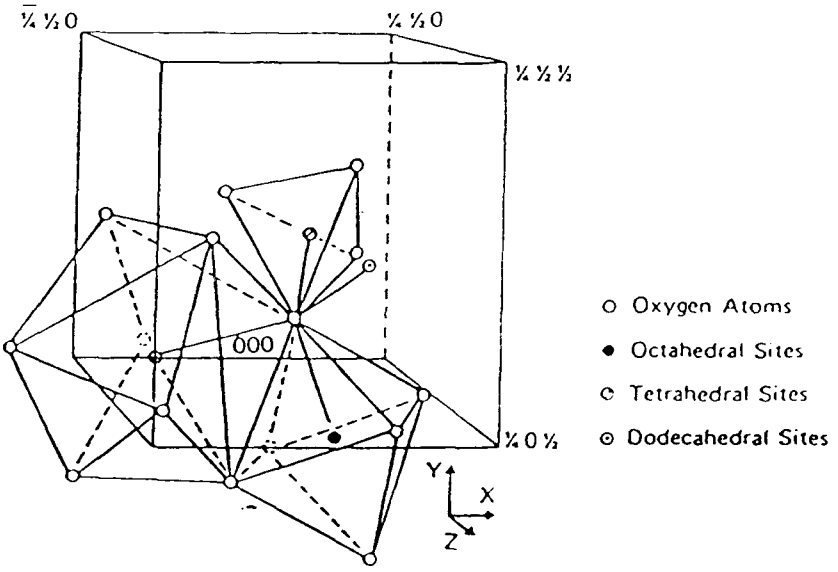

Figure 1. Diagram of lattice sites in garnet crystal structure. (From Eschenfelder [7].)

magnetic interaction, so the net result is the magnetization of one iron ion. The substrate used in these experiments is the paramagnet gadolinium gallium garnet (GGG), $Gd_3Ga_5O_{12}$, which has gallium completely replacing the iron.

Lattice spacing is important in the growth of garnet thin films, as improper matching of film to substrate can result in cracking as well as other effects. The lattice constant for the GGG substrate is 12.383 Å. Pure YIG is very close to this, and so results in a good lattice match. The substitution of bismuth into the dodecahedral site changes this, however. The bismuth ion is much larger than the yttrium. If the bismuth were to completely substitute for the yttrium, the resulting lattice constant would be 12.621 Å. It is for this reason that the rare earth lutetium is used [17]. Pure LuIG has a lattice constant of 12.283 Å. Interpolation does not result in significant error, and so the correct ratio of bismuth to lutetium can be found for lattice match. In the following expression for lattice mismatch,

$$\frac{\Delta a}{a} = \frac{12.383-[(12.621-12.283)x+12.283]}{12.383},$$

setting the mismatch $\Delta a/a$ equal to zero yields a Bi/Lu ratio of .295. This value multiplied by the 3 dodecahedral sites per formula unit yields a final stoichiometric representation of BiLuIG as $Bi_{0.89}Lu_{2.11}Fe_5O_{12}$. for lattice match [13].

The resultant increase in Faraday rotation with increasing bismuth content may be explained by a diamagnetic transition. This transition is an electron transition between energy levels. The upper energy level exhibits a degeneracy into three

separate levels. The two different possible incident polarizations of light result in excitation from the ground state to two different energy levels of the degeneracy. The difference manifests in a large changing response of two elements of the permittivity tensor, at a certain frequency corresponding to the energy gap of the transition.

However, the increase in magnetooptic effect may not be fully accounted for by the intrinsic bismuth transitions. It has been found that the bismuth ion also affects the trivalent iron transitions, on both the octahedral and tetrahedral sublattices. Bismuth increases the intensity of these paired transitions through the superexchange between the iron ions on the opposite sublattices, and also results in a split excited state, adding to the magnetooptic response. These two mechanisms account for most of the noted increase in the magnetooptic effect, but there are also additional smaller contributors [16].

2.2. Growth

The standard growth technique for thin films of garnet is liquid phase epitaxy (LPE). This technique allows the growth of single crystal thin films with a wide variation of properties [18]. The basic method employed is horizontal dipping [19], with other orientations also possible [20]. The substrate is immersed in a high-temperature supersaturated melt of the garnet components in a flux. The substrate acts as a seed crystal, and the garnet constituents crystallize on the wafer surface.

The substrate is a paramagnetic, transparent, $Gd_3Ga_5O_{12}$ single crystal, grown by the Czochralski method of pulling and rotating a seed crystal from a melt of the crystal components, resulting in long round boules. Wafers are then cut from the boules and highly polished.

The dipping technique involves the substrate wafer being suspended from a platinum three-pronged holder horizontally. The holder is attached to a vertical alumina (Al_2O_3) rod which is inserted into the tube of the furnace. The furnace consists of a platinum-rhodium wire wrapped around an alumina core cylinder. The wire winding is divided into three zones, with the current into each zone controlled by a separate temperature controller, monitored by a separate, platinum:10% rhodium-platinum thermocouple. Inside the cylinder is another smaller cylindrical pedestal upon which rests the platinum crucible containing the melt component oxides. There is another thermocouple under the pedestal to measure the temperature right at the melt crucible. The powder oxides are measured into the

crucible and then placed inside the furnace and heated past the saturation temperature of the garnet component oxides in solution in the flux.

The standard flux for the YIG system is a lead oxide-boron trioxide (PbO-B_2O_3) mixture. These oxides melt at a reachable temperature, as low as 700°C depending on composition, and the other garnet components dissolve in the melted flux. Conventionally, the flux composition is described by R-ratios which correspond to different ratios of important components. These have been experimentally determined to be important by Blank and Nielsen [20]. For the PbO-based flux used here, the important ratios are

$$R_1 = \frac{Fe_2O_3}{Lu_2O_3}$$

$$R_3 = \frac{2\ PbO}{B_2O_3 + Na_2O_3}$$

$$R_4 = \frac{Fe_2O_3 + Lu_2O_3}{Lu_2O_3 + Fe_2O_3 + B_2O_3 + Na_2CO_3 + \frac{1}{2}PbO + Bi_2O_3}$$

$$R_6 = \frac{MgO}{2Fe_2O_3 + MgO}\ .$$

In addition, the ratio of PbO to Bi_2O_3 is important.

For this study, the following R-ratios were suggested by Dr. D. Gualtieri at Allied Signal: R_1=20, R_3=14.4, R_4=0.17, R_6=0, and Pb/Bi=1.5. One film was grown from this melt composition at Allied Signal and sent to CMU for analysis [26]. Films were then grown at CMU with R_6 varying from 1% to 3%.

Experimental work has been done with a different flux system using Bi_2O_3 only as the primary flux [5,23]. Films grown at CMU, following a previously reported

lead-free flux, have been unsuccessful due to extremely high viscosity of the melt at the low temperatures required to obtain sufficient bismuth incorporation for lattice match. The viscous flux would adhere to the film upon removal from the melt, and cause further growth at the locations of the adhered droplets. The addition of sodium carbonate to the flux, a precursor of sodium oxide, Na_2O, was attempted in order to reduce the flux viscosity and the subsequent flux adhesion to the newly grown film. The sodium reduced the viscosity somewhat, but small crystallites and other impurities remained in the films. This caused problems for optical waveguiding, contributing to difficulty of prism coupling as well as high optical absorption. A study of the effects of the sodium incorporation into the films on the magnetic and magnetooptic properties was performed as a result of this, and showed no adverse effects [27], so sodium was used in the lead oxide-based melt to help lower the viscosity in that system at low growth temperatures.

The flux oxides were measured to produce a 300 gram melt, which approximately fills the platinum crucible one third of the way to the top when melted. The oxides are originally in powder form, however, and therefore must be compressed in some way. Other studies have used several melting times; heating up and cooling down the crucible with a fraction of the total oxides added to the crucible each time. However, the repeated heating and cooling can cause inhomogeneities in the melt, and so in this study all of the oxide was placed in the crucible at the same time, using a mortar to press in the components. The melt was scaled down to allow all the oxide to fit in at once.

The crucible was covered with a platinum lid, and the oxides in the crucible were then heated to 940°C in the furnace and held there for 24 hours. The melt was then uncovered and stirred, using the three-pronged substrate holder with the ends bent horizontally, at 100 RPM for three hours. The melt was then ready for growth; there were no separate phases or impurities visible on top of the melt.

Before growth, the substrate wafer is mounted in the platinum holder. The combination is soaked clean in a heated soap solution for 20 minutes and then in heated deionized water for 20 minutes. Then the substrate is placed in an ultrasonic bath for 1 minute to further remove any impurities. The holder and wafer are then mounted on the alumina rod suspended from a rack which rotates as well as inserts the rod into the furnace and the melt.

During substrate cleaning, the melt is lowered to the growth temperature. Care is taken to assure that the melt is not below saturation for more than about an hour. Otherwise, separate phases, growth of tiny crystallites, or other inhomogeneities could occur. When the wafer is clean and the furnace is at the growth temperature, the substrate is lowered into the furnace slowly so as to reduce thermal stresses on the substrate and the rod. The substrate is held immediately above the melt for five minutes in order to preheat the wafer to the exact growth temperature. Longer preheating times can result in condensation of lead oxide vapor on the substrate and degradation of the film quality. After the substrate is preheated, growth is commenced. Rotation of the substrate at 50 RPM is started, and the wafer is lowered into the melt. Upon submersion, the start time is noted. Faster rotation rates resulted in surface

marks on the grown films resembling outward spiralling scratches.

Slightly before the end of the growth time, the holder is raised from the melt to ensure complete clearance from the melt in time. The rotation rate is then ramped up to 800 RPM and then braked immediately to 0 RPM to spin off any excess flux from the wafer, as there will be further growth under any droplets of flux. The holder is again slowly raised to prevent thermal shock. Once the holder is removed from the rod it is placed in a warm mixture of 50% each nitric and acetic acids. It is left in the heated acid for several hours in order to remove all remaining flux from the film. The wafer is then carefully removed from the holder and washed off in deionized water and blown dry with compressed nitrogen. The films grown showed a desirable mirror-like finish, but slight surface features could be seen, possibly indicating very small thickness variations resulting from flux adhesion.

Two melts were prepared at an R_6 value, representing MgO content, of 2%, and one melt each was prepared at 1% and 3%. Five films were grown from each melt, at varying growth temperatures. In addition, one film, which was prepared by Dr. D. Gualtieri at Allied Signal from the equivalent melt but with no MgO added, was compared with the other films.

Growth temperature affects many of the properties of the film. For example, and of interest here, the film thickness and also bismuth content are both directly related to the amount of supercooling, that is, the difference between growth temperature and saturation temperature [21]. Saturation temperature therefore yields zero epitaxial growth, as there is no excess of solutes to crystallize on the substrate. The growth rate

and bismuth content versus temperature are shown in Figure 2.

The growth rates for the MgO doped melts are lower, as Mg acts as a growth inhibitor. The incorporation into the dodecahedral sites by trivalent ions is the driving factor for the growth rate. The divalent Mg ion also inserts into these sites, and so charge compensation must occur by causing Fe^{4+} ions to form. This is a slower process as the compensating Fe^{4+} ions are not as readily available in the melt [28].

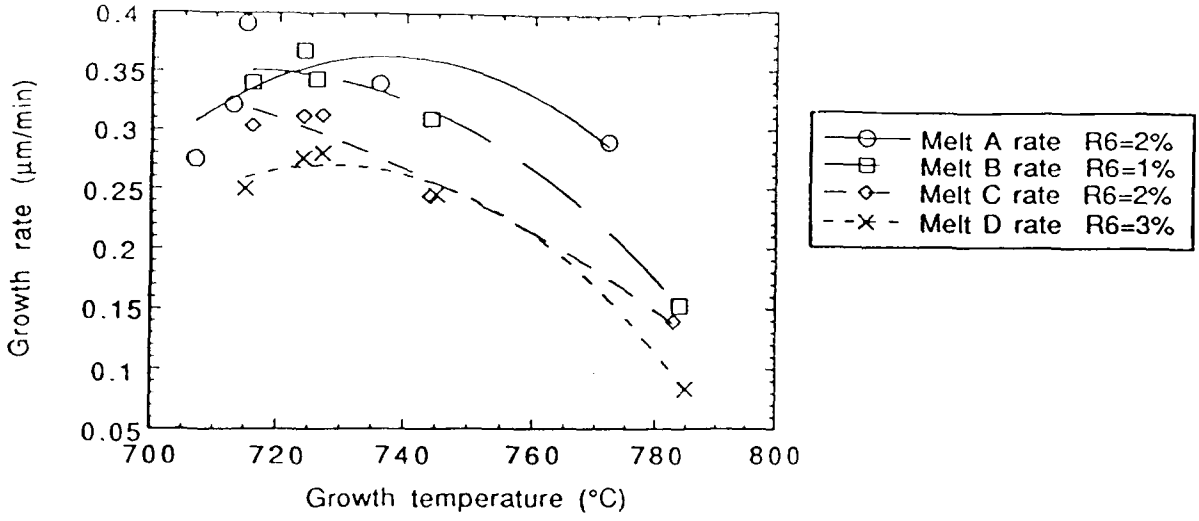

Figure 2a. Growth rate versus growth temperature for varying values of MgO content R_6.

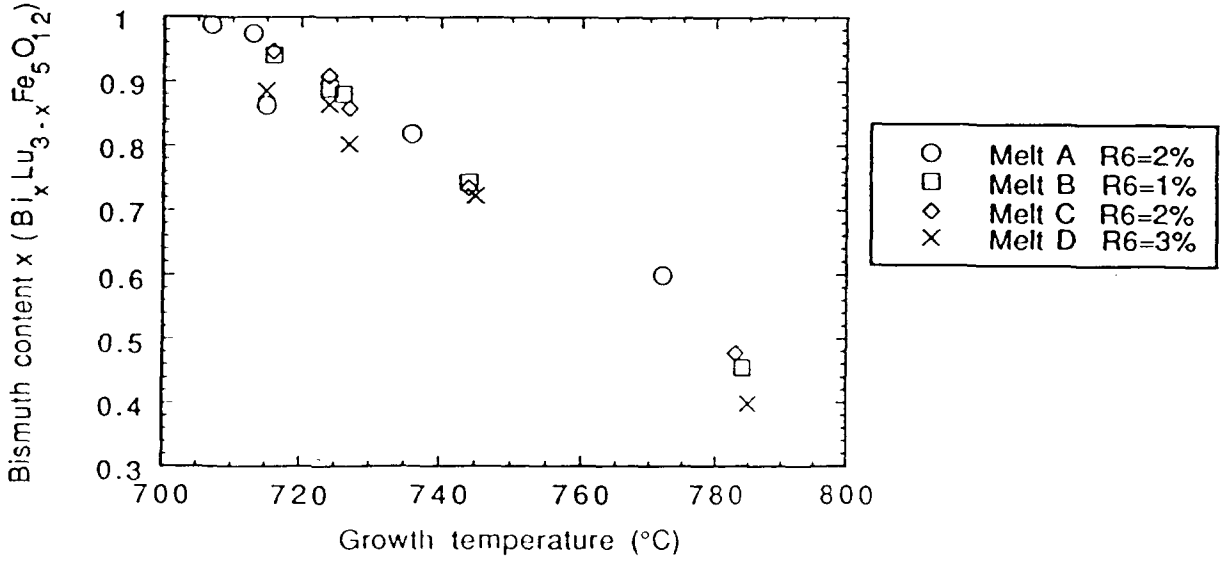

Figure 2b. Bismuth content versus growth temperature for varying values of MgO content R_6.

2.3. Effect of Sodium Doping

To eliminate the effects of lead substitution, an experimental lead-free melt, with bismuth oxide only as the flux, has been used to grow bismuth-substituted lutetium iron garnet thin films. At the low growth temperature required for the incorporation of necessary amounts of bismuth for a significant Faraday rotation value, this melt is highly viscous and flux adhesion impairs the surface morphology of the films. Na_2O is suggested for use in decreasing this viscosity and therefore promoting flux removal in the LPE growth. A study was performed at CMU with the assistance of Dr. Devlin Gualtieri of Allied Signal Corporation and Dr. Mahadevan Ramesh.

BiLuIG films previously grown from the lead-free melt with Na_2O had a more negative uniaxial anisotropy than those grown without sodium. This may be attributable to a growth induced anisotropy. However, growth induced anisotropy is also a function of bismuth content in these films. To isolate the effect of sodium on the growth induced anisotropy in garnet films, YIG was chosen as a model system, eliminating the Bi variable.

YIG layers were grown at Allied Signal on standard GGG substrates from a standard PbO/B_2O_3 flux. Sodium substitution was accomplished by addition of Na_2CO_3, a precursor to Na_2O, in the same molar concentration as B_2O_3, and the other solutes were then adjusted to achieve epitaxy in the same temperature range. Na:YIG films were also prepared at a lower temperature range to encourage sodium

incorporation into the lattice.

Anisotropy field was measured using standard FMR techniques by sweeping the applied magnetic field, noting the resonance field for five different microwave frequencies from 6 to 10 GHz, and averaging.

The controlled YIG measurements of uniaxial anisotropy field are shown in Figure 3. To examine the stability of the noted change in anisotropy field, the films underwent an annealing process. The YIG films were annealed at 970 °C for 4 hours and the anisotropy measurements were repeated. The samples grown with sodium at the same temperature as the pure YIG exhibit a slightly more negative anisotropy field, while those grown at the lower temperature to encourage Na substitution show a significantly lower value. The anneal revealed that the uniaxial anisotropy field increased back to approximately zero.

The Faraday rotation, lattice match, and microwave passband measurements all revealed no appreciable effect of sodium incorporation.

This shows that the uniaxial anisotropy field can be affected significantly without appreciable effect on either microwave losses or the strength of the MSW-optical interaction.

See Reference [27] for complete details of the study of the effect of sodium.

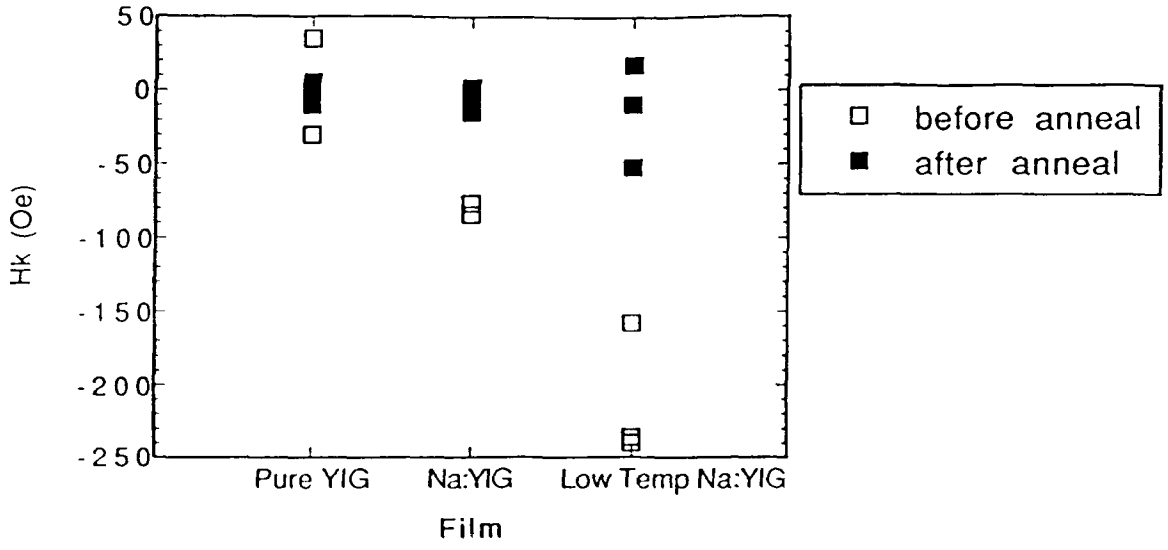

Figure 3. Uniaxial anisotropy field Hk versus sodium content. Low temperature Na:YIG contains a greater amount of sodium.

3. Characterization

The grown films were characterized for several properties, including thickness, bismuth content, optical loss, refractive index, FMR linewidth, and MSW insertion loss. These properties are summarized in Table 1 and discussed in the sections below.

3.1. Composition, Mismatch, Thickness, and Faraday Rotation

Each of the grown films was analyzed by x-ray fluorescence to determine film composition. The film is bombarded with an x-ray beam, and each component element in the film will fluoresce, or re-radiate x-rays, with a given energy profile. The system is calibrated with pure element oxides initially, to have an exact spectrum with the given conditions for that element. With the film under test, each element will then emit x-rays with the given energy profile, but in varying rates over time commensurate with the proportion of elements in the film. As certain spectrum profiles will overlap, a regression curve fitting algorithm is performed on the results, and a weight percentage for each element is obtained. With knowledge of the atomic weight of each component element, the molar percentage, and therefore the stoichiometry, of the film is acquired.

A measurement for lattice match was made by x-ray diffraction, where an x-ray beam is directed at the film at varying angles, and the detector shows the intensity of the x-rays diffracting at that angle. The angles of high intensity correspond directly to lattice constant. Very little ($\Delta a/a < 0.02\%$) lattice mismatch was observed at any MgO

Film No.	MgO R_6 (%)	Growth temperature (°C)	Thickness (μm)	Bi content (x)	Optical loss (dB/cm)	Refractive index n	FMR linewidth (Oe)	MSW insertion loss (dB)
From Allied Signal								
011	0	715	4.7	0.79	18.8	2.342	3.6	55
Grown at CMU								
SSA04	2	736	3.4	0.82				
SSA05	2	707	2.8	0.99				
SSA06	2	713	3.2	0.98				
SSA07	2	772	2.9	0.60				
SSA08	2	715	3.9	0.86				
SSB01	1	726	3.4	0.88	17.5		0.95	
SSB02	1	724	3.7	0.89	21.9		1.3	
SSB04	1	784	1.5	0.46				
SSB05	1	744	3.1	0.74	23.2		0.95	
SSB06	1	716	3.4	0.94	24.6	2.345	0.87	50
SSC01	2	724	3.1	0.91	23.6		0.87	
SSC02	2	783	1.4	0.48				
SSC03	2	744	2.4	0.74	20.7		0.88	
SSC04	2	727	3.1	0.86	21.9		1.1	
SSC05	2	716	3.0	0.95	29.9	2.344	0.87	
SSD01	3	724	2.8	0.87	25.4		1.1	
SSD02	3	715	2.5	0.88				
SSD03	3	727	2.8	0.80	27.2		0.97	
SSD04	3	745	2.5	0.72	21.9		0.90	70
SSD05	3	785	0.83	0.40				

Table 1. Measured properties.

doping level used here.

The mass of each sample was measured using a microbalance. Each substrate was weighed before and after growth, with the difference corresponding to the mass of the film. Thickness was measured by m-line spectroscopy on one sample by fitting the obtained mode angles with the refractive index and thickness. This measurement is obtained in conjunction with the optical attenuation measurement and will be explained in the following section. The thickness could therefore be calibrated to the mass, and the thicknesses of the other films was thus obtained.

The magnetooptic effect is a function of bismuth concentration [16]. BiLuIG films were grown previously at CMU, and the Faraday rotation was measured using a magnetooptic loop tracer. The sample is mounted between the poles of an electromagnet. The poles have a hole through the center. Laser light of a predetermined polarization is aimed through these holes, through the film, and through a device which separates the two orthogonal polarization components. The intensity of each component is detected, and a differential amplifier is used to extract the change in angle of polarization, or Faraday rotation. The magnetic field is swept, and the polarization change at saturation corresponds to the absolute Faraday rotation for that film. This value is then divided by the thickness of the film to determine the desired value of rotation in degrees per unit length through the film. This value was shown to be linearly dependent on Bi content, as expected, for the earlier films, and the magnitude agreed with previously reported films [5] (See Figure 4.)

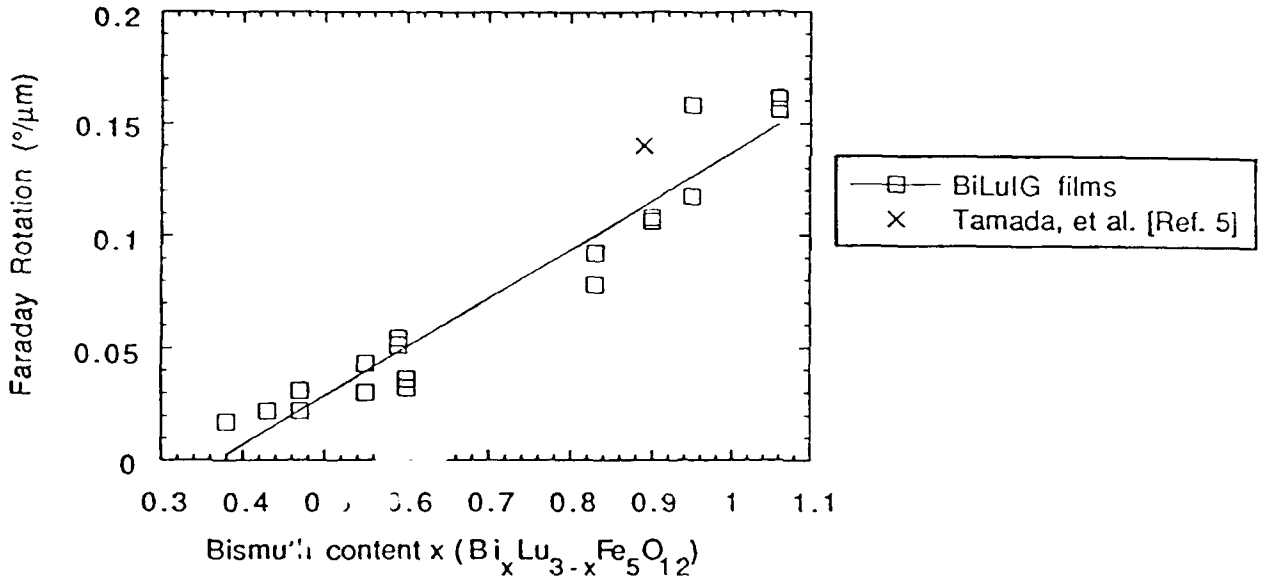

Figure 4. Faraday rotation versus bismuth content for previously grown films.

3.2. Optical Waveguide Properties

The optical properties of the films were measured using a technique based on m-line spectroscopy. The optical attenuation of the films was measured using a method of coupling out of the waveguide with a moveable exit prism on a film of index-matching fluid [29]. Infrared laser light at 1.319 micrometers wavelength is coupled into the waveguide via a prism. The waveguide is mounted vertically at the center of a rotating stage. The exit prism is clamped to the film, and there is a photodetector on the stage, which can be adjusted for output angle. Light is coupled into the film, propagates with loss down the waveguide, is coupled out by the exit prism, and enters the photodetector, and the power incident is noted. The exit prism is moved in increments. At each increment, the output angle of the photodetector is adjusted if necessary to maximize the power received, and the power is noted again, as well as the length of the increment. In this fashion, the increase in power with decreasing propagation length may be calculated, and is equal to the optical attenuation per distance in the film.

Initially, the incident angles for each mode in the films were found. The light is coupled into the same apparatus as above via a prism, and the angle at which the light is incident is variable using the rotation stage. Instead of the photodetector, a paper screen is placed around the top stage, and an infrared video camera is used to see the spots on the screen when the correct angle for the given mode is dialed in. The incident angle corresponding to the third available mode with TM polarization was

used for the optical attenuation measurement of each film.

Mode k-vectors can be obtained given the thickness of the film and the indices of refraction of the film, substrate, and cover by standard slab waveguide theory [30]. An additional birefringence capability was added following the scaling factors introduced by Kogelnik and Ramsawamy [31]. From the individual mode k-vectors, the exit angle may be found. Using a computer program to give these resultant mode angles, values for the film index and thickness with each polarization were varied in order to match the experimental results. This thickness value for one film was used to calibrate the mass-thickness measurement.

No reduction in optical attenuation proportional to magnesium doping was evident; in fact, a very slight increase may be noted (See Figure 5). These values represent guided mode attenuation, and so do not exactly reflect the intrinsic material attenuation, as the reflections off the inside of the waveguide as well as the fact that the ray path can be represented as a zigzag pattern instead of a straight line propagating down the guide contribute to the measured attenuation. However, upon analysis this error proved inconsequential. For sample films with refractive indices as found above, the magnitudes of the reflection coefficients are very close to unity, and with the measured mode angles, the propagation down the waveguide occurs at very shallow angles. For example, the ratio of the actual propagation length down the waveguide versus the corrected length can be represented as the cosine of that reflection angle, θ, where

$$\cos\theta = \frac{\text{measured}}{\text{corrected}} = \frac{\lambda_0 k_1}{2\pi n}$$

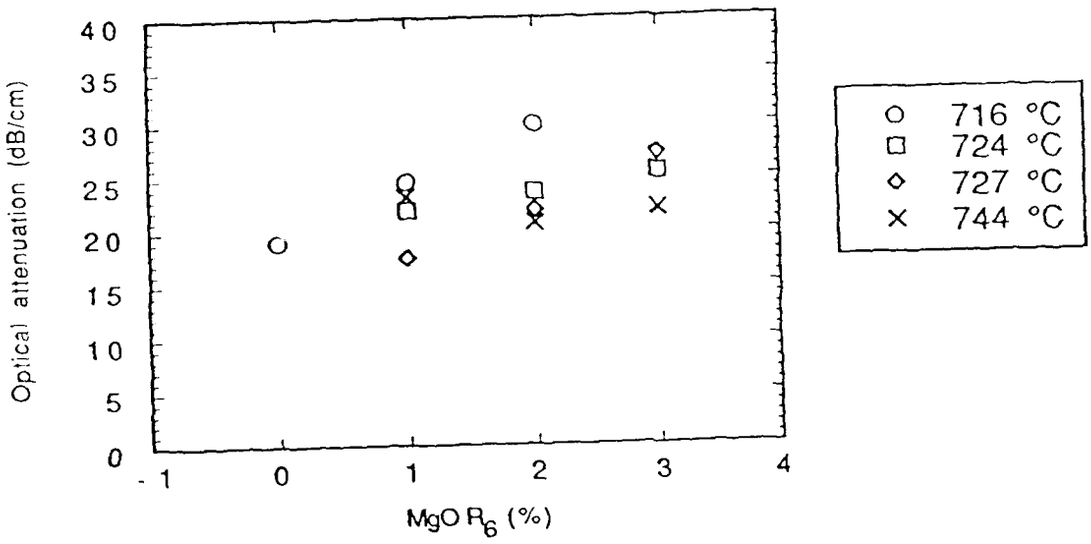

Figure 5. Optical waveguide mode attenuation versus MgO content R_6.

and λ_0 is the incident light wavelength, k_l is the k-vector of the given mode, and n is the refractive index of the film. For several films grown here, this correction factor equals approximately 0.98, and is therefore of little consequence to the plot of attenuation versus magnesium content. This is to be expected, as analysis of the optical attenuation of one film for three different modes was performed. The slope of power detected versus propagation length, i.e. the optical attenuation, is the same for each mode, and since each mode has a different angle, the thickness differences do not matter (See Figure 6).

The most widely held explanation for changes in optical absorption involves charge compensation. In the lead-free melts of Tamada [5], it was postulated that the minimum of optical attenuation with a given amount of Mg^{2+} doping occurs because the Mg^{2+} replaces Fe^{2+} ions that were formed to compensate for Pt^{4+} ions incorporated from the platinum crucible and oxygen vacancies. The Fe^{2+} ions are responsible for a transition which results in higher optical attenuation, but the right amount of Mg^{2+} to compensate for Pt^{4+} and oxygen vacancies will eliminate this. Tamada showed that the amount of Pt^{4+} remains constant over several MgO dopant values, as there is a finite attack on the crucible.

In the PbO-based system, for the film with no Mg^{2+}, there are several mechanisms from the incorporation of lead into the film that manifest in high optical absorption, such as the Pb^{2+}-Pb^{4+} intervalence transition, and Pb^{4+}-oxygen vacancy transitions. The incorporation of Mg^{2+} is initially compensated by the formation of Pb^{4+}, but most of it increases the formation of Fe^{4+}. This ion can account for the slight

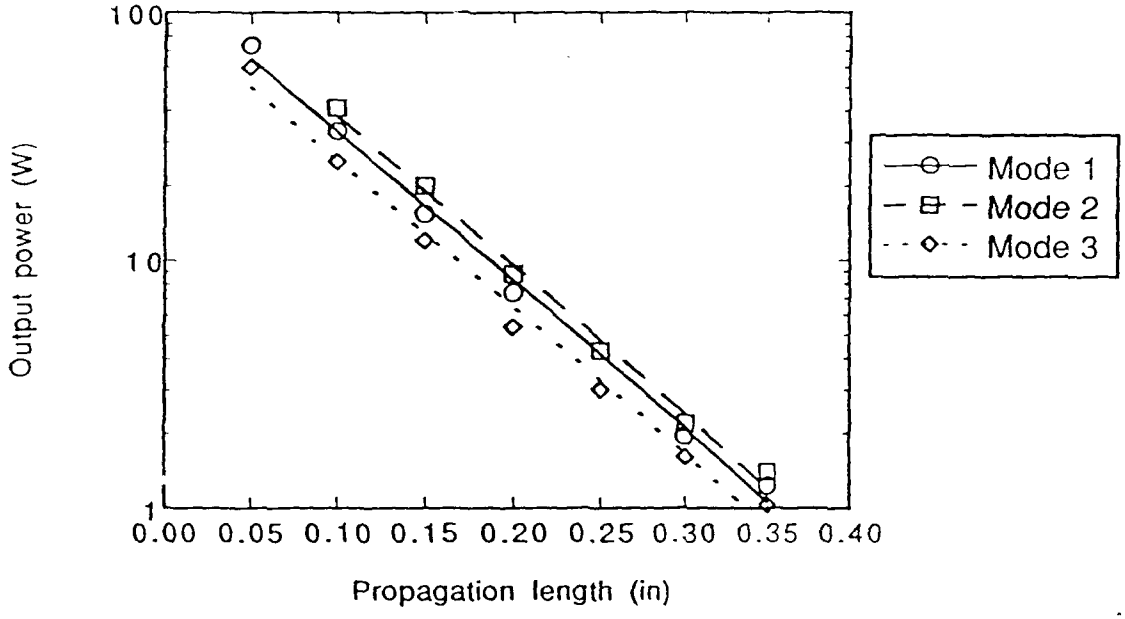

Figure 6. Optical mode detected power versus propagation length in the waveguide for different guided modes.

increase in optical attenuation. However, the optical absorption, while not as low as the lowest achieved by Tamada at critical Mg^{2+} doping levels, was still lower than his optical absorption for other values of MgO including zero. X-ray fluorescence showed no detectable Pt^{4+} in the films, as there is less bismuth in the flux to attack the crucible. This precludes the formation of Fe^{2+}, and so there is no increase of the optical absorption because of this [32].

3.3. Microwave Properties

Ferromagnetic resonance (FMR) linewidth is an important material parameter relating to the excitation of magnetostatic waves. FMR linewidth measurements were performed on the films using an apparatus fashioned after the design by Adam, et al. at Westinghouse [33]. It involves a small hole in the side of the X-band waveguide used to carry the microwave. Around this small hole is a soft magnetic iron plate, and the film is placed near to this hole. The hole and iron plate cause a well in the applied magnetic field, and so only a small localized area will resonate. This method has the advantage of being nondestructive and the entire LPE-grown wafer can be measured without cutting.

The measurements on the films grown from the PbO-based melt with MgO doping showed very low linewidths of less than 1 Oersted. This is significantly lower than the film grown from the equivalent PbO-based melt with no MgO, although there is little observable trend among the different nonzero MgO doping values (See Figure 7).

The drastic reduction in FMR linewidth with only a small amount of MgO doping can also be explained in the domain of charge compensation [34]. The lead in the melt can be incorporated in the film as Pb^{2+} as well as Pb^{4+}. With no Mg^{2+} in the film, differing amounts of Pb^{2+} and Pb^{4+} can cause the occurence of Fe^{4+} and Fe^{2+} respectively. The formation of Fe^{2+} is known to produce an increase in linewidth by the valence exchange mechanism [35]. The addition of Mg^{2+} both prevents the incorporation of Pb^{2+} as well as charge compensating the Pb^{4+} obviating the

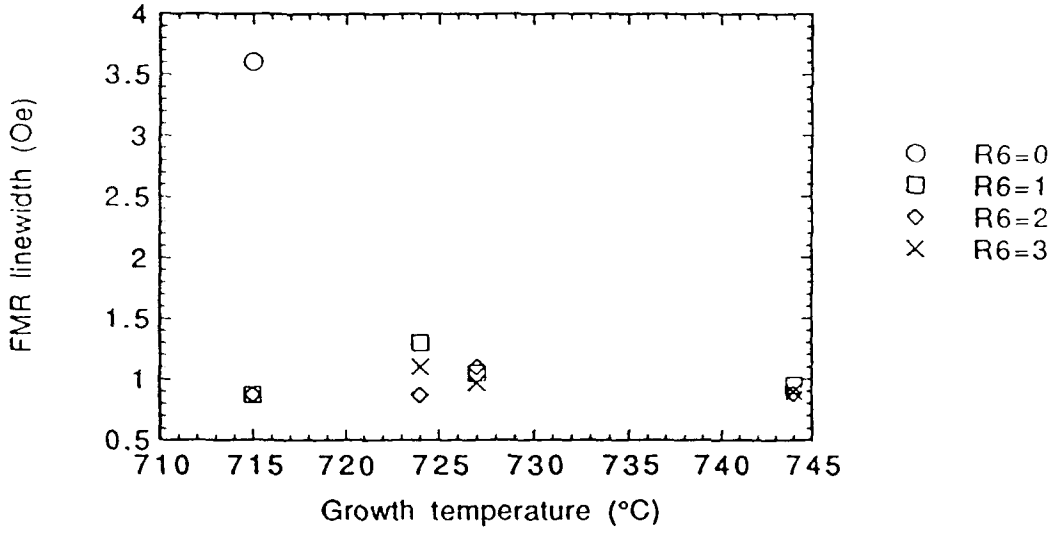

Figure 7. FMR linewidth versus growth temperature for varying values of MgO content R_6.

production of the nontrivalent iron ions and resulting in low linewidth [36].

The films were then measured for MSW passband characteristics. The MSW's were excited by a microwave signal launched by an antenna line in contact with the film and received by a similar antenna after propagating 1/2 inch. This was performed in an applied magnetic field. The passband measurements showed a very poor response (see Figure 8), although one film grown with MgO was shown to have a stronger response than the one grown without MgO. This result is contrary to the very low measured FMR linewidths.

This inconsistency may be explained by the fact that the linewidth is measured in a highly localized area (approximately 1 mm^2), while the MSW passband measurement must cause an MSW to be propagated across a much larger distance (1/2 inch). Further FMR measurements showed a variation in ferromagnetic resonance field at various locations on the same wafer of up to 10 Oe. These different resonance fields across the path length of the MSW suggest the presence of inhomogeneities across the wafer that could adversely affect the MSW propagation characteristics. The low growth temperatures required for bismuth substitution can lead to uneven films [19], as can the lower growth rates caused by MgO substitution [37]. In addition, some researchers use a rotation that changes direction every 10 seconds in order to get a uniform film [38]. Another possibility is the remaining flux on the film. While the droplets are mostly removed by spinning soon after removal from the melt, they are not completely removed and there is growth during the slow removal of the film from the furnace. Faster removal from the furnace might alleviate this problem. Slight variations in the furnace temperature profile could also cause inhomogeneities.

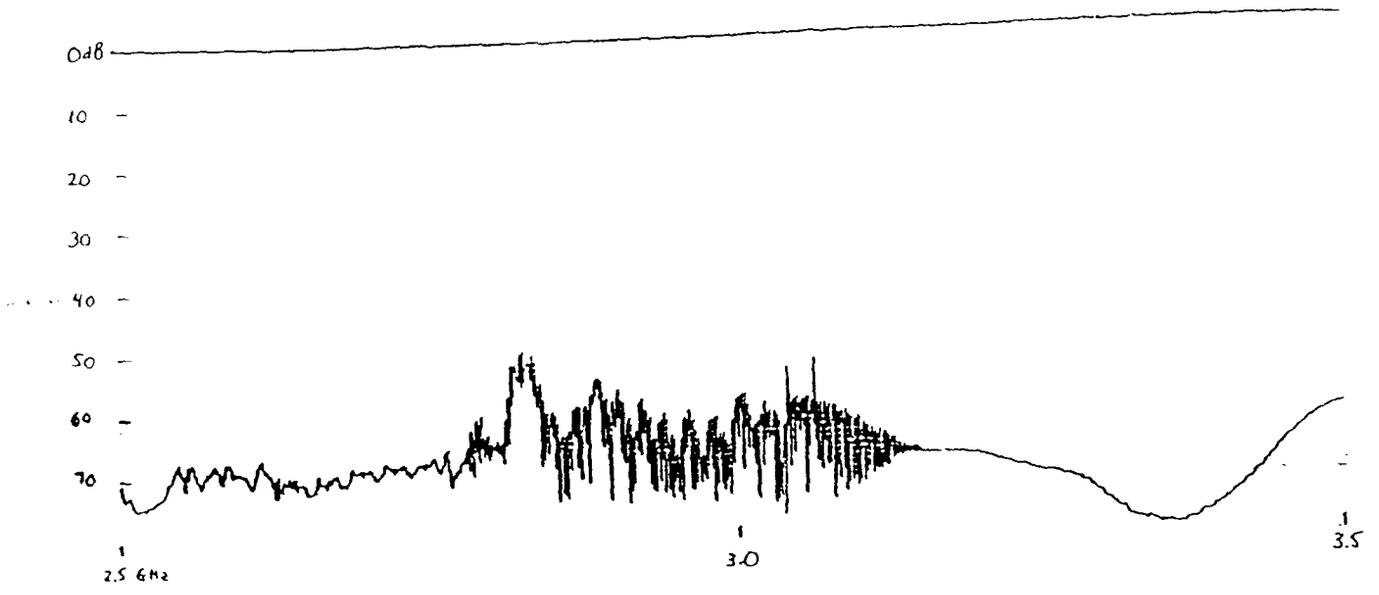

Figure 8a. Magnetostatic wave passband plot of film from melt with no MgO added.

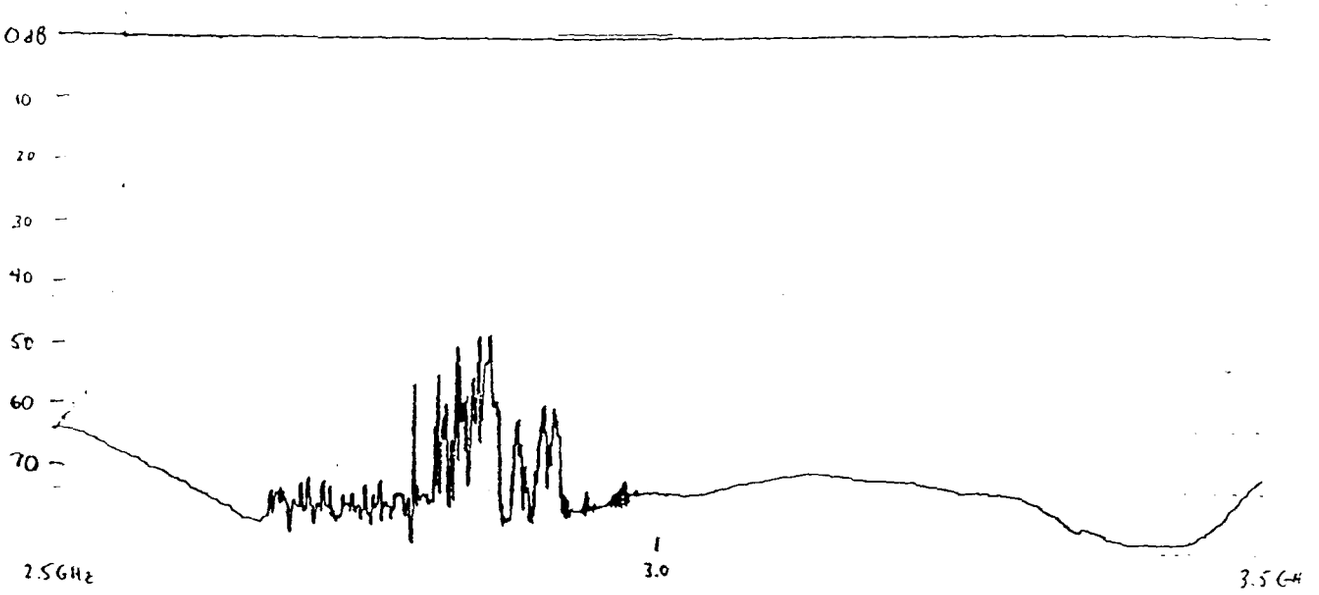

Figure 8b. Magnetostatic wave passband plot of film grown from melt with MgO content R_6=1%.

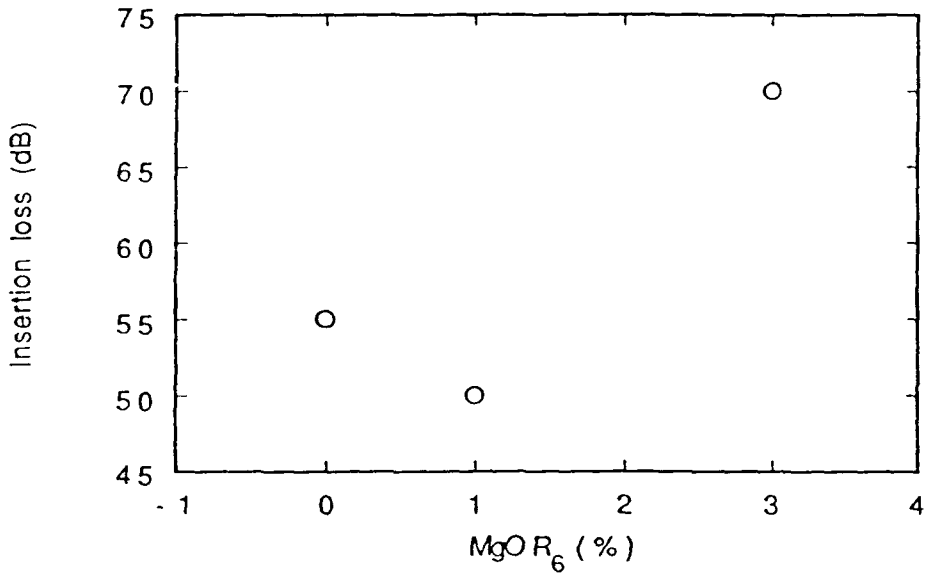

Figure 8c. Microwave insertion loss versus MgO content R_6.

4. Conclusion

Bismuth-doped lutetium iron garnet films for the MSW-optical mode interaction were grown by LPE from a lead-oxide based flux. The flux was doped with varying amounts of MgO, and the effects were compared with previously reported effects on a lead-free melt. It was shown that the magnesium incorporation into the films significantly decreased the FMR linewidth while keeping optical absorption fairly constant. The MSW passbands of the films were not very good, but this may be alleviated in the future by employing switching rotation direction, and precise temperature and furnace removal monitoring to ensure more homogeneous films. Also, adjustment of melt parameters for higher growth rates to compensate for the growth-rate inhibition due to the MgO may improve the homogeneity. The charge-compensation mechanism can be used to explain the observed effects of the magnesium doping.

In addition, the sodium in the melt adds a negative uniaxial anisotropy, which is adjustable by later annealling, and has no detrimental effects. By precision annealling and controlling the anisotropy field, the MSW passband frequency could be tuned to the desired value.

This melt composition is thus found to be a viable alternative to the more difficult lead-free flux. Individual optimization of films grown from this flux into the separate layers of the less restrictive multi-layer structure would ease the requirements further, and this method may show its usefulness in devices exploiting the MSW-optical mode interaction.

References

[1]. P.K. Tien, R.J. Martin, S.L. Blank, S.H. Wemple and L.J. Varnerin, Appl. Phys. Lett. vol. 21, pp. 207-209 (1972).

[2]. A.D. Fisher, J.N. Lee, E.S. Gaynor and A.B. Tveten, Appl. Phys. Lett. vol. 41, pp. 779-781 (1982).

[3]. C.S. Tsai, D. Young, W. Chen, L. Adkins, C.C. Lee and H. Glass, Appl. Phys. Lett. vol. 47, pp. 651-654 (1985).

[4]. S.H. Talisa, IEEE Trans. Magn. vol. 24, pp. 2811-2813 (1988).

[5]. H. Tamada, M. Kaneko and T. Okamoto, J. Appl. Phys. vol. 64, pp. 554-559 (1988).

[6]. D.D. Stancil, IEEE J. Quant. Mech. vol. 27, pp. 61-70 (1991)

[7]. N. Bilaniuk, D.D. Stancil and S.H. Talisa, J. Appl. Phys. vol. 67, pp. 508-510 (1990).

[8]. S.H. Talisa and D.D. Stancil, IEEE Trans. Magn. vol. 25, pp. 3494-3496 (1989).

[9]. Y.K. Fetisov, A.A. Klimov, and V.L. Preobrazhenskii, Int'l Conf. Sol. St. Dev. Mat. 1991, pp. 347-349 (1991).

[10]. V.V. Matyushev, A.A. Stashkevich and J.M. Desvignes, J. Appl. Phys. vol. 69, pp. 5972-5974 (1991).

[11]. K. Matsuda, H. Minemoto, O. Kamada and S. Ishizuka, IEEE Trans. Magn. vol. MAG-23, pp. 3479-3481 (1987).

[12]. D.M. Gualtieri, S.M. Emo and T.R. Kinney, J. Appl. Phys. vol. 69, pp. 5978-5980 (1991).

[13]. P. Hansen, W. Tolksdorf and K. Witter, IEEE Trans. Magn. vol. MAG-20, pp. 1099-1104 (1984).

[14]. R.F. Belt and J.B. Ings, Proc. SPIE vol. 753, pp. 142-149 (1987)

[15]. A.H. Eschenfelder, *Magnetic Bubble Technology* (Springer, Berlin, 1981).

[16]. G.B. Scott and D.E. Lacklison, IEEE Trans. Magn. vol. MAG-12, pp. 292-311 (1976).

[17]. P. Hansen, C.-P. Klages, J. Schuldt and K. Witter, Phys. Rev. B vol. 31, pp. 5858-5864 (1985).

[18]. H.J. Levinstein, S. Licht, R.W. Landorf and S.L. Blank, Appl. Phys. Lett. vol. 19, pp. 486-488 (1971).

[19]. E.A. Giess, J.D. Kuptsis and E.A.D. White, J. Cryst. Growth vol. 16, pp. 36-42 (1972).

[20]. S.L. Blank and J.W. Nielsen, J. Cryst. Growth vol. 17, pp. 302-311 (1972).

[21]. P. Hansen, K. Witter and W. Tolksdorf, Phys. Rev. B vol. 27, pp. 6608-6625 (1983).

[22]. J.M. Robertson, P.K. Larsen and P.F. Bongers, IEEE Trans. Magn. vol. MAG-11, p. 1112 (1975).

[23]. J.E. Davies, J. Matl. Sci. Lett. vol. 11, pp. 976-979 (1976).

[24]. J.M. Robertson, J. Electrochem. Soc. vol. 123, pp. 1248-1249 (1976).

[25]. G.L. Nelson and W.A. Harvey, J. Appl. Phys vol 53, pp. 1687-1689 (1982).

[26]. D.M. Gualtieri, correspondence, 7/15/1991.

[27]. M. Ramesh, D.M. Gualtieri, S.D. Silliman, J. Peruyero and D.D. Stancil, J. Appl. Phys. vol. 70, pp. 6289-6291 (1991).

[28]. W.H. De Roode and J.M. Robertson, J. Cryst. Growth vol. 63, pp. 105-110 (1983).

[29]. H.P. Weber, F.A. Dunn and W.N. Leibolt, Appl. Optics vol. 12, pp. 755-757 (1973).

[30]. A.B. Buckman, Guided-Wave Photonics (Saunders HBJ, Fort Worth, 1992).

[31]. H. Kogelnik and V. Ramaswamy, Appl. Optics vol. 13, pp. 1857-1862 (1974).

[32]. G.B. Scott and J.L. Page, J. Appl. Phys. vol. 48, pp. 1342-1349, (1977).

[33]. J.D. Adam, S.H. Talisa and J.A. Kerestes, IEEE Trans. Magn. vol. 25, pp. 3488-3490 (1989).

[34]. R.D. Henry, P.J. Besser, D.M. Heinz and J.E. Mee, IEEE Trans. Magn. vol. MAG-9, pp. 535-537 (1973).

[35]. H.L. Glass and M.T. Elliot, J. Cryst. Growth vol. 34, pp. 285-288 (1976).

[36]. H. Tamada, M. Saitoh and M. Kandeko, J. Appl. Phys. vol. 67, pp. 949-954 (1990)

[37]. C. Jovanovic, S. Sure, E. Clausing, C. Scharfschwerdt, M. Neumann, H. Alwes, K. Lorenz, H. Dötsch, W. Tolksdorf and P. Willich, J. Appl. Phys. vol. 71, pp. 436-440 (1992).

[38]. H. He, S. Jun, H. Deng, C. Zhu and Z. Feng, IEEE Trans Magn. vol. 25, pp. 3497-3499 (1989).

Acknowledgement

Special thanks are given to Dr. Devlin Gualtieri at Allied Signal Corp. for his assistance and for sharing his expertise in melt determination and film growth, and to Michael Daniel at Westinghouse for his assistance in MSW passband measurement. Additional thanks are given to Professor Daniel D. Stancil for helpful instruction, guidance and encouragement, to Dr. M. Ramesh, Dr. C. Cinbis, and N. Bilaniuk for helpful discussion, and to J. Peruyero for growth of the previous BiLuIG films used for Faraday rotation measurement. The support of Professor Mark Kryder of CMU and the backing of the Air Force Office of Scientific Research and the National Science Foundation are also gratefully acknowledged.